Spring 2019

“Polysoaps” via RAFT Copolymerization to Form Well-Defined Micelles for Water Remediation and Targeted Drug Delivery Applications

Phillip Pickett
University of Southern Mississippi

“POLYSOAPS” VIA RAFT COPOLYMERIZATION TO FORM WELL-DEFINED MICELLES FOR WATER REMEDIATION AND TARGETED DRUG DELIVERY APPLICATIONS

by

Phillip D. Pickett

A Dissertation
Submitted to the Graduate School,
the College of Arts and Sciences
and the School of Polymer Science and Engineering
at The University of Southern Mississippi
in Partial Fulfillment of the Requirements
for the Degree of Doctor of Philosophy

Approved by:

Dr. Charles L. McCormick, Committee Chair
Dr. Sarah Morgan
Dr. Derek Patton
Dr. Daniel Savin
Dr. Douglas Masterson

_____	_____	_____
Dr. Charles L. McCormick Committee Chair	Dr. Jeffery S. Wiggins Director of School	Dr. Karen S. Coats Dean of the Graduate School

May 2019

Published by the Graduate School

ABSTRACT

Amphiphilic copolymers have become increasingly important for environmental and biological applications due to their behavioral characteristics in aqueous solution. For example, structurally-tailored statistical amphiphilic copolymers or "polysoaps" can self-assemble into micelles or other architectures in water at various concentrations. Polysoaps may be differentiated from small molecule surfactant micelles in their capability to self-assemble into unimolecular associates (unimolecular micelles) with no dependence on concentration. Such micelles offer enormous potential for dispersion of hydrophobic species in water at high dilution. Importantly, each polymer chain forms its own micelle and upon dilution, these micelles remain intact and capable of dispersing hydrocarbon material in their core domain. This dissertation focuses on determining the parameters that contribute to the unique unimeric micelle properties of polysoaps. We utilize RAFT copolymerization to prepare well-controlled copolymers with a variety of functional groups, molecular weights, and hydrophobic mole fractions. With this research platform, we achieve a better understanding of how single polymer chains form unimeric assemblies capable of sequestering hydrocarbons in water. With sufficiently high hydrophobic content along a water-soluble backbone, micelles may form, some with unimeric structures. The unimeric micelles have been shown to have higher uptake efficiencies of hydrocarbon into their core domains as compared to multimeric, polymer-based and small molecule, surfactant-based micelle. This work demonstrates the potential utility of polysoaps for contemporary applications including oil spill remediation, water treatment, and targeted drug delivery.

ACKNOWLEDGMENTS

I would like to extend my sincerest thanks to my research advisor, Dr. Charles L. McCormick, for his constant support, patience, and mentorship throughout my graduate career. I am especially grateful to Dr. McCormick for giving me the freedom to explore my intellectual creativity and curiosity. Additionally, I appreciate his influence on my professional development and for encouraging a research environment that stresses the importance of critical thinking and independence. I would also like to thank my graduate committee, Dr. Sarah Morgan, Dr. Derek Patton, Dr. Daniel Savin, and Dr. Douglas Masterson for their support and guidance. Many thanks to Dr. Brett Calhoun and Dr. William Jarrett for additional guidance and help throughout my graduate career.

I am thankful for all the past and current McCormick group members. I especially thank Dr. Brooks Abel, Dr. Keith Parsons, Dr. Christopher Holley, Dr. Wenming Wan, Dr. Marco Oliviera, David Siefker, Mason Dearborn, and Kaden Stevens. Additional thanks go to my past REU students, Austin Ventura and Christopher Kasprzak. I am forever grateful to Dana Froelich for her years of friendship and assistance while in graduate school. Without Dana, routine operation of the McCormick group would not be possible.

I would like to acknowledge and thank Dr. Wayne Reed and his research group at Tulane University for their continuous collaboration on research projects throughout my graduate studies. Thanks especially goes to Dr. Aide Wu for his cooperative efforts on a joint project in the Reed labs. I would also like to thank Dr. Vijay Rangachari and Dr. Jason Azoulay for allowing me the use of their UV-Vis and Fluorescnece spectroscopy instrumentation.

I would also like to acknowledge the financial support for this research, which was provided by the National Science Foundation's Experimental Program to Stimulate Competitive Research (EPSCoR) under Cooperative Agreement No. IIA1430364, by the CMEDS Consortium of GOMRI (grant # SA 12-05/GoMRI-002), and by the National Science Foundation Graduate Research Fellowship Program under Grant GM004636/ GR04355.

Though there are too many to list, I would like to thank all my friends, without whom I would not have been able to succeed in my graduate studies. Their constant support and encouragement kept me focused and gave me the strength to do well. For my friends back home in Maryland, I am greatly appreciative for providing me with a close circle of friends that I can always count on. For the friends I have made in Hattiesburg, I will always cherish our memories and will continue to value your friendship.

Finally, I would specifically like to express gratitude towards my family. My most heartfelt thanks to my mother and father, Isabelle and Steven Pickett, and my brothers and sisters, Stephen, Elizabeth, Hannah, Gregory, Isabelle, and Mary Pickett for their support of my education and for always loving me and staying in touch while I was away from home. They are the best family I could ever wish for and there was no one I looked forward to seeing more over the holidays than my own family.

DEDICATION

This dissertation work is dedicated to my mother and father, Isabelle and Steven Pickett, and my grandparents, Isabelle Fox and Alice and Ralph Pickett. They have shown me limitless love and support and I am forever grateful for their role in my life and for making me the man I am today.

TABLE OF CONTENTS

LIST OF TABLES

LIST OF ILLUSTRATIONS

LIST OF SCHEMES

LIST OF ABBREVIATIONS

CMC	Critical Micelle Concentration
CAC	Critical Aggregation Concentration
HLB	Hydrophilic Lipophilic Balance
UCST	Upper Critical Solution Temperature
LCST	Lower Critical Solution Temperature
RDRP	Reversible Deactivation Radical Polymerization
CRP	Controlled Radical Polymerization
RAFT	Reversible Addition-Fragmentation Chain Transfer
CTA	Chain Transfer Agent
DP	Degree of Polymerization
PAHs	Polycyclic Aromatic Hydrocarbons
AMPS	2-Acrylamido-2-Methylpropane sulfonic acid
AIBN	Azobisisobutyronitrile
DMP	Dodecylsulfanylthiocarbonylsulfanyl-2-methyl propionic acid
DDAM	Dodecylacrylamide
CPDT	2-Cyano-2-Propyl Dodecyl Trithriocarbonate
CEP	4-Cyano-4-(Ethylsulfanylthiocarbonylsulfanyl) pentanoic acid
V-70	2,2’-Azobis(4-Methoxy-2,4-Dimethylvaleronitrile)
SAC	Sulfacetamide
SMZ	Sulfamethazine
4HPhMA	4-Hexylphenyl Methacrylamide
mSAC	Methacryloyl Sulfacetamide

mSMZ	Methacryloyl Sulfamethazine
HPMA	N-(2-Hydroxypropyl) Methacrylamide
DPDMA	(Dodecylpropyledisulfide) Methacrylamide
9-AM	9-Anthracenemethanol
SDS	Sodium Dodecyl Sulfate
^{1}*H-NMR*	Proton Nuclear Magnetic Resonance Spectroscopy
^{13}*C-NMR*	Carbon Nuclear Magnetic Resonance Spectroscopy
DLS	Dynamic Light Scattering
SLS	Static Light Scattering
GPC	Gel Permeation Chromatography
SEC	Size Exclusion Chromatography
MALLS	Multi-Angle Laser Light Scattering
PDI	Polydispersity Index
Mw	Weight Average Molecular Weight
Mn	Number Average Molecular Weight
D_h	Hydrodynamic Diameter
R_h	Radius of Hydration
IC50	Half Minimal Inhibitory Concentration
LMw	Low Molecular Weight
MMw	Medium Molecular Weight
HMw	High Molecular Weight

CHAPTER I - INTRODUCTION

1.1 Small Molecule Surfactants and Critical Micelle Concentration.

Surfactants have gained a wide variety of uses commercially for dispersing insoluble compounds in water. Traditional surfactants are amphiphilic small molecules consisting of a hydrophilic head group and a hydrophobic tail.[1–4] Normally, these surfactants are capable of assembling into spherical structures called micelles with the hydrophobic tails making up the core of the sphere and the hydrophilic head groups the corona. Assembly into such structures requires an overall decrease in Gibbs free energy of the system. For example, micellization occurs as result of the entropically favorable induced assembly of hydrophobic moieties in water due to the expulsion of water in proximity to a hydrophobe to the less-ordered bulk phase.[5]

Surfactants get their name from being "surface-active-agents" in aqueous media, a term that is a consequence of diffusional exchange of the surfactant molecules between the surface and bulk solution.[4,6] Upon saturation of the air-water interface, newly added surfactant molecules accumulate in the bulk water phase and self-assemble into micelles (Figure 1.1).[1–4,6–10] The concentration of surfactant that designates this point is called the critical micelle concentration (CMC). Beyond the CMC, diffusional partitioning of the surfactant molecules between the surface and bulk solution increases, leading to sharp decreases in surface tension.[4] Larger surfactant molecules, especially polymeric surfactants, diffuse more slowly, and therefore exhibit smaller drops in surface tension at the CMC.[4] However, some polymeric surfactants can form unimeric micelles with minimal surface activity and an absence of a CMC.

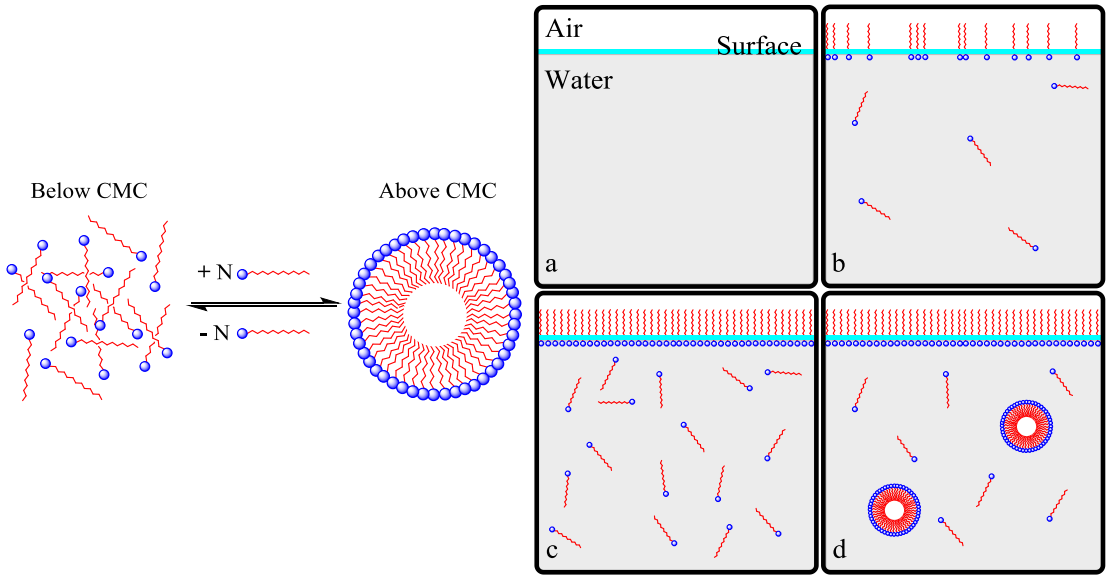

Figure 1.1 Top: visual aid of transition between non-ordered surfactant and spherical surfactant micelle at the CMC. Bottom: a) no surfactant present in water; b) surfactant below CMC align at water surface; c) surfactant at the lower limit of CMC form monomer layer at water surface; d) surfactant above CMC form micelle in water solution.[1–4,6–10]

1.2 Hydrophilic-Lipophilic Balance.

In order to form a stable assembly in water, a polymeric system must have an appropriate hydrophilic-lypophilic balance (HLB).[11–14] The importance of this value is as a predictive tool to determine how a given surfactant will behave in oil/water mixtures, dictating the identity of the continuous phase. A simple way to calculate HLB is through the Griffin method[11,15] which uses the equation

$$HLB = 20 \times \frac{M_h}{M_{tot}}$$

in which M_h is the molecular weight of the hydrophilic portion of a surfactant and M_{tot} is the total molecular weight of the surfactant. However, when using this method for ionic surfactants, HLB values are often observed to be lower than expected because they do not

account for the increased hydrophilicity of the charged groups. Therefore, a correction factor (C_h) is added to the equation.

$$HLB = 20 \times \frac{M_h}{M_{tot}} + C_h$$

Most emulsifying surfactants have an overall HLB value that range from 1 to 20.[14] Values closer to 1 represent surfactants that produce water in oil emulsions. Conversely, surfactants with values closer to 20 produce oil in water emulsions.

There are other methods of calculating HLB. A more complicated one is Davies method[15,16] which considers every contributing functional group in its calculation based on group values. Davies equation is

$$HLB = 7 + \sum H_i - n(0.475)$$

in which H_i is the group value of contributing hydrophilic groups and n is the number of aliphatic carbons (-CH-, -CH_2-, or -CH_3) in the hydrophobic portion of the surfactant. Values for individual functional groups arbitrarily range from 1-40 with hydrophilic character increasing HLB and hydrophobic character decreasing HLB. The arbitrary group values can be found in reference 16. Surfactant mixtures can also be used to achieve HLB values for desired emulsification properties. For example, an HLB of a mixture of A and B surfactants is directly influenced by the weighted contribution of the HLB of each component based on molar or mass fraction (f_x).[17]

$$HLB_{AB} = f_A \cdot HLB_A + f_B \cdot HLB_B$$

1.3 Polysoaps.

Amphiphilic copolymers have been of great interest for decades because of their ability to self-assemble in water.[18–20] The associative properties of several architectural

types have been studied in solution. These include block,[21–23] graft,[24,25] segmental block,[26–28] dendritic,[29,30] star,[31,32] and soap-like[4,33,34] copolymers (Figure 1.2). From these architectures, multimeric assemblies such as micelles, vesicles, and worm-like micelles have been achieved.[ref] Soap-like copolymers or "polysoaps" are unique in that they can spontaneously organize into unimolecular micelles without a concentration dependence, resulting in no measurable CMC for these systems.[4,20,35–37]

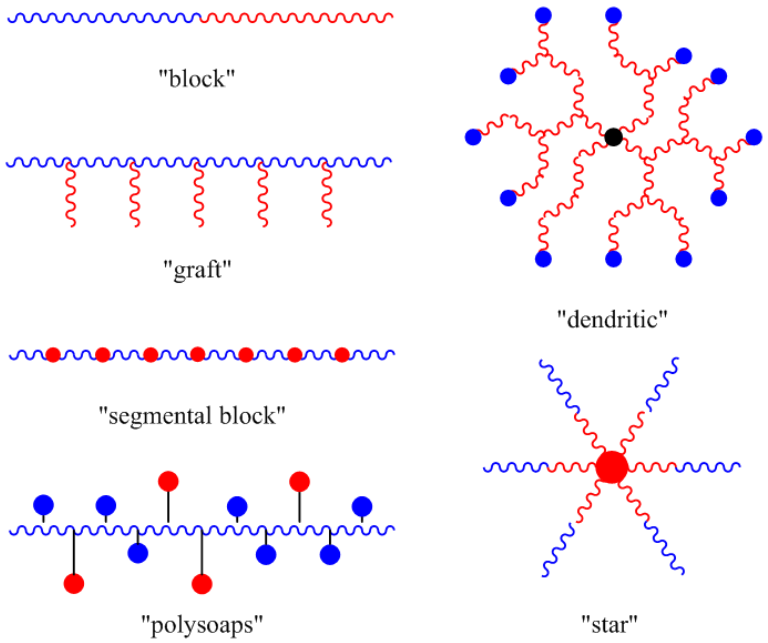

Figure 1.2 Notable amphiphilic copolymer architectures that form polymeric micelles (blue: hydrophilic; red: hydrophobic).[4,21,30–34,22–29]

Early studies with micelle-forming polymers by Strauss and coworkers[33,34] revealed that amphiphilic copolymers consisting of hydrophobic pendant groups along a hydrophilic backbone possessed surfactant-like characteristics. These first studies of polysoaps were conducted with cationic polymers of poly(2- and 4-vinylpyridine) that were partially N-substituted with n-dodecylbromide, resulting in both uni- and multi-

molecular micelles that could solubilize hydrocarbons in water.[33–35,38] Laschewsky, in an extensive 1995 review article,[4] described the structural variations and behavioral characteristics of micellar copolymers, including those of traditional "polysoaps" with head, mid-tail, and tail-end attachment to the macromolecular backbone, and main-chain type hydrophilic moieties (Figure 1.3).[4,36,39–47] Hydrophilic groups can be non-ionic (acrylamide and acrylic acid)[48–50], cationic (ammonium salts)[51–55], anionic (carboxylate and sulfonate)[26,42,47,56–58], and zwitterionic (sulfobetaines and carboxybetaines).[59–61] Hydrophobic units can be varied from hydrocarbons with different chain lengths (C_6-C_{18}),[48,50,58] to aromatic (benzene, pyrene, and naphthalene)[26,51,53] or vinyl ethers,[54,58] and may even be stimuli-responsive.[47,56,58,59] In addition, several molecules possessing pyrenyl,[42,53,62–66] naphthyl,[47,56,65] or dansyl[47,58,67] moieties have been employed as fluorescent probes or labels that respond to changes in their local environment.

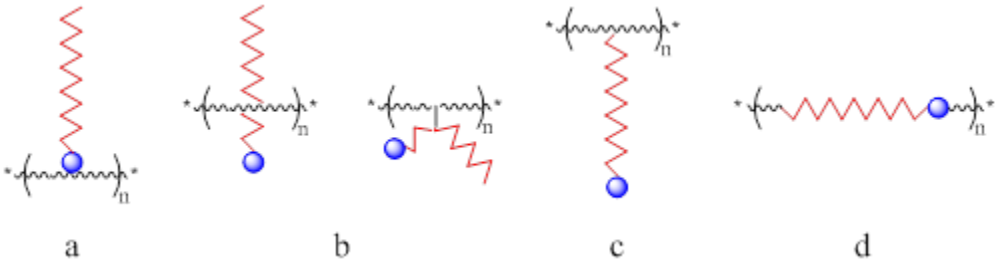

Figure 1.3 Structural variations of surfactant analogs on polysoap chain: a) head type; b) mid-tail type; c) tail-end type; d) main chain type.[4,40]

By 2000, major symposia and research reviews[68–72] were focused on specific architectures in which self- or stimuli-induced intra- and intermolecular hydrophobic associations could lead to various nanostructures in water. A number of models have been proposed for micelle formation in such polysoap systems. Literature supports the "local micelle" and "molecular micelle" models that originated from Srauss' work

(Figure 1.4).[4,40,63,64,73–80] The local micelle model suggests that only a limited number of neighboring hydrophobes on a single chain will associate within a domain, resulting in multiple associations per a polysoap chain (Figure 1.4a). The molecular micelle model holds that every hydrophobe in the polysoap contributes to a single domain, thus one micelle per chain (Figure 1.4b).[4,75] The "regional micelle" model (Figure 1.4c) assumes that both intra- and intermolecular interactions can participate in micelle-like domains, suggesting that increases in volume fraction will allow for gradual shift from intra- to intermolecular associations.[4,40,75]

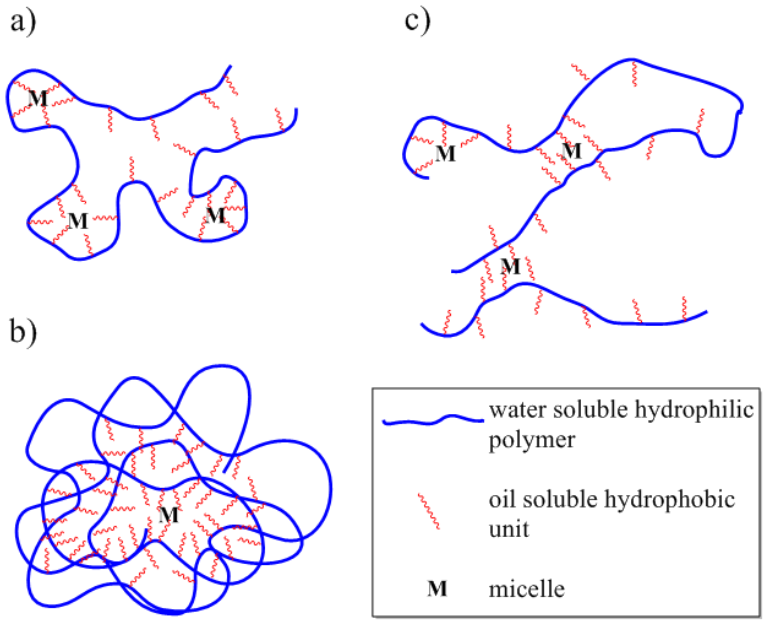

Figure 1.4 Micelle models for polysoaps: a) local micelle; b) regional micelle; c) molecular micelle.[4,75]

Extending some elements of the local micelle and molecular micelle models, more recent work of Morishima and coworkers led to the "flower-like" micelle model (Figure 1.5).[27,81–86] At sufficiently low hydrophobic content, a micelle is formed in which associated hydrophobes form a core that is surrounded by water soluble loops of the

corona. These flower-like micelles are largely intramolecular, however, interpolymer associations at higher concentration allow bridged, multipolymer micelles as well.[82] When the hydrophobic content increases, intramolecular associations dominate; the flower-like micelles collapse through further association of the hydrophobes in a manner analogous to that of the molecular micelle model.[27,81,82] However, this can only happen if the micelles are sufficiently stabilized in the corona.

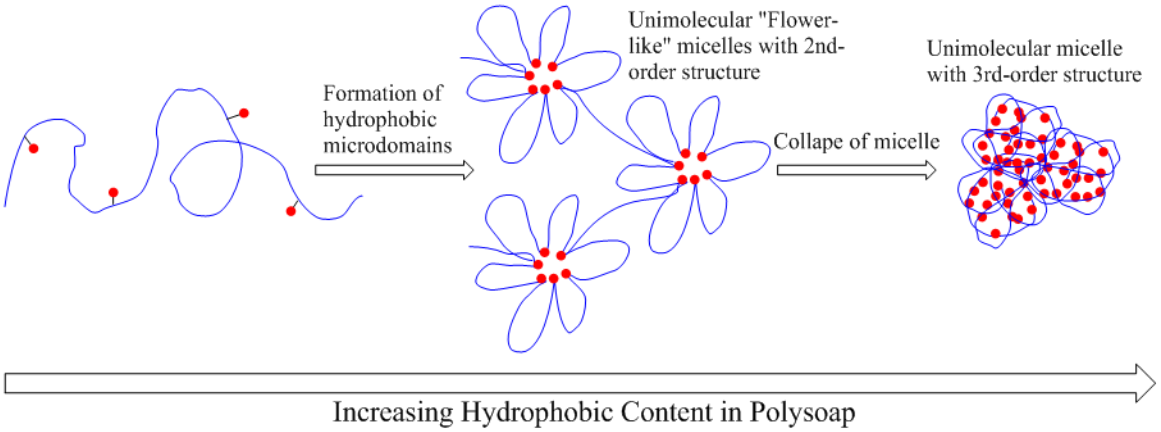

Figure 1.5 Illustration of "flower-like" micelle concept of unimolecular micelles of second- and third-order structures.[81]

Additional experiments by Morishima examined the influence of copolymer hydrophobic content on the secondary and tertiary structures of unimeric assemblies.[27] As the molar hydrophobic content increased along the polymer backbone, a shift from intra- to inter-molecular association was observed. Initially, the copolymers formed loosely folded second-order structures at lower hydrophobic content of 10-30%. Between 30-50%, unimeric third-ordered structures of compacted micelles were observed. These unimeric structrures formed without a concentration dependence. As the mole fraction of hydrophobe increased past 50%, interchain associations dominated and multimeric micelles emerged. These studies were conducted on polymers with molecular weights

ranging between 15 - 30 kDa, produced via uncontrolled, free radical copolymerization techniques. Though the studied polymers were in a small range of molecular weights, it is difficult to assess whether the assembly properties were due to the hydrophobic content or the differences in polymer degree of polymerization.

McCormick and coworkers[55] studied the effects of hydrophobic monomer distribution along the polymeric backbone on solution properties. Hydrophobically-modified water-soluble acrylamide copolymers were synthesized in which the hydrophobes were distributed statistically and in micro-blocky segments along the polymers backbone. At low concentrations and low hydrophobic content, the solution viscosity of the blocky polysoaps increased exponentially with concentration owing to intermolecular association of the hydrophobes. The statistical polymers did not exhibit this dramatic increase in viscosity since intermolecular associations were not present at low concentrations. Interestingly, these polymers were shear thickening in water as result of a critical shear stress that disrupted intramolecular association of the hydrophobes, thus allowing extended polymer chains to interact inermolecularly.[55]

1.4 Stimuli-responsive polymers.

Stimuli-responsive, associating polymers that exhibit changes in chemical structure, conformation, or physical properties are important for biomedical, water purification, and environmental remediation applications.[69,87] These polymers exhibit reversible solution behaviors in response to pH, ionic strength, or temperature. Also, by tethering responsive polymeric backbones to hydrophobic, water-soluble, or other responsive (co)polymers, responsive materials with a variety of assembly and rheological properties can be achieved.[77,88]

Polyelectrolytes are a class of responsive polymers that contain many charged groups, often with a charge at each repeating unit.[77,89,90] These charges can be either along or pendent to the polymer backbone. Anionic and cationic polyelectrolytes respond to variations in ionic strength of a solution via a rod-to-coil conformational change. This is commonly referred to as the polyelectrolyte effect.[91] Initially, due to the highly charged nature, the polymer chain is extended into a rod-like conformation due to repulsive forces. When simple electrolytes are added, the charges are screened and the polymer collapses into a coil, often resulting in phase separation. Zwitterionic polymer backbones, however, exhibit anti-polyelectrolyte effect behavior[92] which results from the chain initially adopting a collapsed, coil-like conformation due to intra- and inter-polymer charged dipole interactions (typically observed from units with sulfobetaine, phosphobetaine, or carboxybetaine functionalities). When an electrolyte is introduced, the charged dipole interactions break, and the polymer becomes extended and soluble in water.

Polymers that contain acidic or basic functional groups are polyelectrolytes with pH-dependent solution properties.[31,93] Changing the pH of the solution results in varying the degree of ionization of the polymer. Normally, with pH-responsive polymers the degree of ionization can be tuned from 100% charged to completely neutral depending on solution pH and the functional group pK_a value. This relationship is expressed in the Henderson-Hasselbalch equation shown below

$$pH = pK_a + \log\frac{[A^-]}{[HA]}$$

where pK_a is the -log(K_a), with K_a being the acid dissociation constant, [HA] is the concentration of protonated acid, and [A^-] is the concentration of the acid's conjugate base. The transition between the charged and neutral states of a polymer is typically broad as the poly(acid or base) acts as a buffer in solution. Poly(acids) undergo a shift from charged to neutral when the pH of the solution is greater than the pK_a of the acidic functional group. Conversely, poly(bases) become ionized when the pH of the solution increases above the pK_a of the base. In water, shifts in solubility make these types of pH-responsive polymers relevant for biomedical and environmental applications. Common acidic and basic monomers used to synthesize pH-responsive polymers are shown in Figure 1.6.

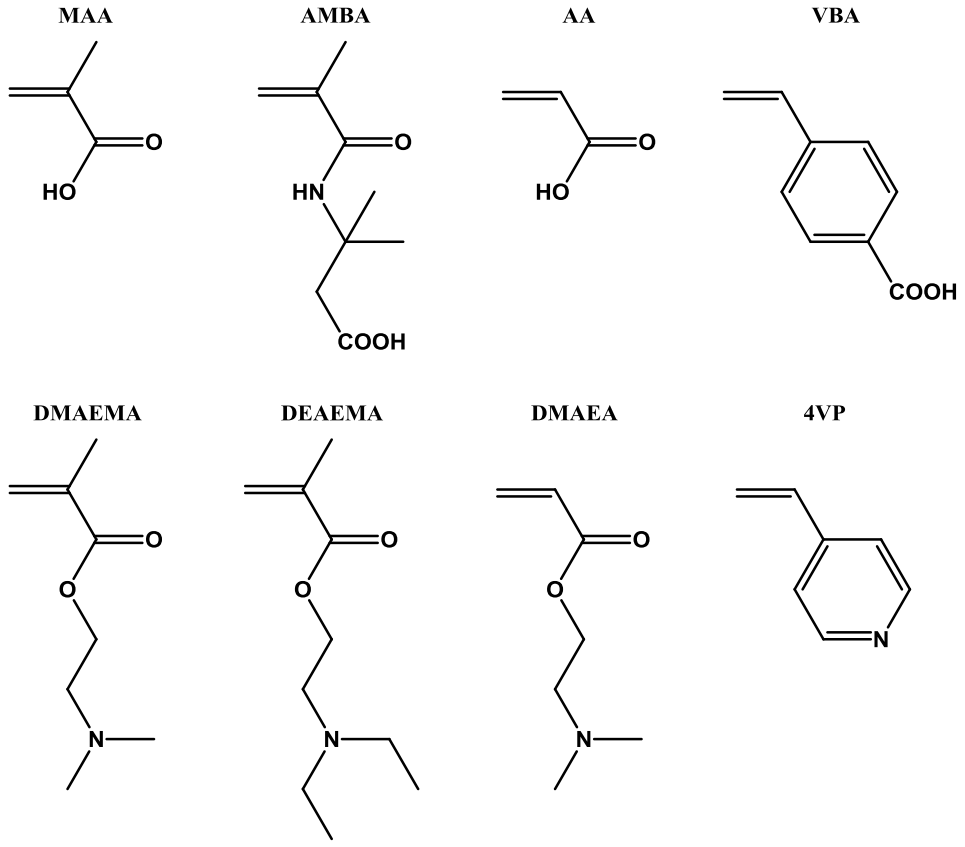

Figure 1.6 Common acid and base functionalized monomers used to synthesize pH-responsive polymers.[93]

Thermally-responsive polymers possess the property of changing conformation and thus hydrodynamic volume with temperature.[29,93,94] This transformation is often associated with a change in the Gibbs free energy of mixing (ΔG) of polymer in solution, which is a function of enthalpy (ΔH) and entropy (ΔS).

$$\Delta G = \Delta H - T\Delta S$$

Polymers that exhibit an increase in solubility as temperature increases, possess a positive ΔS of mixing. These polymers have an upper critical solution temperature (UCST).[94] On the other hand, polymers that exhibit a decrease in solubility as temperature increases have a negative ΔS of mixing and a lower critical solution temperature (LCST).[94] In water, this entropy driven process is influenced by the interaction and ordering of water molecules with and around the polymer chain. Common functional monomers used to make thermally-responsive polymers are shown in Figure 1.7.

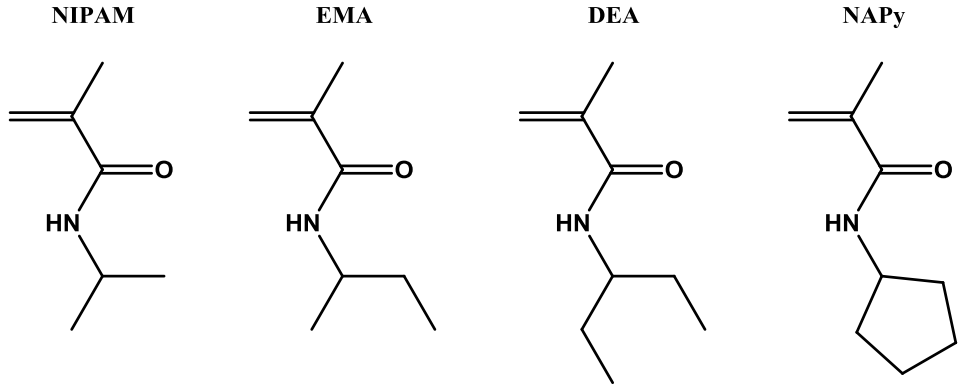

Figure 1.7 Common monomers used to synthesize thermally-responsive polymers.[93]

1.5 pH-Responsive sulfonamide-based polymers.

Recently, our group has demonstrated the tunable pH- and CO_2-responsive behavior of sulfonamide-based homopolymers achieved by varying the sulfonamide

substituents (and thus pK_a values) of the constituent monomers (Scheme 1.4). Most significantly, the corresponding polymers exhibit narrow, reversible pH-dependent solubility transitions with an "on/off" type of behavior.[95] When the solution pH > pK_a of the sulfonamide proton the monomer and analogous homopolymer is water soluble; conversely when the solution pH < pK_a of the sulfonamide proton then the monomer and resulting homopolymer is water insoluble. Additionally, if the pK_a of the sulfonamide functionality is high enough, CO_2 can be used to induce reversible phase separation through the formation of carbonic acid in solution.

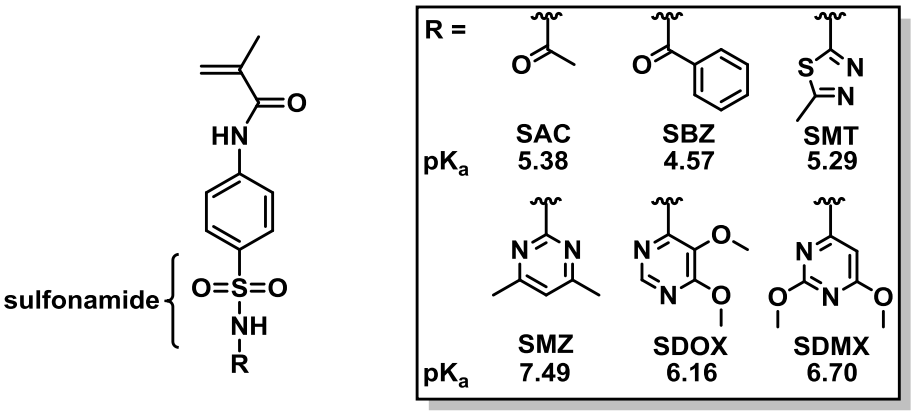

Scheme 1.1 Sulfonamide monomer structure and varying R-groups with respective pK_a values.[95]

1.6 RAFT Polymerization.

Prior to the development of reversible deactivation radical polymerization (RDRP) techniques,[96–98] control over molecular weight and polymer structure was not possible. With broad polydispersities, poor functional monomer selection and lack of structural control, the synthesis of systems with conformational response and assembly features to mimic biomolecules was difficult. Among important RDRP techniques is reversible addition–fragmentation chain transfer (RAFT) polymerization. This technique

was first reported by Rizzardo and coworkers.[98,99] The RAFT process in Scheme 1.3 demonstrates the concentration suppression and control of the propagating radical through a degenerative chain transfer mechanism. This reduces chain transfer reactions to monomer or solvent, and termination reactions via radical coupling or disproportionation, which allows for a quasi-living propagating chain end to exist. Because of this, RAFT polymerization is a versatile technique that offers control over molecular weight and narrow polymer molecular weight distributions. In addition, RAFT can tolerate a wide variety of monomer functionalities and solvents.[23,97,98,100–107] The powerful synthetic tools developed for RAFT polymerization and subsequent advances in the technique now allow polymerization of highly functional monomers under benign conditions (in water and at room temperature) to afford complex, but highly controlled architectures with a tailorable range of responses to external stimuli.[97,98]

A key characteristic of RAFT is the use of a chain transfer agent (CTA), often trithiocarbonates or dithioesters with R and Z stabilizing groups. These R and Z groups are chosen for a given set of conditions such that the R group is capable of rapid fragmentation and efficient re-initiation of monomer. The Z group affects the rate of radical addition to the CTA, the lifetime of the radical intermediate, and the direction of fragmentation. For sufficient polymerization control, the rate of addition (k_{add}) of the initiator-derived radical must be significantly higher than the rate of propagation (k_p).

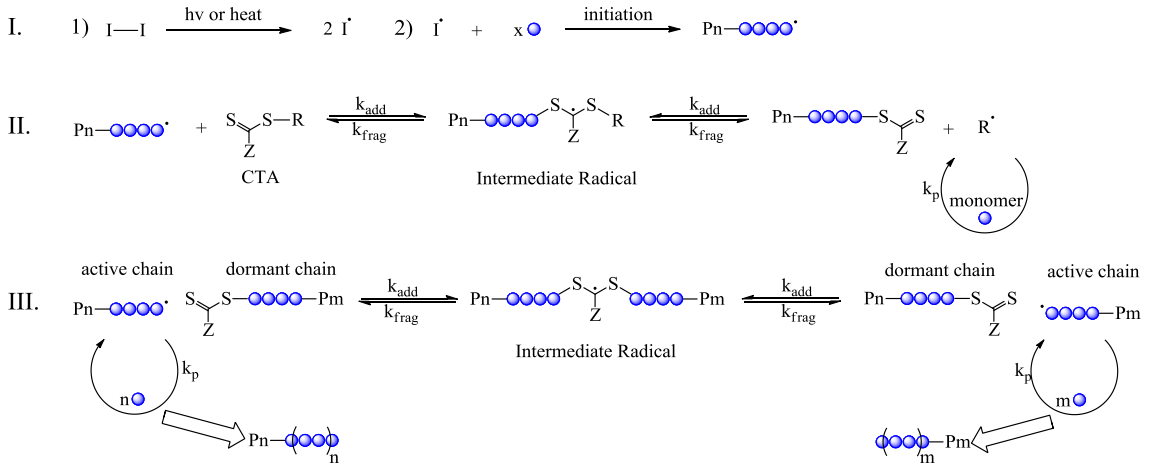

Scheme 1.2 Generic RAFT polymerization scheme: I) initiation; II) initialization period; III) addition/fragmentation and propagation.[98,101–105]

Once the degenerative chain-transfer step of RAFT polymerization establishes an equilibrium state, propagation proceeds as it does in conventional free radical polymerization; the rate of propagation (R_p) follows pseudo-first order kinetics with respect to monomer concentration ([M]) and is calculated as

$$R_p = k_{app}[M]$$

where k_{app} is the apparent propagation rate constant equal to $k_p[P_n\cdot]$ when a steady state of propagating radical concentration ($[P_n]$) is maintained throughout the polymerization. The theoretical degree of polymerization (DP) is often determined by the ratio of initial monomer concentration ($[M]_o$) to CTA concentration ([CTA]), as well as monomer conversion (ρ). This assumes that almost all the polymer chains are derived from CTA R-groups. The theoretical DP is calculated by

$$DP = \frac{\rho[M]_o}{[CTA]}$$

CHAPTER II – RELEVANCE AND OBJECTIVES OF RESEARCH

2.1 Relevance of Research.

Materials with the ability to sequester and disperse hydrocarbon molecules in water are important for oil spill remediation, water treatment, and biomedical applications. Polymeric surfactants offer a unique route to achieving the desirable properties for such applications. Specifically, for the work presented in this dissertation, polymers that form unimeric micelles are of interest. The following discussions highlight the relevance of research to specific applications.

2.1.1 Oil Spill Remediation

The Deepwater Horizon oil spill (2010) accentuated the need for advanced remediation technologies, materials, and methods. Utilization of conventional surfactants in this incident and the Exxon Valdez spill in 1989 has proven to be insufficient for remediation of the oil. Although, bacterial break-down of crude oil can be enhanced by surfactant-induced micro-dispersion,[108,109] a critical micelle concentration (CMC) of surfactant must be maintained for oil emulsification. Furthermore, the micelle lifetime must exceed the time required for petroleum biodegradation. In the ocean, maintaining a concentration above the CMC is not possible with small molecule surfactants due to the enormous dilution effect (Scheme 1.1). After migration and dilution of initially dispersed oil, surfactant levels fall below the CMC and oil is released back into the marine environment, appearing as plumes at various depths, oil slicks on the surface, and deposits on the sea floor.[110,111] Therefore, polymeric surfactants that can maintain core domain structure regardless of concentration would be invaluable for oil spill cleanup in open sea waters.

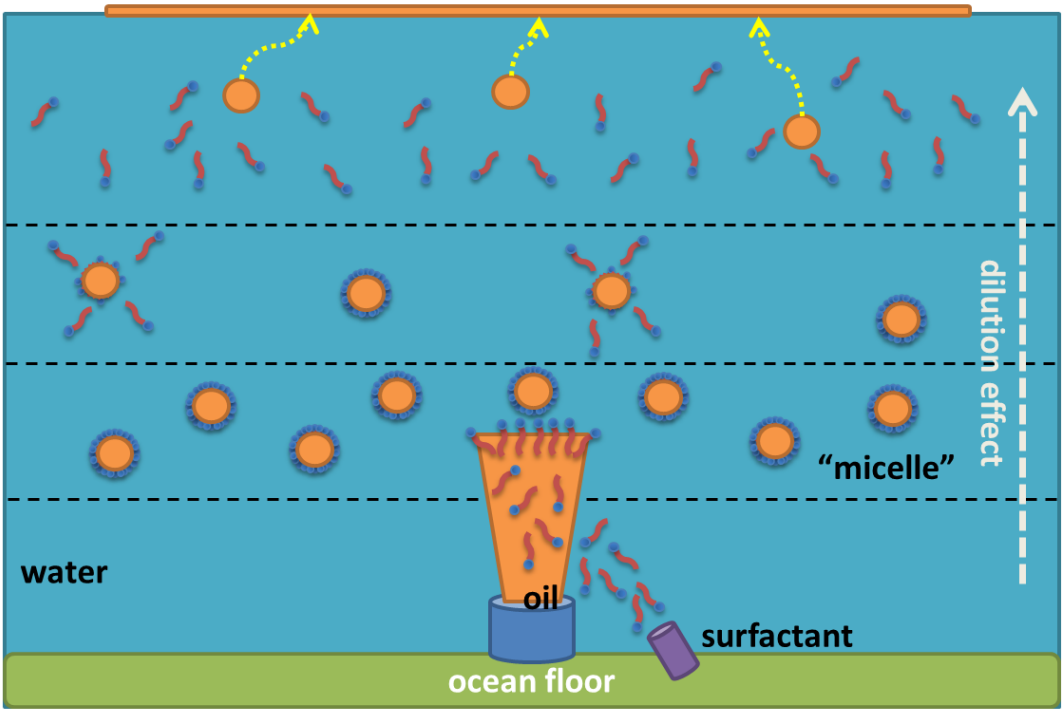

Scheme 2.1 The fate of surfactant/oil in open sea water due to the dilution effect.

2.1.2 Water Treatment

Assuring the quality and availability of clean drinking water is a major global objective, spurred recently by well-documented reports of contamination by pollutants including pharmaceuticals, pesticides, and polycyclic aromatic hydrocarbons (PAHs).[112–118] These types of chemicals typically enter water sources through sewer drainage and water runoff or from industrial waste disposal.[117–120] The presence of PAHs and related hydrophobic compounds in water sources has been linked to cancer and birth defects.[9–11] Unfortunately, removal of these harmful chemicals has proven to be challenging due to the low efficiency and high cost of commercial purification techniques.[123–125] Therefore, developing a sustainable polymer that could sequester foulant and purify the water though removal of the material would greatly improve water treatment technologies.

2.1.3 Targeted Drug Delivery

Many chemotherapeutic drugs are small, hydrophobic molecules that require water-soluble, biocompatible nanocarriers for enhanced vascular circulation. Existing polymeric carriers either conjugate the therapeutic along a copolymer backbone or sequester hydrophobic drugs within a protected interior domain to be delivered to specific sites in the body. However, the former route requires complex, multi-step syntheses and the latter is subjected to inherent dilution effects in the body, limiting the efficiency of drug delivery at the targeted site. One way to circumvent a number of these issues is by using biocompatible, stimuli-responsive polymers that are capable of unimeric micelle formation, hydrophobic drug delivery, and triggered release, regardless of dilution effects. Ideally, the synthesis of these polymers would be facile and the sequestration properties would be amenable to a variety of therapeutic payloads.

2.1.4 Overall Research Platform

The research presented in this dissertation aims to develop materials that circumvent the inescapable dilution effect encountered with conventional surfactants by utilizing functional amphiphilic copolymers that form unimolecular micelles or "polysoaps". The use of these polysoaps for efficient water remediation or drug delivery applications is possible since, in principle, each polymer chain forms its own micelle that is capable of hydrophobe/foulant sequestration regardless of dilution effects. Additionally, this allows us to build a research platform that encompasses multiple generations of these unimeric polymer-based micelles with practicality in variety of applications (Scheme 1.2).

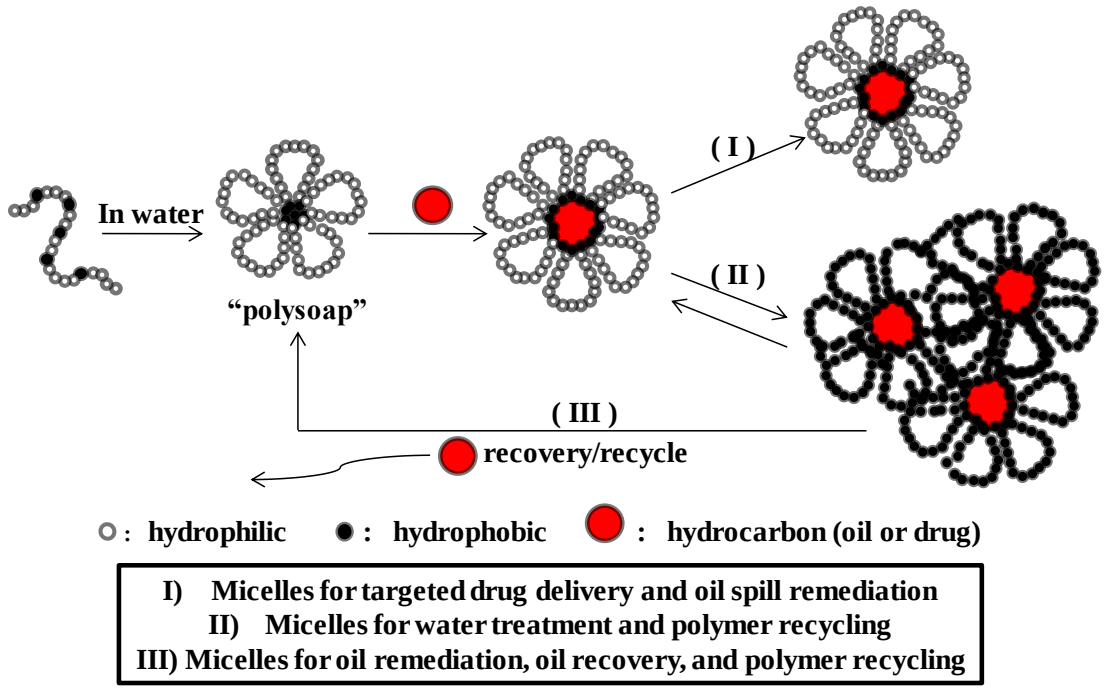

Scheme 2.2 Polymeric micelles (polysoaps) for water remediation and targeted drug delivery applications: I) first-generation polysoap; II) second-generation polysoap; III) third-generation polysoap.

A first-generation micelle would be useful for targeted drug delivery and oil spill remediation technologies. A second-generation micelle can be used for sustainable water treatment technologies. Lastly, a third-generation polymeric micelle would be advantageous for oil remediation, recovery, and polymer recycling.

2.2 Objectives of Research

The overall goal of this dissertation is to develop unimolecular polymeric micelles capable hydrocarbon sequestration for use in enhanced environmental remediation applications and for targeted drug delivery of hydrophobic cancer therapeutics. This is accomplished by focusing on the parameters that contribute to the unique unimeric micelle formation of statistical amphiphilic copolymers called "polysoaps". The work utilizes RAFT copolymerization to afford polymers with controlled molecular weights

and narrow molecular weight distributions. This is advantageous because we can prepare a series of copolymers with varying molecular weights, architectures, and monomer content.

The specific objectives of this research are to:

1) Synthesize a library of linear anionic amphiphilic copolymers (first-generation polysoaps) capable of micelle formation via RAFT copolymerization of DDAM and AMPS.
2) Characterize the anionic polysoaps for their micellar solution properties (micelle size, surface activity, core domain hydrophobicity, and hydrophobe uptake efficiency) as a function of hydrophobic content and polymer concentration.
3) Investigate the cell toxicity of anionic polysoaps using cell viability experiments.
4) Systematically investigate how hydrophobic content and copolymer molecular weight in polysoap systems effect micelle size, core domain formation, and hydrocarbon uptake efficiencies.
5) Synthesize a library of pH/CO_2-responsive second-generation, amphoteric polysoaps via the RAFT copolymerization of mSAC or mSMZ, and 4HPhMA.
6) Investigate the micellar properties of second-generation, amphoteric polysoaps.
7) Determine the pH and CO_2 -dependent phase behavior of second-generation, amphoteric polysoaps.
8) Demonstrate the hydrocarbon removal capabilities of second-generation, amphoteric polysoaps.
9) Synthesize a library of third-generation, polysoaps through the RAFT copolymerization of mSAC and mSMZ.

10) Investigate the micellar properties of third-generation polysoaps as a function of solution pH.
11) Determine the pH and CO_2-responsive phase behavior of third-generation polysoaps.
12) Demonstrate the capability for third-generation polysoaps to remove hydrocarbons from water followed by foulant isolation and polymer recovery.
13) Synthesize biocompatible, responsive polysoaps via the RAFT copolymerization of HPMA and DPDMA for the delivery of hydrophobic cancer drugs.
14) Investigate the micellar properties of biocompatible, responsive polysoaps.
15) Determine the responsive behavior and payload release of biocompatible, responsive polysoaps.
16) Investigate the cell toxicity of biocompatible, responsive polysoaps.

This dissertation is presented in three sections. The first section involves preparing first-generation polysoaps from hydrophobic dodecyl acrylamide (DDAM) and hydrophilic 2-acrylamido-2-methylpropanesulfonic acid (AMPS) to be used for oil-spill remediation. These polysoaps form both unimeric and multimeric micelles based on composition. The unimeric micelles are especially promising since each copolymer forms its own micelle capable of hydrocarbon (foulant) sequestration, even at high dilution.

The second section is directed at understanding the structural contributions to micelle formation and hydrocarbon uptake capability. Within these studies, a library of anionic AMPS-based polysoap were prepared. Three molecular weights (15kDa, 50kDa, and 120kDa) were studied, each series containing copolymers with 10, 20, 30, 40, 50, and

60 mol% DDAM. These polymers were characterized as a function of concentration using dynamic light scattering for hydrodynamic diameters and UV-Vis and fluorescence spectroscopy using pyrene as a model hydrocarbon to probe uptake efficiencies and to probe hydrophobic core domain formation of the micelles, respectively.

Based on the original polysoap concept, the third section incorporates responsive functionalities into the polysoap backbone in attempt to obtain a system that is recoverable for water treatment applications. This second-generation polysoap was realized utilizing sulfonamide-based monomers which are pH- and CO_2-responsive. The unique characteristics provided by the sulfonamide copolymers are narrow solubility transitions and tunable pK_a values. When the solution pH > pK_a of the sulfonamide moiety, the group is charged and micelles form in solution; conversely, when the solution pH < pK_a the functional group is neutral, water-insoluble, and phase separation occurs. An advantageous property of these polymers is that they can be recycled to clean multiple batches of contaminated water before reaching saturation of their core domains.

This dissertation includes two additional projects included in Appendix A and Appendix B. The research presented in Appendix A involves a third-generation polysoap that is synthesized by the RAFT copolymerization of mSAC and mSMZ. This copolymer possesses three characteristics depending on pH: 1) micellization for sequestration of hydrocarbon in water, 2) precipitation for the removal of the polymer and foulant from water, and 3) full solubility in water for separation and release of the hydrocarbon foulant from the copolymer so that the polysoap can be fully recycled.

The research presented in Appendix B comprises the design and preparation of biocompatible, responsive polysoaps for the targeted drug delivery of hydrophobic cancer

therapeutics. These types of polysoaps contain hydrophobic units that can be cleaved via reduction of a disulfide bond, which results in the dissolution of the core domain, allowing for controlled release of a hydrophobic payload.

CHAPTER III - EXPERIMENTAL

3.1 Structurally controlled "polysoaps" via RAFT copolymerization of AMPS and n-doedcyl acrylamide for environmental remediation.

3.1.1 Materials.

2-Acrylamido-2-methylpropane sulfonic acid (AMPS, **1**, Figure C.1) (99%), acryloyl chloride and azobisisobutyronitrile (AIBN, **2**, Figure C.2) (98%) were purchased from Sigma Aldrich. The monomer, AMPS, was recrystallized from methanol. The initiator, AIBN, was purified by recrystallization from ethanol. All other purchased reagents were analytical grade and used as received. The RAFT chain transfer agent, 2-dodecylsulfanylthiocarbonylsulfanyl-2-methyl propionic acid (DMP, **3**, Figure C.3) was synthesized according to a previously reported method.[126] ^{1}HNMR, δ(TMS, ppm): 0.90 (t, 3H, -CH3), 1.37-1.47 (m, 20H, -(CH2)10-), 1.75 (s, 6H, 2-CH3), 3.42 (t, 2H, -CH2S), 13.05 (s, 1H, -COOH); yellow crystals, m.p. 61-62 ^{o}C. The synthesis of n-dodecyl acrylamide (DDAM, **4**, Figure C.4) is outlined below.

3.1.2 Synthesis of n-dodecyl acrylamide.

n-Dodecyl acrylamide (DDAM) was synthesized by reacting n-dodecyl amine with acryloyl chloride in THF using triethylamine (TEA) as an acid receptor (Figure 3.1). A typical procedure is as follows: in a 500 mL flask equipped with stir bar, dodecylamine (0.1 mol) and TEA (0.13 mol) were added to 100 mL of THF. Then the solution was cooled to 0 °C in an ice bath and acryloyl chloride (0.13 mol) in 100 mL THF was then added to the reaction flask slowly over 2 hours. Afterwards, the flask was removed from the ice bath and kept at room temperature for another 2 hours. Following filtration and evaporation of THF, the crude product was twice recrystallized from acetone at -25 °C.

[1]HNMR, δ(TMS, ppm): 0.90 (t, 3H, -CH3), 1.20-1.30 (m, 18H, -(CH2)9-), 1.55 (m, 2H, -CH2-), 3.22 (t, 2H, -CH2NHCO), 5.61 (m, 1H, C=CHCO), 6.20 (m, 1H, CH2=C); white powder, m.p. 54-55°C.

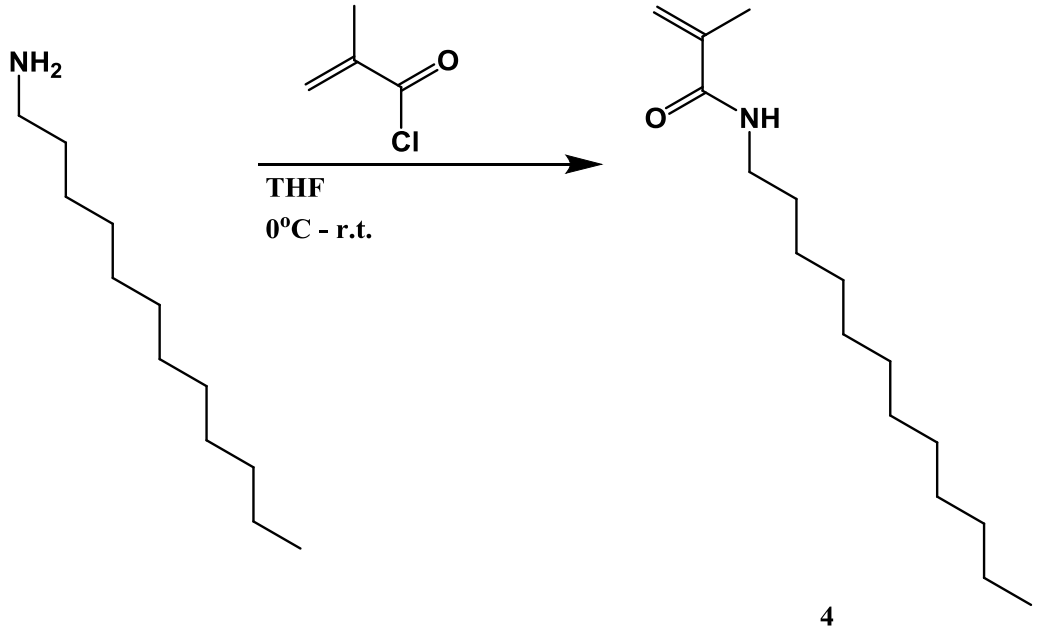

Figure 3.1 Synthesis of n-dodecylacrylamide (DDAM, **4**, Figure C.4).

3.1.3 RAFT copolymerization of AMPS and DDAM.

The general procedure is as follows. The DDAM and AMPS with desired feed ratio, for example, DDAM (0.9717 g, 3 mmol), AMPS (0.6224 g, 3 mmol), DMP (4.9 mg, 0.013 mmol), DMF (3 mL) and AIBN (0.7 mg, 0.007 mmol) with the molar ratios of DDAM: AMPS: DMP: AIBN= 450: 450: 2: 1, were added to a 10 mL polymerization flask equipped with a magnetic stir bar. After purging with N_2 for 30 minutes, the flask was placed in an oil bath at 60 °C while stirring. After a desired polymerization time of 10 hours, the flask was removed from the oil bath and immediately cooled with liquid nitrogen. The crude reaction solution was then dialyzed against methanol for 1 day

followed by water with small amount of NaOH for another 3 days. The purified product was isolated by lyophilization resulting in fine, white powders.

3.1.4 Pyrene uptake of the poly(AMPS-stat-DDAM) series.

To study the uptake characteristics of the polysoaps, 10 uL of 50 mg/mL pyrene solution in acetone was added to 1.5 mL centrifuge tube. After all of acetone was evaporated, 1 mL of polysoap in DI water with the desired concentration was added to this centrifuge tube to solubilize the pyrene deposited on the surface. The contents were sonicated and allowed to equilibrate with shaking over a one-day period. Afterwards, the sample was centrifuged at 10k RPM for 10 minutes and the amount of pyrene in solution was determined by UV absorbance spectroscopy at a wavelength of 339 nm.

3.1.5 Characterization.

Dynamic Light Scattering (DLS) measurements at 90o of the polysoap series in DI water were performed using a DLS detector (Malvern-zetasizer Nano Series) with a 22 mW He-Ne laser operating at $\lambda = 632.8$ nm, an avalanche photodiode detector with high quantum efficiency, and an ALV/LSE-5003 multiple τ digital correlator electronics system. Data analysis of DLS measurements was performed using the CONTIN method.

Static light scattering (SLS) measurements at 90^{o} were made using incident light at 633 nm from a Research Electro Optics HeNe laser operating at 40 mW. The time-averaged scattering intensity (over two min) was measured from a Brookhaven Instruments BI-200SM goniometer with an avalanche photodiode detector and TurboCorr correlator.

Gel permeation chromatography measurements were performed with multiangle laser light scattering (SEC-MALLS) at 25 ^{o}C using TOSOH Biosciences TSK-GEL

columns [Super AW3000 G3000 PWXL (<50 000 g mol-1, 200 A) and G4000PWXL (2000-300 000 g mol-1, 500A)]. A Wyatt Optilab DSP interferometric refractometer (λ = 690nm), a Polymer Laboratories LC 1200 UV/Vis detector (λ = 310 nm for polymers and λ = 274 nm for monomers) and a Wyatt DAWN DSP multi-angle laser light scattering detector (λ = 633 nm) were used with 0.2 M $LiClO_4$ in methanol as the eluent at a flow rate of 1 mL/min.

Surface Tension measurements of samples at specified concentrations were performed with a Kruss Tensiometer at room temperature. Samples were prepared and equilibrated for one day prior to measurement.

Steady State Fluorescence measurements were recorded with a Quantamaster from Photo Technology International. The excitation wavelength was 338 nm. The step size for emission and excitation was set to 1 nm.

Cell viability tests were performed using a Vybrant MTT cell proliferation assay kit (Invitrogen). Cells were seeded in the 96-well microplate (Nunclon) with cell density of 5,000 KB cells in 100 μL per well for 24 hours before incubation with different concentrations of the polysoaps. Cells were cultured for 2 days before adding 10 μL of 12 mM MTT reagent to each well. Then cells were further incubated at 37 ^{o}C for 4 hours, followed by adding 100 μL of the SDS (10%) HCl (0.01 M) solution to each well and mixing thoroughly using the pipette. The absorbance was read at 570 nm with a Synergy2 MultiMode Microplate Reader (BioTek).

3.2 Structurally controlled anionic "polysoaps" to serve as dispersants for hydrocarbon uptake in aqueous media: Structural contributions of hydrophobic content and molecular weight.

3.2.1 Materials.

2-Acrylamido-2-methyl-1-propanesulfonic acid sodium salt solution (AMPS, **1**, Figure C.1) (50% v/v in water), 2-Cyano-2-propyl dodecyl trithiocarbonate (CPDT, **5**, Figure C.5) (>97%), and azobisisobutyronitrile (AIBN, **2**, Figure C.2) (98%) were purchased from Sigma Aldrich. Dodecylacrylamide (DDAM, **4**, Figure C.4) (>97%) was purchased from TCI America and used as received. The monomer, AMPS, was isolated and purified via precipitation from acetone and collected via vacuum filtration and dried under high vacuum. The initiator, AIBN, was purified by recrystallization from methanol. The RAFT chain transfer agent, CPDT, was purified via column chromatography prior to use.

3.2.2 Synthesis of poly(AMPS-stat-DDAM) series.

The general procedure is as follows. The DDAM and AMPS with desired feed ratio, for example, DDAM (0.9717 g, 3 mmol), AMPS (0.6224 g, 3 mmol), CPDT (4.9 mg, 0.013 mmol), DMF (3 mL) and AIBN (0.7 mg, 0.007 mmol) with the molar ratios of DDAM: AMPS: DMP: AIBN= 450: 450: 2: 1, were added to a 10 mL polymerization flask equipped with a magnetic stir bar. After purging with N_2 for 30 minutes, the flask was placed in an oil bath at 70 °C while stirring. After a desired polymerization time, the flask was removed from the oil bath and immediately cooled with liquid nitrogen and opened to atmospheric pressure. The crude reaction solution was then dialyzed against methanol three times over 1 day followed by water with small amount of HCL three

times over another day. The purified product was isolated by lyophilization resulting in fine, white powders. Compositional data for each polymer in the series are given in Table 1. In addition to self-assembly in water into micelles, copolymers are soluble in DMF and methanol which disrupt hydrophobic interactions and thus allow characterization studies of the non-associated systems via ^{1}H-NMR and SEC-MALLS.

3.2.3 Preparation of UV-Vis and Fluorescence Spectroscopy Samples.

To study the uptake characteristics of the polysoaps, 5 uL of 50 mg/mL pyrene solution in acetone was added to 0.5 mL well of a 96-well plate. After all of acetone was evaporated, 0.5 mL of polysoap in DI water with the desired concentration was added to the respective well to solubilize the pyrene deposited on the surface. The contents were allowed to equilibrate with shaking over a one day period. Afterwards, a 0.2 mL aliquot of polysoap solution was removed and transferred to a new 96-well plate and the amount of pyrene in solution was determined by UV-Vis absorbance spectroscopy at a wavelength of 341 nm. Fluorescence spectroscopy was also used to probe the hydrophobic domain formation of the micelles via the I_3/I_1 ratio of pyrene in solution.

3.2.4 Characterization.

Dynamic light scattering (DLS) measurements were collected using incident light at 633nm from a Research Electro Optics HeNe laser operating at 40mW. The time-dependent scattering intensities were measured from a Brookhaven Intruments BI-200SM goniometer at 60, 75, 90, 105, and 120 degrees with an avalanche photodiode detector and TurboCorr correlator.

UV-Vis spectroscopy and fluorescence spectroscopy for pyrene absorbance and fluorescence were measured with a TECAN Safire 96-well plate spectrometer running on

integrated Microsoft Excel software. Absorbance was measured at 341 nm and fluorescence was measured via emission scan from 350 to 550 nm with an excitation wavelength of 341 nm.

Structural data for the polymer series were collected using 1H-NMR for % conversion and %DDAM content and gel permeation chromatography for molecular weight and PDI information. Gel permeation chromatography measurements were performed with a Viscotek TDA302 triple detector array system equipped with TOSOH Biosciences TSK-Gel columns (SuperAW3000 and SuperAW4000). The eluent was 0.2M $LiClO_4$ in methanol at a flow rate of 0.6 ml/min.

3.3 Amphoteric, sulfonamide-functionalized "polysoaps": CO_2-induced phase-separation for water remediation.

3.3.1 Materials.

4-cyano-4-(ethylsulfanylthiocarbonylsulfanyl)pentanoic acid (CEP, **7**, Figure C.7) was synthesized according to literature procedures.[127] Methacryloyl chloride (Aldrich, 97%) was distilled under vacuum and stored under N_2 at −10 °C prior to use. N, N′-Dimethylformamide (DMF) from Acros (extra dry with sieves) was stirred under vacuum at room temperature for 60 min prior to use to remove traces of dimethylamine. The initiator (96%) 2,2′-Azobis(4-methoxy-2,4-dimethylvaleronitrile) (V-70, **6**, Figure C.6) from Wako was stored in a sealed container at -10°C. Sulfonamide precursors (>97%) sulfacetamide (SAC) from Sigma-Aldrich and (99%) sulfamethazine (SMZ) from Acros Organics were used as received. 4-N-hexylaniline (>98%) was purchased from Alfa Aesar and was distilled immediately prior to use. Trimesic acid (96%) was purchased from Sigma-Aldrich and used as received. Standardized 0.1 N NaOH and 0.05 N HCl solutions were purchased from Fisher Scienctific and used as received. The hydrophobic probes, pyrene (>99%) and 9-anthracenemethanol (97%) from Sigma-Aldrich, were used as received.

3.3.2 Synthesis of 4-cyano-4-(ethylsulfanylthiocarbonyl)sulfanylpentanoic acid (CEP).

CEP was synthesized using the following procedure (Figure 3.2). A suspension of NaH (95%) (2.11 g, 83.5 mmol) in anhydrous diethyl ether (150 mL) was cooled to 0 °C using an ice bath, upon which ethanethiol (5.73 g, 92.3 mmol) was added over 15 min accompanied by a vigorous evolution of hydrogen gas. The reaction was stirred for an

additional 15 min at 0 °C followed by dropwise addition of carbon disulfide (7.03g, 92.3 mmol) over 5 min and the reaction stirred for 60 min at room temperature. The reaction mixture was then diluted with pentane (100 mL) and the resulting yellow precipitate isolated by vacuum filtration before drying under vacuum yielding Sodium ethyl trithiocarbonate (12.07 g, 90%) as a hygroscopic yellow solid. To a suspension of sodium ethyl trithiocarbonate (9.89g, 61.7 mmol) in diethyl ether (200 mL) at room temperature was added solid I_2 (8.63g, 34.0 mmol) over 5 min. The reaction was stirred for 60 min at room temperature and the precipitated NaI salts removed by vacuum filtration and washed with 50 mL diethyl ether. The filtrate was transferred to a separatory funnel and washed with 5% $Na_2S_2O_4$ (1 x 150 mL), H_2O (1 x 150 mL), and brine (1 x 150 mL) before drying over $MgSO_4$. The solvent was removed via rotary evaporation followed by drying in-vacuo to yield bisethyl trithiocarbonate (96%) as a yellow solid. A solution of bis-ethyltrithiocarbonate (5.00g, 18.2 mmol) and 4,4′-Azobis(4-cyanopentanoic acid) (V-501) (7.66g, 27.3 mmol) in EtOAc (250 mL) was prepared in a 500 mL 3-necked flask equipped with stir bar and condenser. The solution was purged with N_2 for 40 mins prior to heating at reflux for 18 h, upon which the reaction was quenched via exposure to air and cooled to room temperature. The solvent was removed via rotary evaporation and the crude raft agent purified via column chromatography on SiO_2 (60:35:5 Hexanes:EtOAc:Acetic acid). To remove the acetic acid, the column fractions containing CEP were combined and transferred to a separatory funnel and washed with 0.05N HCl (2 x 150 mL), brine (1 x 150 mL), dried over $MgSO_4$, and the solvent removed via rotary evaporation followed by drying under vacuum to yield CEP as a yellow solid. Yield:

7.10g (74%). mp: 43-45°C; 1H NMR (300 MHz, $CDCl_3$): δ 3.38 (q, 2H), 2.70 (t, 2H), 2.55 (m, 2H), 1.85 (s, 3H), 1.40 (t, 3H).

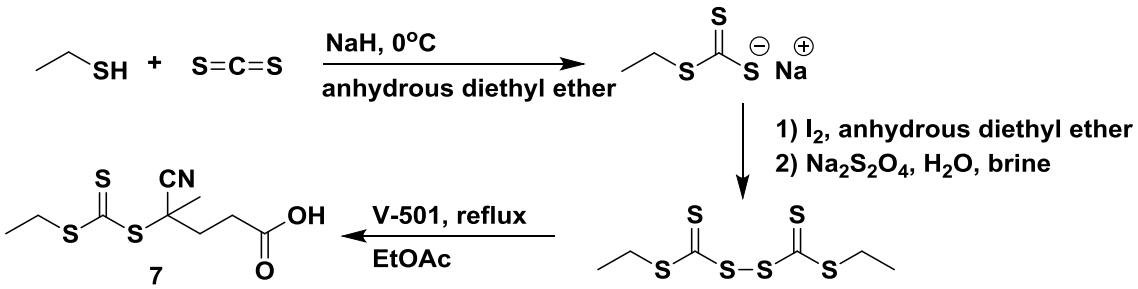

Figure 3.2 Synthesis of RAFT chain transfer agent, CEP (**7**, Figure C.7).

3.3.3 Synthesis of 4-Hexylphenyl Methlyacrylamide (4HPhMA).

Using an adjusted procedure,[44] 4HPhMA was synthesized (Figure 3.3) by the following procedure. 4-Hexylaniline (40.0 mmol) was dissolved in 160 mL of a 1:1 (v:v) mixture of acetone and 0.5 N aqueous NaOH and stirred while cooling in an ice bath. Methacryloyl chloride (4.10 mL, 42.0 mmol) was then added dropwise over 30 min followed by removing the flask from the ice bath and stirring the reaction at room temperature for an additional 60 min. The acetone was removed by rotary evaporation, followed by adjusting the solution to pH = 2 with 12 N HCl. The resulting solids were isolated using vacuum filtration and washed with 100 mL of dilute HCl (0.01 N) prior to drying under vacuum for 48 h, yielding the desired monomer as a white powder. Yield: 9.22 g, 94%; mp: 43-45°C; 1H NMR (300 MHz, $CDCl_3$): δ 7.58 (s, 1H), 7.47 (d, 2H), 7.14 (d, 2H), 5.77 (s, 1H), 5.42 (s, 1H), 2.56 (t, 2H), 2.04 (s, 3H), 1.58 (d, 2H) 1.26 (s, 6H), 0.88 (s, 3H).

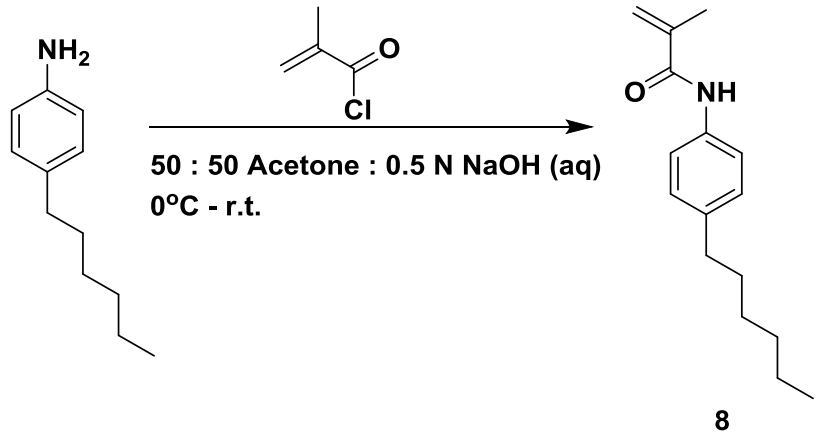

Figure 3.3 Synthesis of 4HPhMA (**8**, Figure C.8).

3.3.4 Synthesis of Methacryloyl Sulfacetamide (mSAC).

Using a similar procedure previously outlined,[44] mSAC was synthesized (Figure 3.4). Sulfacetamide (40.0 mmol) was dissolved in 160 mL of a 1:1 (v:v) mixture of acetone and 0.5 N aqueous NaOH and stirred while cooling in an ice bath. Methacryloyl chloride (4.10 mL, 42.0 mmol) was then added dropwise over 30 min followed by removing the flask from the ice bath and stirring the reaction at room temperature for an additional 60 min. The acetone was removed via rotary evaporation, followed by adjusting the solution to pH = 2 with 12 N HCl. The resulting solids were isolated using vacuum filtration and washed with 100 mL of dilute HCl (0.01 N) prior to drying under vacuum for 48 h, yielding the desired monomer as a white powder. Yield: 10.29 g, 91%; mp 203−205 °C; 1H NMR (300 MHz, DMSO-d6): δ 11.99 (s, 1H), 10.20 (s, 1H), 8.11−7.65 (m, 4H), 5.84 (s, 1H), 5.58 (s, 1H), 1.93 (s, 3H), 1.89 (s, 3H).

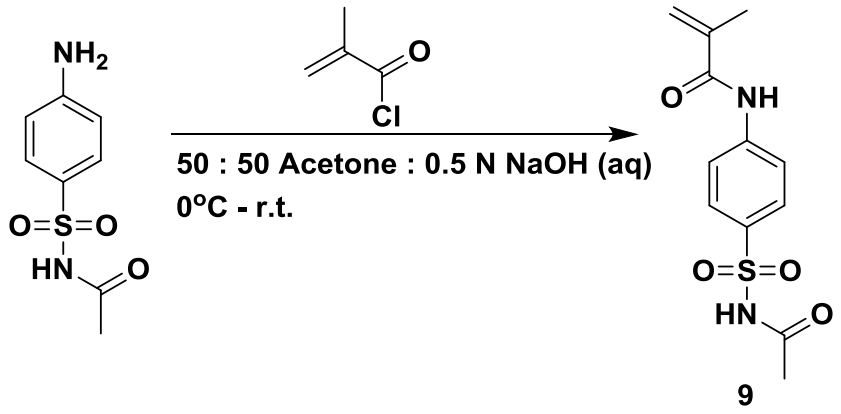

Figure 3.4 Synthesis of mSAC (**9**, Figure C.9).

3.3.5 Synthesis of Methacryloyl Sulfamethazine (mSMZ).

Using a similar procedure previously outlined,[44] mSMZ was synthesized (Figure 3.5). Sulfamethazine (30.5 g, 109.5 mmol) was dissolved in 500 mL of a 1:1 (v:v) mixture of acetone and 0.5 N aqueous NaOH and stirred while cooling in an ice bath. Methacryloyl chloride (14.4 g, 137.7 mmol) was then added dropwise over 30 min followed by removing the flask from the ice bath and stirring the reaction at room temperature for an additional 60 min. The acetone was removed via rotary evaporation, followed by adjusting the solution to pH = 2 with 12 N HCl. The resulting solids were isolated using vacuum filtration and washed with 100 mL of dilute HCl (0.01 N) prior to drying under vacuum for 48 h, yielding the desired monomer as a white powder. Yield: 35.87 g, 96%; mp 203−205 °C; 1H NMR (300 MHz, DMSO-d6): δ 11.58 (s, 1H), 10.09 (s, 1H), 7.98−7.80 (m, 4H), 6.73 (s, 1H), 5.81 (s, 1H), 5.54 (s, 1H), 2.22 (s, 6H), 1.91 (s, 3H).

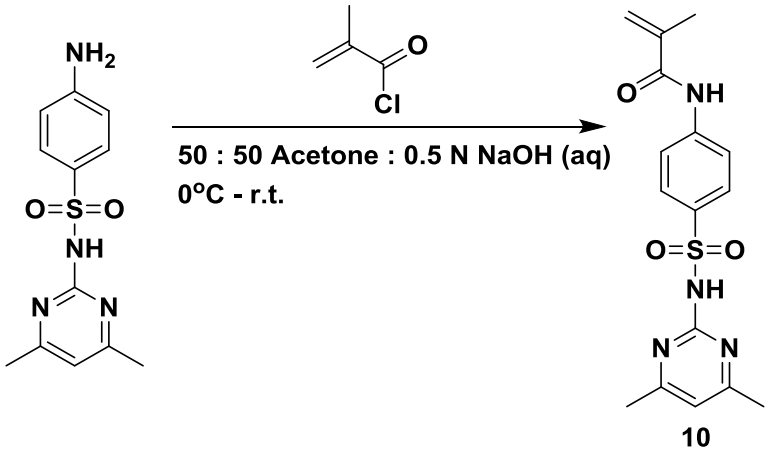

Figure 3.5 Synthesis of mSMZ (**10**, Figure C.10).

3.3.6 Statistical Copolymerization of 4HPhMA and mSAC via RAFT.

A representative copolymerization procedure for preparing the amphoteric copolymers is as follows: 4HPhMA (0.279 g, 1.13 mmol), mSAC (2.89 g, 10.23 mmol), CEP (7.86 mg, 0.006 mmol), DMF (15 mL), and V-70 (1.8 mg, 0.007 mmol) with the molar ratios of $[4HPhMA]_0$:$[mSAC]_0$:$[CEP]_0$:$[V\text{-}70]_0$ equal to 38:340:1.0:0.2. Trimesic acid (50 mg) was added as an internal standard. The flask was then sealed and purged with ultra-high purity N_2 for 60 min in an ice bath. An initial aliquot of 200 μL was taken prior to commencing the polymerization at 30°C in an oil bath while stirring. After the desired polymerization time of 24 hours, an aliquot was taken and analyzed by ^{1}H NMR (DMSO-d_6) to determine monomer conversion by comparing the relative integral areas of the trimesic acid aromatic protons (8.64 ppm, 3H) to the monomer vinyl proton (5.84 ppm, 1H). SEC-MALLS (5% AcOH, 0.02M LiBr in DMF) was used to monitor the molecular weight and dispersity (Đ) of each polymerization. Polymers isolated for solubility studies were purified by precipitating the reaction mixture into a 10-fold excess

of MeOH, followed by isolating the resulting solids by ultracentrifugation. The isolated polymers were then precipitated three times from DMF into MeOH. The resulting solids were removed by vacuum filtration before drying overnight in vacuo.

3.3.7 Dissolution of the amphoteric sulfonamide copolymers.

Based on the molar equivalents of sulfonamide monomer in the mSAC (A) and mSMZ (B) series, a 1.25 molar excess of sodium hydroxide was added to the aqueous polymer solutions to deprotonate the sulfonamide units and ensure sample dissolution. For example, a 250 mg sample of the A10 containing 0.971 mmol of -SO_2NH- was solubilized with 1.21 mmol of NaOH into 10 mL of DI water. The sample was then diluted in a volumetric flask to 25 mL to prepare a 10 mg/mL stock solution (pH ~ 12) for characterization experiments. Sequential dilutions from the stock solution were utilized to prepare concentrations of 0.1, 0.5, 1.25, 2.5, 3.75, 5, 7.5, and 10 mg/mL.

3.3.8 Pyrene absorbance/fluorescence studies.

The extent of pyrene uptake and the environment of the micelle core domains in series A and B were studied using UV-Vis and fluorescence spectroscopy. Into each well of a 96-well plate was added 5 μL of a 50 mg/mL stock solution of pyrene in acetone. The acetone was then evaporated and 0.5 mL of the desired polysoap solution subsequently added. The well plate was covered and placed on a shaker for 24 hours to allow the solutions to equilibrate. Then, 200 μL of the polysoap/pyrene solution from each well was transferred to a second 96-well plate for analysis via UV-Vis absorbance and fluorescence spectroscopy with a TECAN Safire spectrometer.

3.3.9 Absorbance and turbidimetric titration experiments.

Into a 50 mL centrifuge tube was added 50 μL of a 50 mg/mL stock solution of pyrene in acetone. The acetone was then allowed to evaporate and 5 mL of a 10 mg/mL polysoap solution (pH ~ 12) was added to the tube and the contents placed on the shaker for 24 hours. The contents of the tube were then centrifuged to remove residual pyrene, and the solution subsequently transferred to a 20 mL scintillation vial. While stirring, the solution was titrated with 0.01N HCl at 10 μL increments. % transmittance and pyrene absorbance were measured as a function of pH via UV-Vis spectroscopy.

3.3.10 Turbidity measurements during CO_2/N_2 entrainment cycles.

To a disposable 50 mL centrifuge tube, 10 mL of polysoap solution (10 mg/mL, pH ~ 12) was added along with a stir bar. The initial % transmittance was measured for the samples. The solution was then purged with CO_2, allowing sufficient time for the solution to become turbid for subsequent measurement of % transmittance. The sample was then purged with N_2 for a selected period of time; % transmittance was again measured. The procedure was repeated for multiple cycles.

3.3.11 Remediation of 9-anthracenemethanol from water.

The following procedure was utilized to determine behavior of B10 and B20 in multiple cycles of remediation of water containing 9-anthracenemethanol (9-AM): To a 1.5 mL microcentrifuge tube was added 10.3 mg of polymer, 1 mL of 0.1 mM 9-AM in water, and 200 uL of 0.2 N NaOH. After vortexing, the contents were equilibrated while shaking for 30 mins. The resulting solution (pH ~ 12) was centrifuged at 10,000 rpm and the absorbance was measured at 388 nm. The solution was then sparged with CO_2 for 3 mins, followed by centrifugation at 10,000 rpm for 10 mins. The supernatant was

removed, and the absorbance value measured at 388 nm. A new 1 mL aliquot of 0.1 mM 9-AM solution and 200 μL of 0.2 N NaOH was added to the centrifuged pellet, allowing it to re-dissolve while vortexing for 30 minutes.

3.3.12 Calculating the 9-AM uptake capacity for B10 and B20.

To determine the uptake capacity for amphoteric polysoaps B10 and B20, the number of moles of polymer was first calculated for each initial solution during the 9-AM remediation experiments ($1.53x10^{-7}$ and $2.28x10^{-7}$ moles, respectively). Then the number of moles of 9-AM at the saturation limit was calculated ($7.0x10^{-7}$ and $12.0x10^{-7}$ moles for B10 and B20, respectively). These values were then used to determine the moles of 9-AM per a mole of copolymer chains. When converted to molecules of each species using Avogadro's number, the result is molecules of 9-AM per a polymer chain (4.5 and 5.2, for B10 and B20, respectively).

3.3.13 Characterization.

Dynamic light scattering (DLS) measurements were conducted at 633nm utilizing a Research Electro Optics HeNe laser operating at 40mW. The time-dependent scattering intensities were measured with a Brookhaven Instruments BI-200SM goniometer at 60, 75, 90, 105, and 120 degrees with an avalanche photodiode detector and TurboCorr correlator.

Gel permeation chromatography (GPC) was performed using a Viscotek TDA 302 equipped with a triple detector array of RI, low, and right-angle light scattering and viscosity detectors. The GPC system was equipped with Tosoh TSKgel Super AW guard column, Super AW3000, and Super AW4000 columns in series. The eluent used for the sulfonamide polysoaps was 5% AcOH, 0.02M LiBr in DMF.

UV-Vis spectroscopy and fluorescence spectroscopy for pyrene absorbance and fluorescence were measured with a TECAN Safire 96-well plate spectrometer running on integrated Microsoft Excel software. Absorbance was measured at 341 nm and fluorescence was measured via emission scan from 350 to 550 nm with an excitation wavelength of 341 nm. For the pH titrations, CO_2-reversibility, and hydrocarbon removal experiments, percent transmittance and absorbance were determined using an Agilent Technologies Carey Series UV-Vis-NIR Spectrophotometer run with Carey WinUV software.

3.4 pH-Responsive sulfonamide-based polysoaps via RAFT copolymerization for oil remediation and recovery (Appendix A).

3.4.1 Materials.

Methacryloyl chloride (Aldrich, 97%) was distilled under vacuum and stored under N_2 at −10 °C prior to use. The RAFT agent precursors; ethanethiol (Sigma Aldrich, 98%), carbon disulfide (Sigma Aldrich, 99.9%), and 4,4′-Azobis(4-cyanopentanoic acid) (V-501) were used as received. The solvents; diethyl ether (Fisher Scientific, Spectranalyzed), pentane (Fisher Scientific, HPLC grade), and acetone (Sigma Aldrich, anhydrous) were used as received. N, N′-Dimethylformamide from Acros (extra dry with sieves) was stirred under vacuum at room temperature for 60 min prior to use to remove traces of dimethylamine. The initiator (96%) 2,2′-Azobis(4-methoxy-2,4-dimethylvaleronitrile) (V-70, 6, Figure C.6) was purchased from Wako and stored in a sealed container at -10°C. The hydrophilic sulfonamide precursor (>97%) sulfacetamide (SAC) was purchased from Sigma-Aldrich and (99%) sulfamethazine (SMZ) from Acros Organics. The internal standard of (96%) trimesic acid was purchased from Sigma-Aldrich and used as received. The 0.1 N NaOH (Fluka Analytical, standardized) and 0.05 N HCl (Alfa Aesar, standardized) solutions were both purchased and used as received.

3.4.2 Synthesis of 4-cyano-4-(ethylsulfanylthiocarbonyl)sulfanylpentanoic acid (CEP).

Please see Section 3.3.2 for the synthetic procedure of CEP (**7**).

3.4.3 Synthesis of Methacryloyl Sulfacetamide (mSAC).

Please see Section 3.3.4 for the synthetic procedure of mSAC (**9**).

3.4.4 Synthesis of Methacryloyl Sulfamethazine (mSMZ).

Please see Section 3.3.5 for the synthetic prodedure of mSMZ (**10**).

3.4.5 Statistical copolymerization of mSAC and mSMZ via RAFT.

The general procedure is as follows. The mSAC, mSMZ, CEP, and V-70 with desired feed ratio were added to a 25 mL polymerization flask equipped with a magnetic stir bar. For example, mSAC (0.279 g, 1.13 mmol), mSMZ (2.89 g, 10.23 mmol), CEP (7.86 mg, 0.006 mmol), DMF (15 mL) and V-70 (1.8 mg, 0.007 mmol) with the molar ratios of mSMZ : mSAC : CEP : V-70 = 71 : 641 : 1 : 0.2. Trimesic acid (50 mg) was added as an internal standard. The flask was then sealed and purged with ultra-high purity N_2. After purging with N_2 for 60 mins, an initial aliquot of 200 μL was taken prior to commencing the polymerization at 30°C in an oil bath while stirring. After the desired polymerization time of 24 hours, an aliquot was taken and analyzed by 1H NMR (DMSO-d6) to determine monomer conversion by comparing the relative integral areas of the trimesic acid aromatic protons (8.64 ppm, 3H) to the monomer vinyl proton (5.84 ppm, 1H). An SEC-MALLS instrument (95% DMF/5% CH_3COOH, 20 mM LiBr) was used to monitor the molecular weight and molecular weight distribution (Mw/Mn) of each polymerization. The polymer was purified using dialysis against water followed by isolation via lyophilization. The polymer was a fluffy white solid.

3.4.6 Preparation of polysoap solutions.

Polysoap solutions were prepared via sequential dilution in an aqueous 20 mM phosphate buffer composed of sodium phosphate monobasic and sodium phosphate dibasic. The pH of the phosphate buffer was measured to ensure the desired pH of 6.5. All solutions were vortexed before further dilution and an automatic micropipette was

used to ensure precision. Polysoap solutions with concentrations of 0.1, 0.5, 1.0, 2.5, 3.75, 5.0, 7.5, and 10mg/mL in an aqueous phosphate buffer at pH 6.5 were prepared.

3.4.7 Pyrene uptake into the core domains of the polysoaps.

To study the uptake characteristics of the polysoaps, the following procedure was used for a single trial. To a single 1.5 mL centrifuge was added 10 μL of 50 mg/mL pyrene solution in acetone. The acetone was evaporated leaving the pyrene behind. Into the centrifuge tube was then added the desired polysoap solution in water (1.5 mL). The contents were vortexed and allowed to shake for 24 hours for the solution to equilibrate. Then the solution was centrifuged, and 1 mL of the polysoap/pyrene solution was transferred to another centrifuge tube prior to measurement via UV-Vis spectroscopy and fluorescence spectroscopy.

3.4.8 Light scattering titration experiments.

The following procedure was performed for each polysoap sample to determine the light scattering intensity and hydrodynamic diameter as a function of pH for a 10 mg/mL sample: To a light scattering test tube was added 1.5 mL of the desired polysoap solution that was filtered through a 0.45 μm PVDF syringe filter. The pH was measured, and static and dynamic light scattering was performed on the sample. The sample was then titrated with minimal 0.1 M HCl (10-50 μL) to slightly lower the pH of the solution. The sample was again filtered into a new light scattering test tube using a 0.45 μm PVDF syringe filter and measured via static and dynamic light scattering.

3.4.9 Hydrocarbon removal and polysoap recovery experiment.

The following procedure was performed for each polysoap. An aqueous solution of 0.1 mM 9-anthracenemethanol was used to prepare 5mL of a 5mg/mL solution of each

copolymer. The solutions were titrated to pH 6.5 and shaken overnight to allow for hydrocarbon uptake. Afterwards, UV-Vis was performed on the solutions. Then, the solutions were titrated again to a pH of 2.5. The samples were then centrifuged, and UV-Vis was performed on the resulting supernatant. The supernatant was then returned to the polymer pellets and titrated to a pH of 10. 1 mL of ether was introduced and an extraction was performed on the solutions. Afterwards, the ether was removed and UV-Vis was performed on both the ether and aqueous layers.

3.4.10 Characterization.

Dynamic light scattering (DLS) measurements were collected using incident light at 633nm from a Research Electro Optics HeNe laser operating at 40mW. The time-dependent scattering intensities were measured from a Brookhaven Instruments BI-200SM goniometer at 60, 75, 90, 105, and 120 degrees with an avalanche photodiode detector and TurboCorr correlator. The decay rate was collected from a quadratic fit of the autocorrelation function. The data was processed using Mathcad with the following steps. Decay rate was plotted versus q^2 to generate a straight line. The slope of the line is the diffusion coefficient. The diffusion coefficient was then used in the Stokes-Einstein equation to calculate a hydrodynamic radius of the particles. The radius was multiplied by two to produce the hydrodynamic diameter which was reported for the DLS experimental data. Example data processing in the appendix.

Gel permeation chromatography (GPC) was performed using an assembled instrument with a Hewett Packard Series 1100 HPLC pump in line with a Viscotek T60A Dual Detector and a Viscotek VE3580 IR detector. The GPC system was equipped with Tosoh TSKgel Super AW guard column, Super AW3000, and Super AW4000 columns in

series. The eluent used for the sulfonamide polysoaps was0.2 M $NaHCO_3$ / Na_2 CO_3 Buffer at pH 9.0 in water with 0.02 M LiBr. The SEC software used to process the data was OmniSEC version 4.7.

UV-Vis spectroscopy measurements were conducted with an Agilent Technologies Carey Series UV-Vis-NIR Spectrophotometer run by Carey WinUV software. Steady state fluorescence measurements were recorded using a PTI-Horiba QuantaMaster 400 spectrofluorimeter equipped with a 75 W Xe arc lamp.

3.5 Biocompatible, responsive "polysoaps" via RAFT copolymerization for the delivery of hydrophobic cancer drugs (Appendix B).

3.5.1 Materials.

The monomer precursors; D,L-1-amino-2-propanol (TCI, 98%), sodium methanesulfinate (AK Scientific, 92%), sulfur (Sigma Aldrich, 100 mesh), bromo propylamine hydrobromide (AK Scientific, 98%), and dodecanethiol (Sigma Aldrich, 98%) were used as received. Methacryloyl chloride (Aldrich, 97%) was distilled under vacuum and stored under N_2 at −10 °C prior to use. The RAFT agent precursors; ethanethiol (Sigma Aldrich, 98%), carbon disulfide (Sigma Aldrich, 99.9%), and 4,4′-Azobis(4-cyanopentanoic acid) (V-501) were used as received. The solvents; diethyl ether (Fisher Scientific, Spectranalyzed), pentane (Fisher Scientific, HPLC grade), acetone (Fisher Scientific, Optima grade), anhydrous methanol (Sigma Aldrich), and 200 proof ethanol (Decan Laboratories, anhydrous) were used as received. The initiator (96%) 2,2′-Azobis(2-methylpropionitrile) (AIBN, **2**, Figure C.2) was purchased from Sigma Aldrich and recrystallized from methanol prior to use. The internal standard of trioxane was purchased from Sigma-Aldrich and used as received. The detailed synthesis of the RAFT chain transfer agent 4-cyano-4-(ethylsulfanylthiocarbonylsulfanyl)pentanoic acid (CEP, **7**, Figure C.7) and monomers N-(2-hydroxypropyl)methacrylamide (HPMA, **11**, Figure C.11) and (dodecylpropyldisulfide)methacrylamide (DPDMA, **12**, Figure C.12) are described below.

3.5.2 Synthesis of 4-cyano-4-(ethylsulfanylthiocarbonyl)sulfanylpentanoic acid (CEP).

Please see Section 3.3.2 for the synthetic procedure of CEP (**7**).

3.5.3 Synthesis of N-(2-hydroxypropyl)methacrylamide (HPMA).

The synthesis of HPMA is as follows (Figure 3.6). To a 2-L round bottom flask was added D,L-1-amino-2-propanol (102.307 g) dissolved in 1 L of MeCN. A stir bar was added, and the round bottom was sealed with a septum and placed into an ice bath. To the reaction mixture was added methacryloyl chloride (67.80 g) dropwise over 3 hours. The round bottom was then removed from the ice bath and allowed to reach room temperature, and then the contents were stirred for an additional 2 hours. Solvent was removed via rotary evaporation at 30 ^{o}C. After 2/3 of the solvent had been removed, a white crystalline salt had formed. The salt isolated via vacuum filtration and purified by recrystallization from minimal acetone at room temperature. The resulting product was white crystals. mp: 65-67 °C; ^{1}H NMR (300 MHz, D_2O): δ 6.60 (b, 1H), 5.70 (s, 1H), 5.30 (s, 1H), 3.90 (b, 1H), 3.70 (d, 1H), 3.10-3.60 (m, 2H), 1.9 (s, 3H), 1.2 (d, 3H).

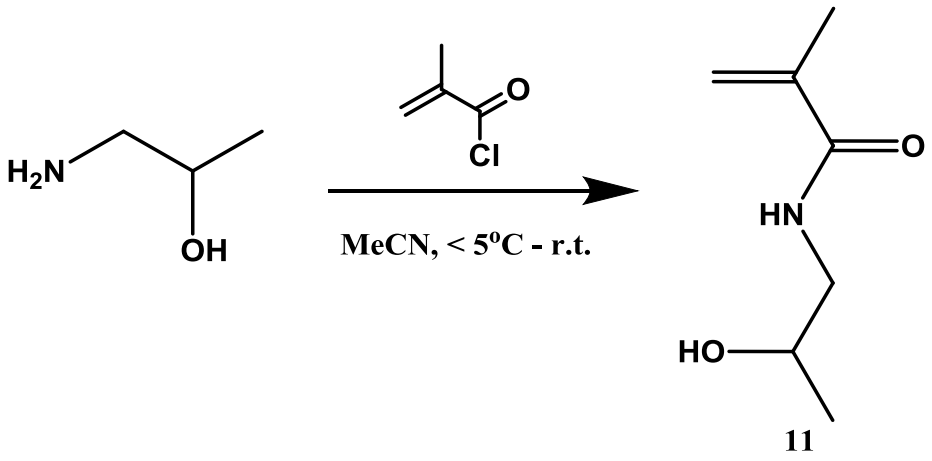

Figure 3.6 Synthesis of HPMA (**11**, Figure C.11).

3.5.4 Synthesis of (dodecylproplydisulfide) methacrylamide (DPDMA).

The synthesis of DPDMA is as follows (Figure 3.7). A mixture of sodium methanesulfinate (10 g, 98 mmol) and sulfur (3.14 g, 98 mmol) in dry methanol (1.2 L) was heated to reflux using a heating manifold (set voltage to 50 V) and a condenser (with drying tube inserted into a rubber septum). After 18 hours, the sulfur had dissolved, and the reaction was stopped. The solvent was removed by rotary evaporation leaving behind an off-white residue. To the residue was added 500 mL of 200 proof ethanol to dissolve the desired product. After stirring for 1 hour, not all the solids dissolved, and the solution was filtered via vacuum filtration. The filtrate was then concentrated by rotary evaporation and the product was dried under high vacuum for 4 hours resulting in a white powder, sodium methanethiosulfonate. To a round bottom flask containing water (150 mL), bromo propylamine hydrobromide (5.04 g, 23.0 mmol) and sodium methanethiosulfonate (6.01 g, 44.8 mmol) were added. The mixture was stirred at 70 °C for 18 hours. The reaction was then removed from the heat and the solvent was removed via rotary evaporation leaving an off-white powder. The crude powder was then suspended in ethanol while vortexing, at which point the solution became light yellow and the powder became white as impurities dissolved. The product was then collected via vacuum filtration and washed with ethanol followed by drying overnight on high vacuum. The pure product was a white powder, aminopropyl sodium methanethiosulfonate. Aminopropyl sodium methanethiosulfonate (11.25 g, 54.6 mmol) was dissolved in dry methanol (200 mL) and dodecanethiol (80 mL, 332 mmol) was added and the solution was stirred for 18 hours at room temperature. The contents of the reaction were then transferred to a separatory funnel. The excess dodecane thiol was the

bottom layer and methanol the top layer. The dodecane thiol was removed from the methanol and then hexanes were added to the separatory funnel to wash the methanol layer. The product remained in the bottom methanol layer. The methanol layer was removed and concentrated using rotary evaporation leaving a white powder. The product was then washed with hexanes and collected via vacuum filtration and then dried via high vacuum. The product was further purified via column chromatography on silica gel using chloroform with 3% TEA as the eluent. After the product was isolated it was a white powder, aminopropyl dodecyl disulfide. Aminopropyl dodecyl disulfide (14.0 g, 43.0 mmol) was added to a round bottom flask. To the flask was then added 300 mL of acetone and triethylamine (15.0 mL). The flask was charged with a stir bar, sealed with a rubber septum, and then placed in an ice bath. Methacroylchloride (7.0 mL, 71.6 mmol) was then added dropwise while stirring in the ice bath. The vessel was then removed from the ice bath and allowed to reach room temperature and the reagents stirred for an additional 18 hrs. A white precipitate had formed after adding the methacroylchloide and it was removed via vacuum filtration. The supernatant was then collected and removed via rotary evaporation leaving a brownish orange oil. The crude product was then purified via column chromatography using $CHCl_3$ as the eluent. The pure product was isolated and dried under high vacuum resulting in a white powder, (dodecylpropyldisulfide) methacrylamide. Yield: 4.0 grams (25%); mp: 41-43 °C; ^{1}H NMR (300 MHz, CDCl3): δ 5.98 (s, 1H), 5.70 (s, 1H), 5.30 (s, 1H), 3.45 (q, 2H), 2.70 (q, 4H), 1.98 (b, 5H), 1.65, (m, 2H), 1.25 (b, 18H), 0.80 (t, 3H).

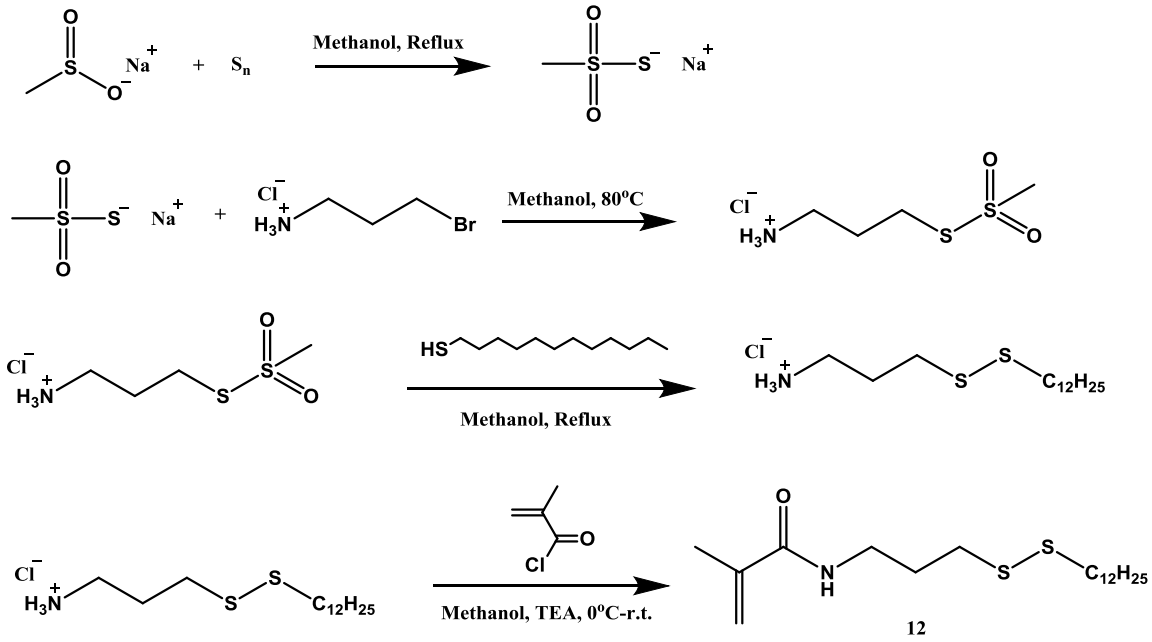

Figure 3.7 Synthesis of DPDMA (**12**, Figure C.12).

3.5.5 Statistical copolymerization of HPMA and DPDMA via RAFT.

The general procedure is as follows. The HPMA, DPDMA, CEP, and AIBN with desired feed ratio were added to a 25 mL polymerization flask equipped with a magnetic stir bar. For example, HPMA (2.83 g, 19.9 mmol), DPDMA (0.377 g, 1.05 mmol), CEP (6.50 mg, 24.7 μmol), MeOH (20 mL) and AIBN (0.811 mg, 4.94 μmol) with the molar ratios of HPMA : DPDMA : CEP : AIBN = 950 : 50 : 1 : 0.2. Trioxane (250 mg) was added as an internal standard. The flask was then sealed and purged with ultra-high purity N_2. After purging with N_2 for 60 mins, an initial aliquot of 200 μL was taken prior to commencing the polymerization at 70 °C in an oil bath while stirring. After the desired polymerization time of 48 hours, an aliquot was taken and analyzed by ^{1}H NMR (MeOH-d4) to determine monomer conversion by comparing the relative integral areas of the signal from the trioxane protons to that of the monomer vinyl protons. An SEC-MALS

instrument (eluent of 0.2 M $LiClO_4$ in MeOH) was used to monitor the molecular weight and molecular weight distribution (M_w/M_n) of each polymerization. The polymer was purified via precipitation from acetone and isolated via centrifugation. The polymer pellet was then washed with acetone five times, followed by drying overnight under vacuum to yield a white powder. The final product was analyzed by ^{1}H-NMR in MeOH-d4 (Figures A7 and A8).

3.5.6 Preparation of polysoap solutions.

Polysoaps were solubilized in DI water, followed by sonication, vortexing, and shaking for 48 hours. Solutions were prepared via serial dilutions, using an automatic micropipette and 25 mL volumetric flasks for precision. This yielded solutions with concentrations of 0.1, 0.5, 1.0, 3.75, and 5.0 mg/mL in deionized water.

3.5.7 Pyrene uptake into the core domains of the polysoaps.

To study the uptake characteristics of the polysoaps, the following procedure was used for a single trial. To a single 1.5 mL centrifuge tube was added 10 μL of 50 mg/mL pyrene solution in acetone. The acetone was evaporated leaving the pyrene behind. Into the centrifuge tube was then added the desired polysoap solution in water (1.5 mL). The contents were vortexed and allowed to shake for 24 hours for the solution to equilibrate. Then the solution was centrifuged, and 1 mL of the polysoap/pyrene solution was transferred to another centrifuge tube prior to measurement via UV-Vis spectroscopy and fluorescence spectroscopy.

3.5.8 Hydrocarbon retention and release experiments.

Hydrocarbon retention in water was performed using the following procedure. Into a 1.5 mL centrifuge tube was added 1 mL of 5 mg/mL polysoap solution. The

solution was prepared using 0.1 mM 9-anthracenemethanol. The contents of the centrifuge tube were allowed to equilibrate over 24 hours. Then the solution was transferred to a dialysis bag (molecular weight cutoff of 1,000 g/mol). The bag with the solution was then dialyzed against DI water. An initial aliquot was taken for UV-Vis spectroscopy followed by sampling and measurement at desired times. Each aliquot was returned to the dialysate after measurement. After several measurements, 50 mmol of glutathione was added to the dialysate and aliquots were taken and measured via UV-Vis spectroscopy.

The following procedure was used for the hydrocarbon release experiment. To a 50 mL centrifuge tube was added 5 mL of 5 mg/mL polysoap solution. The solution was prepared using 0.1 mM 9-anthracenemethanol. The contents of the centrifuge tube were allowed to equilibrate over 24 hours. Ethyl acetate (5 mL) was added to the centrifuge at the start of the experiment. An initial aliquot of the ethyl acetate was taken for UV-Vis spectroscopy followed by sampling and measurement of the ethyl acetate layer at desired times. Each aliquot was returned to the centrifuge tube after measurement. After several measurements, 50 mmol of glutathione was added to the centrifuge tube and aliquots were taken and measured via UV-Vis spectroscopy.

3.5.9 Cell toxicity experiment.

To determine cell toxicity of the polysoaps, a standard MTT cell assay was conducted. Cells (10,000 cells per mL, 100 μL) were seeded in a 96 well plate (Corning Inc.). Cells were treated with 10 μL of a polymer stock solution (50, 25, 10, and 5 μg/mL). Cell proliferation was determined via a standard MTT assay (Vybrant MTT Cell Proliferation Assay Kit; Invitrogen). Cells were incubated for 24 hours prior to adding 10

μL of a 12 mM MTT reagent to each well. The cells were further incubated for an additional 4 hours, followed by adding 100 μL of a SDS (10%)/HCl (0.01 M) solution to each well. The absorbance was then determined utilizing a Biotek Synergy2 MultiMode Microplate Reader. All studies were performed in triplicate.

3.5.10 Characterization.

Dynamic light scattering (DLS) data were collected using incident light at 633nm from a Research Electro Optics HeNe laser operating at 40 mW. The time-dependent scattering intensities were measured with a Brookhaven Instruments BI-200SM goniometer at 60, 75, 90, 105, and 120 degrees with an avalanche photodiode detector and TurboCorr correlator. The decay rate was collected from a quadratic fit of the autocorrelation function. The data was processed using Mathcad with the following steps. Decay rate was plotted versus q^2 to generate a straight line. The slope of the line is the diffusion coefficient. The diffusion coefficient was then used in the Stokes-Einstein equation to calculate hydrodynamic radius of the particles. The radius was multiplied by two to produce the hydrodynamic diameter which was reported for the DLS experimental data. An example of the DLS data processing can be found in the appendix.

Gel permeation chromatography (GPC) was performed using an assembled instrument with a Hewett Packard Series 1100 HPLC pump in-line with a Viscotek T60A Dual Detector and a Viscotek VE3580 IR detector. The GPC system was equipped with Tosoh TSKgel Super AW guard column, Super AW3000, and Super AW4000 columns in series. The eluent used for the polysoap was 0.2 M $LiClO_4$ in MeOH. The SEC software used to process the data was OmniSEC version 4.7.

UV-Vis spectroscopy measurements were conducted with an Agilent Technologies Carey Series UV-Vis-NIR Spectrophotometer run by Carey WinUV software. Steady-state fluorescence measurements were recorded using a PTI-Horiba QuantaMaster 400 spectrofluorimeter equipped with a 75 W Xe arc lamp.

CHAPTER IV – RESULTS AND DISCUSSION

4.1 Structurally controlled "polysoaps" via RAFT copolymerization of AMPS and n-doedcyl acrylamide for environmental remediation.[128]

4.1.1 Overview.

In this section, the synthesis and physical characterization of copolymers that self-assemble into polymeric micelles are presented. These amphiphilic systems are designed for dispersion and subsequent remediation of spilled oil in salt water (brine). These copolymers, which fall under the "polysoap" sub- category, have been synthesized for the first time to our knowledge in a controlled fashion utilizing RAFT copolymerization. This experimental design of single or unimeric micelle assemblies draws heavily from the extensive research of Morishima, Francoise Winnik, and others referenced in the introduction. Controlled radical polymerization (RAFT) techniques and conditions previously developed in our laboratories are utilized to prepare a range of statistical copolymers from 2-acrylamido-2-methylpropanesulfonic acid (AMPS) and n-dodecyl acrylamide (DDAM). Precise control over composition, Mw, and PDI afforded by RAFT should allow a more complete interpretation of surface tension, association, and sequestration properties which depend on segmental chain length. The ultimate objective of this research is to prepare unimolecular micelles capable of efficient capture and eventual *in situ* remediation of oil. In this case, each polymeric surfactant forms its own micelle, circumventing inherent dissociation (and release of dispersed oil) experienced by small molecule surfactants diluted below their CMC. Efficient oil sequestration by unimolecular micelles of defined structure should, in principle, allow natural bacterial

remediation of entrapped oil in the marine environment and potentially prevent the re-deposition of emulsified oil (Scheme 4.1).

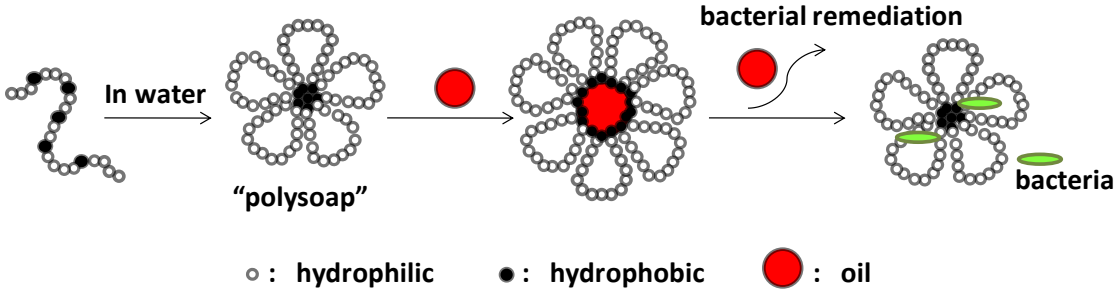

Scheme 4.1 Unimeric micelles capable of oil sequestration and subsequent bacterial remediation.

4.1.2 Structural design and synthesis of the poly(AMPS-stat-DDAM) series.

Sodium dodecyl sulfate (SDS) is one of the most widely used small molecule detergents with demonstrated oil dispersing capability above its critical micelle concentration in water of 8.2 mM.[129,130] Analogous side-chain polysoaps were prepared via statistical controlled radical polymerization of the hydrophilic monomer 2-acrylamido-2-methylpropane sulfonic acid, AMPS, and the hydrophobic monomer n-dodecyl acrylamide, DDAM. A range of copolymer compositions (10, 20, 30, 40, 50, and 60 mol % DDAM) was targeted, keeping constant the number of AMPS units and varying the DDAM units in the feed as shown in Table 4.1. In order to control molecular weight and molecular weight distribution, these copolymerizations were conducted via RAFT at 60^{o}C under homogeneous conditions in DMF utilizing DMP as the chain transfer agent (Scheme 4.2).

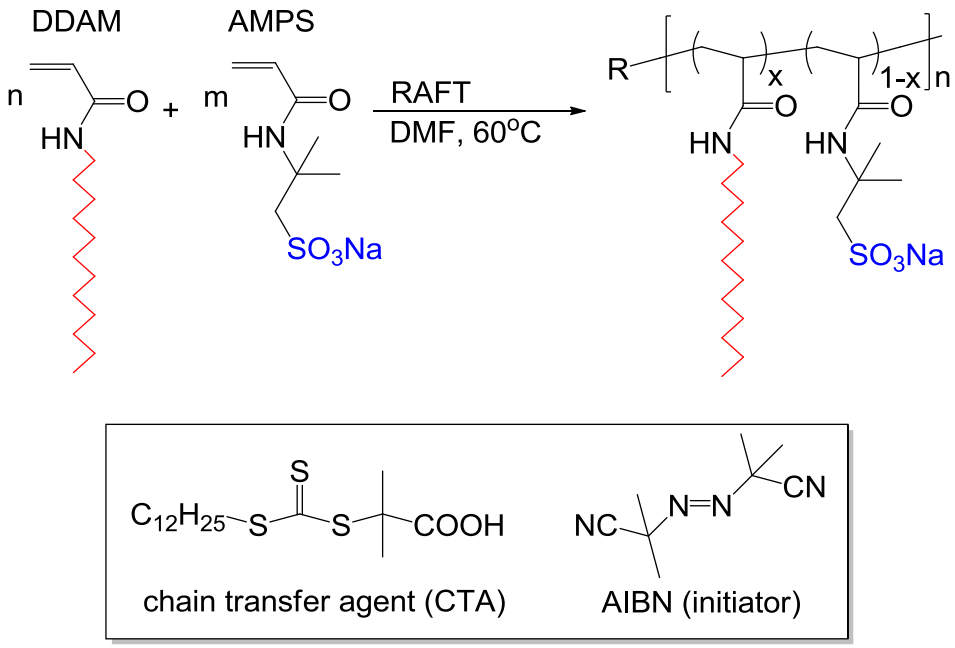

Scheme 4.2 Statistical copolymerization of AMPS and DDAM via RAFT in DMF.

The monomer AMPS was chosen for its ability to remain permanently water soluble even at low pH values and at moderate salt concentrations. The monomer DDAM, a C-12 substituted acrylamide, possesses the same hydrophobic group as SDS.[131–133] The amide groups on both monomers and on their respective statistical copolymers are resistant to hydrolysis.[131–134] When the resulting amphiphilic copolymers self-assemble into micelles in water, the DDAM will form the core of the micelle and the AMPS will reside in the corona, stabilizing the micelle in aqueous solution. To verify the hydrophobic content and chemical structure of the amphiphilic copolymers, ^{1}H-NMR was used. As an example, the ^{1}H-NMR of the amphiphilic copolymer with 40% hydrophobic content (PS40) is shown in Figure 4.1. Ratios of the integrated signals corresponding to the protons alpha to the sulfonate functionality in AMPS at 3.1-3.5ppm (corrected for the overlapping solvent peak) and those of the terminal CH_3 protons in

DDAM at 0.9ppm were compared to calculate the molar compositions of the respective copolymers. These values of mol % incorporation of DDAM shown in Table 4.1 agree well with the respective molar feed compositions.

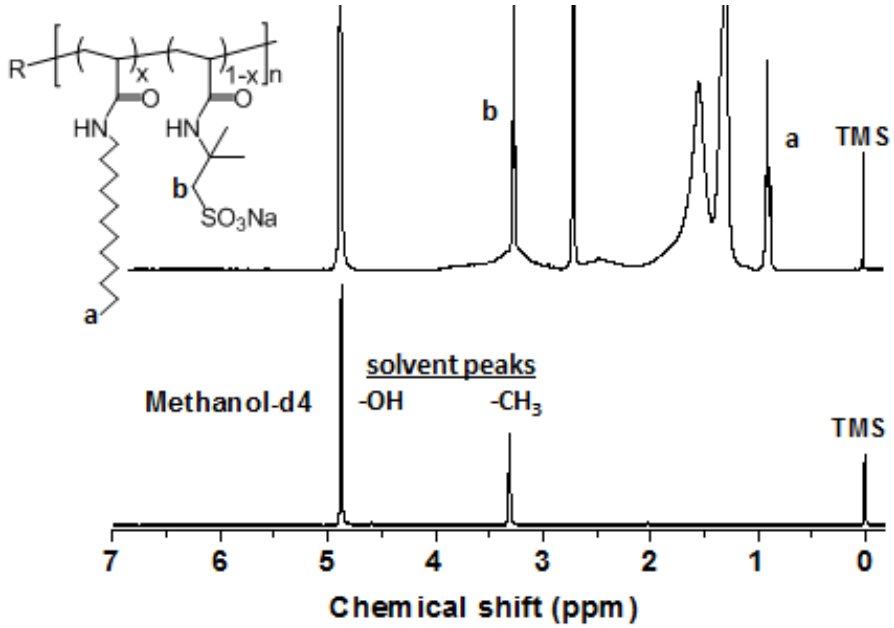

Figure 4.1 ^{1}H NMR spectrums of Methanol-d_4 and poly(AMPS-stat-DDAM) with 40% of hydrophobic monomer content (PS40) in Methanol-d_4.

Table 4.1 Compositional and structural data for the poly(AMPS-stat-DDAM) series.

Sample	Feed composition [a]	Conversion [b]	DDAM content [c]	$M_{n,\,exp}$ / kDa [d]	$M_{n,\,theo}$ / kDa	PDI [d]
PS10	50 : 450: 2: 1	81%	11%	51.2	48.7	1.07
PS20	113: 450: 2: 1	89%	21%	64.4	62.5	1.08
PS30	193: 450: 2: 1	85%	29%	69.2	70.7	1.10
PS40	300: 450: 2: 1	87%	42%	87.6	89.5	1.12
PS50	450: 450: 2: 1	84%	52%	107.8	104.9	1.05
PS60	675: 450: 2: 1	90%	61%	139.5	145.1	1.11
PS60a	112.5: 75: 2: 1	88%	62%	22.6	23.6	1.07

[a]Molar feed composition of DDAM: AMPS: CTA: AIBN.
[b]Determined by UV detector on GPC at the wavelength of 274 nm.
[c]Determined by ^{1}H NMR.
[d]Determined by GPC.

4.1.3 Structural control of the poly(AMPS-stat-DDAM) series.

The controlled nature of the RAFT copolymerization of DDAM with AMPS in DMF was confirmed using ^{1}H-NMR to determine monomer conversion as a function of time (kinetics) and GPC to determine Mw and PDI as a function of monomer conversion. Data for each sample of the series are listed in Table 1. As an example, for the feed composition of 30 mol% DDAM (PS30), the linear pseudo-first order kinetic plot (Figure 4.2a) indicates a constant radical concentration over the 10 hour polymerization time. A linear relationship was found between Mw and conversion with a narrowing of molecular weight distribution (Figure 4.2b) at higher conversion. As well, GPC traces shown for aliquots at 3, 5, and 10 hours (Figure 4.2c) demonstrate the evolution of molecular weight and symmetric, unimodal molecular weight distributions.

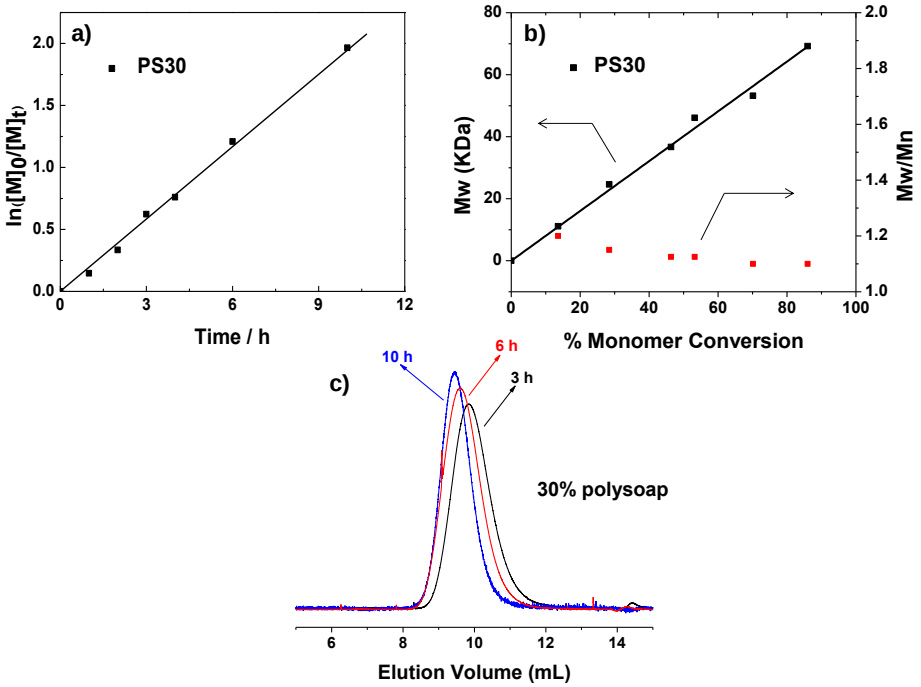

Figure 4.2 Kinetic (a), Mw and PDI vs conversion (b), and GPC (c) plots for statistical copolymerization of DDAM and AMPS at 60^{o} in DMF with DDAM:AMPS:DMP:AIBN = 193:450:2:1.

Also shown in Table 4.1, the PDI of all copolymers remain 1.12 or lower and the experimental number average Mw values closely agree with the theoretically-predicted molecular weights. It is important to note that the solubility of the amphiphilic copolymers in water not only depends on the % hydrophobic content but also on the molecular weight of the copolymer. For example, an attempt to dissolve the 60 mol % DDAM copolymer with a Mw of 139.5 KDa (Table 4.1, PS60) in water was not successful. However, given the ability to control the molecular weight with RAFT copolymerization, a lower molecular weight polymer of the same composition was synthesized with a Mw of 22.6 KDa (Table 4.1, PS60a) which was soluble in water. This single experiment shows the great advantage of utilizing CRP methods, here RAFT, as compared to conventional free radical polymerization when examining structure/behavior of amphiphilic copolymers.

4.1.4 Dynamic light scattering studies of poly(AMPS-stat-DDAM) series.

A fact well-established in the literature, dating back to the early work of Strauss, is that amphiphilic copolymer structures falling under the polysoap classification can form both unimolecular and multimolecular micelles. The transition from a single extended polyelectrolyte chain in water to one with intramolecular associations depends on the sequence distribution, compositional balance, spacing, and flexibility of the constituent charged and hydrophobic segments. With increasing concentrations both intra- and intermolecular associations of hydrophobic groups in water can occur if structurally allowed. In order to determine the nature of the RAFT-generated amphiphilic copolymer series, we first utilized dynamic light scattering (DLS) in order to assess the hydrodynamic size as a function of concentration for each copolymer in water.

The experimental data in Figure 4.3 indicate that PS10, PS20, and PS30 exhibit significant increases in D_h as the concentration increases, consistent with formation of multimolecular micelles. PS10 at 0.78 mg/mL has a D_h value of approximately 22 nm, but 50 nm at 10 mg/mL. The same trend is observed for PS20 and PS30, however, with more dramatic increases in average hydrodynamic size. These polysoaps exhibit transitions near 0.9 and 2.0 mg/ml, respectively, with nearly 30-fold increases in apparent hydrodynamic diameter at 10 mg/ml. By contrast, PS40, PS50, and PS60a with higher DDAM content have quite compact (likely unimolecular) structures in water throughout the concentration range probed. PS40 is the most collapsed, remaining at ~2 nm. PS50 and PS60a samples show compaction from 9nm and 23nm respectively to approximately 5nm over the same concentration range. It is unclear which factors are specifically responsible for the experimentally observed decreases in size for the latter two; however, the small, reproducible D_h values are consistent with assembly into stable micelles with distinct hydrophobic cores and hydrophilic coronas. This behavior is also quite consistent with the higher order self-assembly model and experimental data on related AMPS/alkyl-methacrylamide copolymers prepared by conventional free radical polymerization.[27,135]

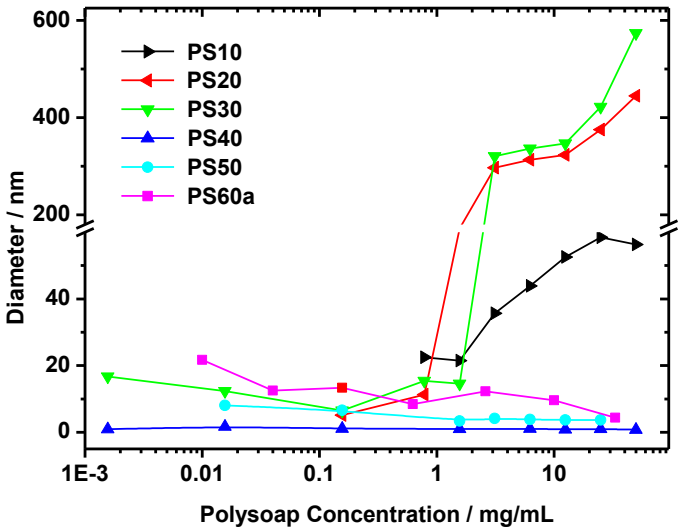

Figure 4.3 Concentration dependence of average hydrodynamic diameter of the poly(AMPS-stat-DDAM) series as measured by DLS.

4.1.5 SLS of poly(AMPS-stat-DDAM) series.

SLS is an ideal technique to discern inter vs. intramolecular assembly. First, it is known that larger particles contribute to higher scattering intensity since intensity scales with d^6. In addition, to a first approximation, the normalized excess scattering intensity as a function of concentration *c* is related to molecular weight by

$$\frac{I_{ex}}{I_o} \approx KcM$$

in which $I_{ex} = (I_{soln} - I_o)$ is the excess intensity, I_o is the scattering from pure solvent, M is molecular weight of the scattering species and $K = 4\pi^2 n^2 (dn/dc)^2 / N_A \lambda^4$ is the optical constant with N_A being Avogadro's number. For a constant molecular weight scatterer (intramolecular assembly), the normalized excess intensity should increase linearly with concentration. A plot of I_{ex}/cI_o vs. c would then yield a line with zero slope. In the case of intermolecular assembly, such a plot would have a positive slope from the increase in

molecular weight of the scattering species with increasing concentration. While there may be subtle effects related to the form factor (serves to decrease I_{ex}) or the second virial coefficient (serves to increase I_{ex},) significant changes in I_{ex}/cI_o vs. c indicate intermolecular association.

Figure 4.4 shows the time-averaged scattering intensities as a function of concentration of the polysoaps with differing hydrophobic content in deionized water. The scattering intensities correlate fairly well with the DLS data shown previously. In general, the PS20 and PS30 polysoaps show higher scattering intensity, consistent with larger particles observed in DLS. In addition, the scattering intensities of the PS40 and PS50 polysoaps remain relatively low, which is in agreement with the consistently small particle sizes observed in the DLS experiments (Figure 4.3). In the case of PS10, the scattering intensities are moderately low, even at higher concentrations. This may be expected based on the DLS data (Figure 4.3); the particle sizes do not increase as much and stay relatively low when compared to the particle sizes of the 20% and 30% polysoaps at high concentrations. The 60% polysoap shows the most unique scattering intensity profile whereby the intensities are much higher than the other polysoaps at lower concentrations. If the scattering intensities were dominated by the size contributions, then the scattering intensities should be closer to those of the 40% and 50% polysoaps. With PS60a there appear to be additional contributions to the scattering intensities.

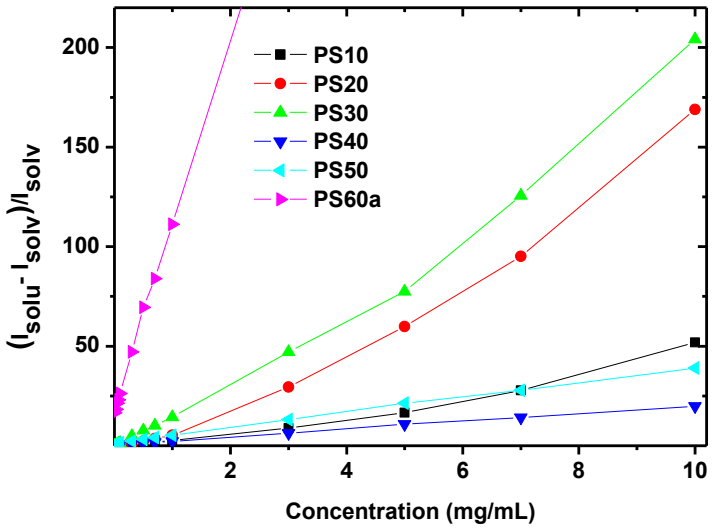

Figure 4.4 Concentration dependence of light scattering intensity ratio of polysoaps in water. Solu and solv are short for solution and solvent, respectively.

From Figure 4.4 it can also be seen that the slopes of some of the scattering intensity profiles do not always remain constant, which can be attributed to an increase in particle molecular weight, likely due to intermolecular complexation or assembly. The 10%, 20%, 30% and 60% polysoaps exhibit transition points; a change in slope is observed as the concentration increases. The slope markedly changes around 5 mg/mL for the 10%, 20% and 30% polysoaps (Figure 4.4) which is consistent with the increase in particle size seen from the DLS experiments (Figure 4.3). The 60% polysoap shows a slight decrease in slope around 0.5 mg/mL (Figure 4.4) which also is consistent with the decrease in particle size observed from the DLS data (Figure 4.3).

Another method used to observe the effects of concentration on particle size involves normalizing the excess scattering intensity to concentration by plotting I_{ex}/cI_o vs. c. Although this method is strictly qualitative, it provides information regarding particle

size contribution to scattering intensity as the concentration increases. This type of analysis compliments the DLS experiments well so that a change in particle size correlates to a change in normalized scattering intensity regardless of the concentration.

The plot of I_{ex}/cI_o vs. c is shown in Figure 4.5. The lower hydrophobic content polysoaps (PS10, PS20, and PS30) show an increasing trend in normalized scattering intensities as concentration increases. This indicates that the particle molecular weights are, on average, increasing as the concentration increases, which supports the DLS results that show increasing diameters with concentration. This increase in particle size is most likely due to intermolecular assembly. In contrast, the higher hydrophobic content polysoaps (PS40, PS50, and PS60a) show the opposite trend in which a decreasing relationship between normalized scattering intensity and concentration is observed, which again is consistent with DLS data indicating decreasing diameters as concentration increases. Note that the shaded region on Figure 4.5 indicates data points that have large amounts of error; at low concentrations (i.e.: below 1 mg/mL) the excess intensities are small (on the order of the noise in count rate) and are being divided by very small concentrations. This produces apparent asymptotic features in the data.

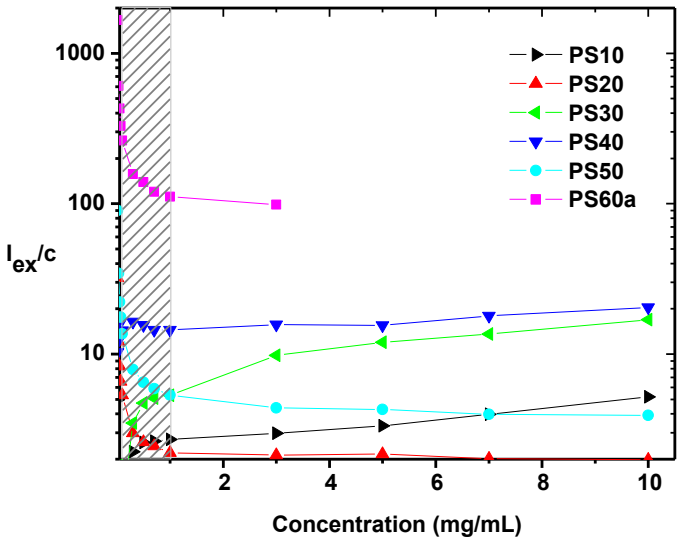

Figure 4.5 Concentration dependence of light scattering intensity ratio of polysoap in water normalized to concentration. I_{ex} is short for $(I_{solu}-I_{solv})/I_{solv}$.

4.1.6 Surface activity of the poly(AMPS-stat-DDAM) series.

Small molecule surfactants are usually characterized by semi-logarithmic plots of surface tension vs concentration. At low concentrations, individual molecules are in equilibrium with a monolayer formed at the air/water interface. As concentration increases, surface tension decreases as more surfactant migrates to the interface. A critical concentration (CMC) is reached at which the interface is saturated and micelles begin to form in the bulk solution. Beyond this concentration, additional surfactant goes only to new micelles being formed in solution and the surface tension remains constant. This typical behavior with a definitive CMC and a rapid decrease in surface tension is shown for SDS in Figure 4.6. Also shown in Figure 4.6 are the surface tension behaviors of each poly(AMPS-stat-DDAM) in deionized water. The lower hydrophobic content polysoaps, PS10, PS20, and PS30, have discernible CMC values and noticeably sharp

decreases in surface tension (from ~ 73 mN/m to around 62 mN/m) as the concentration increases. The higher hydrophobic content polysoaps, PS40, PS50, and PS60a show no discernible break in the semi-logarithmic plots and only gradual decreases in surface tension from their low concentration values of 72-73 mN/m to 67, 65, and 65 mN/m, respectively. These data when combined with the small, stable particle sizes measured by DLS suggest no CMC and thus unimeric micelle behavior.

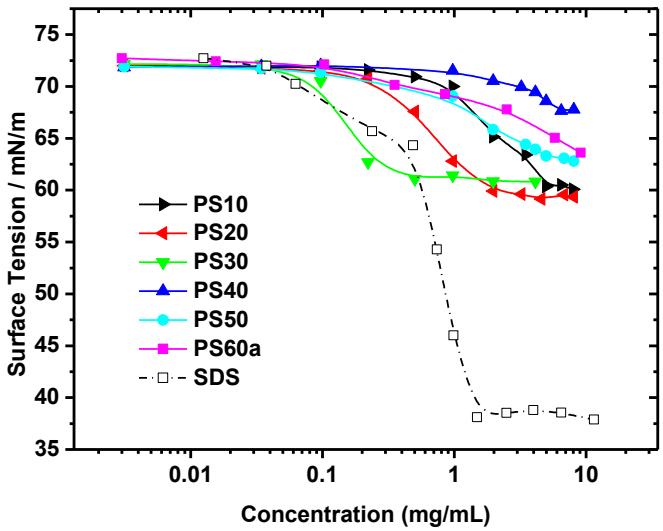

Figure 4.6 Concentration-dependence of surface tension of poly(AMPS-stat-DDAM).

4.1.7 Fluorescence measurements with pyrene to probe the hydrophobic domain of the poly(AMPS-stat-DDAM) series.

Pyrene is a unique chromophore as it has five vibrational modes that contribute to five discernible peaks in its fluorescence spectrum.[72,136] The intensity ratio of I_3/I_1 is often used to probe the polar/hydrophobic microenvironment of the system. A higher I_3/I_1 ratio is obtained in more hydrophobic environment; conversely, a lower ratio indicates a

more polar environment. For example, the I_3/I_1 ratio of pyrene in hexane and water are 1.6393 and 0.54347, respectively while in SDS micelles in water the ratio is 0.87719.[136]

Utilizing the technique described in the experimental section, pyrene was allowed to phase transfer into microdomains of each polysoap and the I_3/I_1 fluorescence intensity ratios of pyrene were measured with increasing copolymer concentrations in water. Experimental data shown in Figure 4.7 indicate increased I_3/I_1 ratios with increases in concentration for each polysoap in the series. The greatest increase in I_3/I_1 is evidenced in PS30 solutions where the ratio increases from 0.66 at low concentrations to 0.99 at higher concentrations. PS10 also has an I_3/I_1 ratio of 0.66 at low concentration that increases to 0.80. PS20 has a slightly higher ratio of 0.73 at lower concentrations which increases to ~0.86 at higher concentrations. The high DDAM content PS40, PS50, and PS60a solutions have high I_3/I_1 values of ~0.85 at the lowest concentration and increase to ~0.93, indicating hydrophobic microdomains. These values for the higher hydrophobic content polysoaps surpass that of SDS which reaches ~0.88 above its CMC. Also, at low concentrations of polysoap, the hydrophobic domains are almost as defined as the SDS above its CMC indicating micelle formation at lower concentrations and supporting unimolecular micelle behavior for the higher hydrophobic content polysoaps.

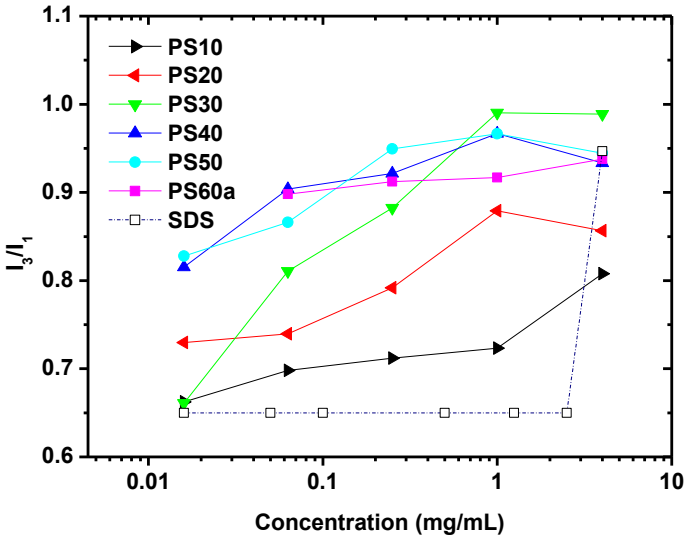

Figure 4.7 I_3/I_1 value vs polysoap concentration for the polysoap series in aqueous solution with 10^{-6}M pyrene as probe. Excitation wavelength was 338 nm.

4.1.8 UV absorbance spectroscopy to measure the sequestration of pyrene in the poly(AMPS-stat-DDAM) series.

The high extinction coefficient and hydrophobicity of pyrene have resulted in its use as a model compound for accurately determining CMC and sequestration or dissolution capability of common surfactants and micellar polymers. The capabilities of amphiphilic copolymers of the polysoap series to phase-transfer pyrene into hydrophobic domains are shown in Figure 4.8 in which absorbance values in deionized water of pyrene at 338 nm are plotted vs copolymer concentration. As the concentration of polysoap increases, more pyrene is transferred into solution as evidenced by linear increases in absorbance values, thus confirming no change in molar absorptivity and the validity of the Beer-Lambert relationship over the concentration range utilized in these experiments. As a control, SDS has relatively low absorbance and an observed CMC of

about 2.8 mg/mL, consistent with literature values of around 2.3 mg/mL (8.2 mM).[129,130] Unimeric micelles PS40, PS50, and PS60a have much greater absorbance vs concentration slopes (Figure 4.8) as compared to those of the multimeric micelles PS10, PS20, and PS30. This is to be expected since the former are more compact and thus have greater total surface areas at specific polymer concentrations. Clearly the unimeric micelles under conditions of this study do not aggregate (due to electrosteric stabilization) with increasing concentration and yet maintain pyrene sequestrating ability.

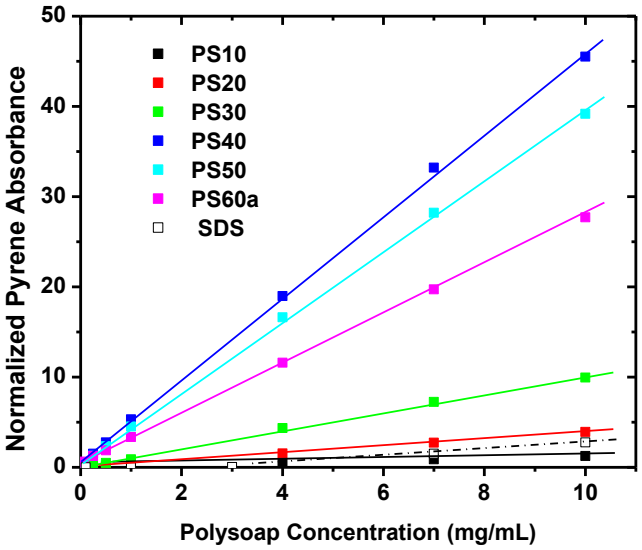

Figure 4.8 Pyrene sequestration as measured by UV absorbance at 339 nm as a function of copolymer concentration for the polysoap series.

4.1.9 Cell toxicity of the poly(AMPS-stat-DDAM) copolymers using the MTT assay.

One major approach to environmental remediation from disasters such as the 2010 Deepwater Horizon oil spill in the Gulf of Mexico has been the use of dispersants that emulsify oil for sufficient periods of time to allow break-down by endogenous marine bacteria. Unimolecular micelles formed by amphiphilic polysoaps, such as PS40

and PS50 in this work, could in principle sequester oil in hydrophobic domains and remain stable (no CMC) at high dilution. However, toxicity to cells, both the advantageous bacterial cells and those of marine organisms, should be considered in assessing the suitability for such application. Cell viability studies have been conducted as outlined in the experimental section for each amphiphilic copolymer in the PS series and for the control surfactant, SDS. Figure 4.9 shows the cell viability of KB cells upon exposure to increasing concentrations.

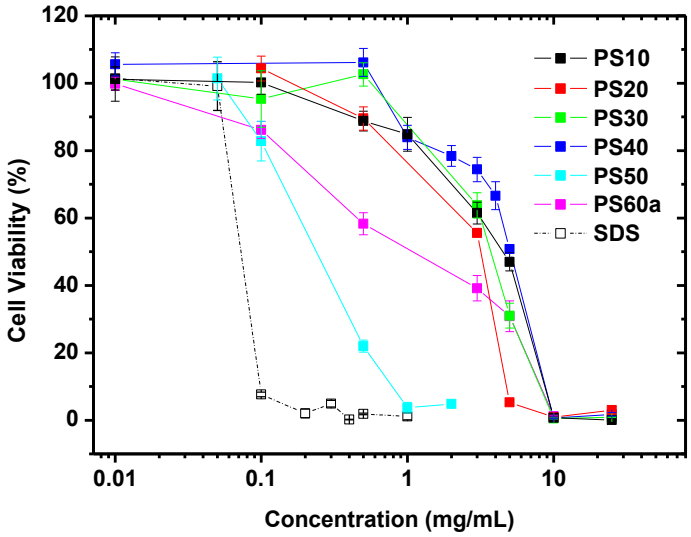

Figure 4.9 KB Cell viability as a function of poly(AMPS-stat-DDAM) concentration.

The IC50 of SDS is around 0.07 mg/mL and essentially no cells survive at concentrations beyond 0.2 mg/mL, a value significantly below its CMC of 2.3 mg/mL (8.2 mM). The semi-logarithmic curves for the polysoaps are quite different in shape from those of SDS. Onset of cell toxicity occurs later and IC50 values are as much as 60 times higher for all samples in the poly(AMPS-stat-DDAM) series except for PS50 and PS60a. Even the latter copolymers are significantly less cytotoxic to KB cells than SDS

above its CMC. As a note, to ensure that the cytotoxicity was not dependent on cell line, the same experiments were conducted using SKOV3 cells and similar results were obtained.

In order to investigate the molecular weight effects of poly(AMPS-stat-DDAM) on cell toxicity, RAFT copolymerization was utilized to prepare four well-defined PS40 (40 mol% DDAM) compositions with differing values of M_w. Figure 4.10 show cell viability vs concentration plots for 10.4, 23.9, 60.1, and 87.6 kDa Mw copolymers indicating IC50 values of 0.32, 0.73, 1.65, and 5.07 mg/mL, respectively. This study indicates that higher molecular weight polysoaps of the same copolymer composition show lower cytotoxicity.

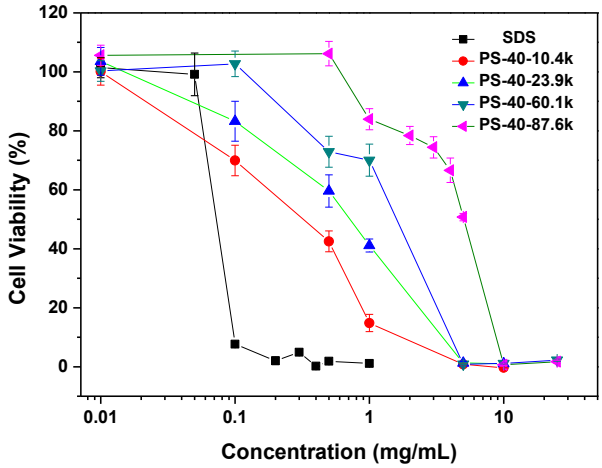

Figure 4.10 Molecular weight dependence of Cell toxicity of PS40 polysoaps with KB cells.

4.2 Structurally Controlled Anionic "Polysoaps" to Serve as Dispersants for Hydrocarbon Uptake in Aqueous Media: Structural Contributions of Hydrophobic Content and Molecular Weight.

4.2.1 Overview.

The studies in the previous section (4.1) measured effects of concentration and hydrophobic content on micelle assembly properties. However, the work presented in this section provides a more systematic approach to study both the molecular weight and hydrophobic content contributions to polymeric micelle size, hydrocarbon uptake capabilities, and core domain definition. It is possible that there are synergistic structural effects that may contribute to these important properties and to unimeric vs. multimeric association in water. As in section 4.1, a library of anionic polysoaps were prepared from AMPS and DDAM for this study (Scheme 4.2).

4.2.2 Structural design and synthesis of poly(AMPS-stat-DDAM) polysoap series.

In this work, using SDS as a respective small molecule surfactant model, anionic polysoaps were studied for their micelle forming and hydrocarbon uptake properties. Important parameters to consider when forming these polymeric micelles are the molecular weight of the copolymers (i.e. degree of polymerization (DP)) and the hydrophobic content along their respective backbones. In order to study these structural contributions to polymeric micelles, the statistical RAFT copolymerization of hydrophobic dodecyl acrylamide (DDAM) and hydrophilic 2-acrylamido-2-methyl-1-propane sodium sulfonate (AMPS) was utilized to prepare copolymers with controlled molecular weights and narrow molecular weight distributions. To study the aforementioned structural parameters systematically, three molecular weight series were

synthesized (low, medium, and high), each with varying amounts of hydrophobic DDAM comonomer content (10, 20, 30, 40, 50, and 60 mole %). Within each molecular weight series, a constant total monomer DP was targeted (50, 250, and 500), and pertinent structural data are reported in Table 4.2. The polysoap samples are labeled as PS for anionic polysoap, followed by a number indicating the targeted hydrophobic content (mole % DDAM) and a subscript indicating the molecular weight series, low (L), medium (M), or high (H). Since RAFT allows us to achieve consistent polymer DPs and monomer content, we can use these samples to determine the individual affect that molecular weight and hydrophobic content have on polymeric micelle size, core domain definition, and hydrocarbon sequestration. It is possible that there are cooperative structural affects that may contribute to these important properties and to unimeric vs. multimeric association in water.

Table 4.2 Structural Data for Low Molecular Weight poly(AMPS-stat-DDAM) Polysoap Series.

Sample	% Conversion [a]	Hydrophobic content [a]	M_w / kDa [b]	M_n / kDa [b]	PDI [b]
		Low Molecular Weight			
$PS10_L$	90%	12%	14.5	12.2	1.18
$PS20_L$	94%	21%	16.7	13.1	1.27
$PS30_L$	89%	30%	16.6	13.4	1.24
$PS40_L$	81%	41%	15.6	12.7	1.23
$PS50_L$	76%	50%	14.2	11.8	1.20
$PS60_L$	80%	62%	14.7	14.5	1.18
		Medium Molecular Weight			
$PS10_M$	58%	10%	43.6	35.3	1.23
$PS20_M$	76%	22%	63.4	51.7	1.22
$PS30_M$	75%	32%	60.0	49.0	1.22
$PS40_M$	73%	39%	55.7	46.8	1.19
$PS50_M$	68%	48%	50.4	43.2	1.17
$PS60_M$	56%	62%	57.6	52.6	1.09
		High Molecular Weight			
$PS10_H$	81%	10%	130.0	98.9	1.31
$PS20_H$	66%	19%	112.8	87.4	1.29
$PS30_H$	57%	30%	122.1	94.9	1.28
$PS40_H$	73%	41%	110.5	84.5	1.30
$PS50_H$	67%	49%	110.2	85.0	1.29
$PS60_H$	59%	60%	125.7	99.9	1.26

[a] Conversion and DDAM mole % determined by ^{1}H NMR.
[b] Determined by SEC-MALLS.
[c] Feed ratio of Monomer: CTA: Initiator was 250: 5: 1.
[d] Feed ratio of Monomer: CTA: Initiator was 1250: 5: 1.
[e] Feed ratio of Monomer: CTA: Initiator was 2500: 5: 1.
[*] All polymerizations were conducted using CPDT as the CTA, AIBN as the initiator, and at 70^{o}C in DMF until desired monomer conversion.

4.2.3 Concentration-dependent properties of poly(AMPS-stat-DDAM) polysoaps in water.

DLS was used to measure the hydrodynamic diameters (Dh) of polymeric micelles as a function of polymer concentration for each molecular weight series (low, medium, and high) (Figure 4.11). The low molecular weight (LMw) samples exhibit an increase in size as concentration increases for all polymers. Additionally, for the 10, 20, 30, 40, and 50% DDAM samples, the hydrodynamic diameters level off to 170, 139, 80, 117, and 195 nm, respectively. $PS60_L$ displays significantly larger sizes and an even greater increase in size from 290 nm at 7.5 mg/mL to 420 nm at 10 mg/mL. This indicates that $PS60_L$ forms unstable multimeric aggregates at higher concentrations and the 10, 20, 30, 40, and 50% DDAM samples in the LMw series form relatively stable multimeric micelles up to 10 mg/mL.

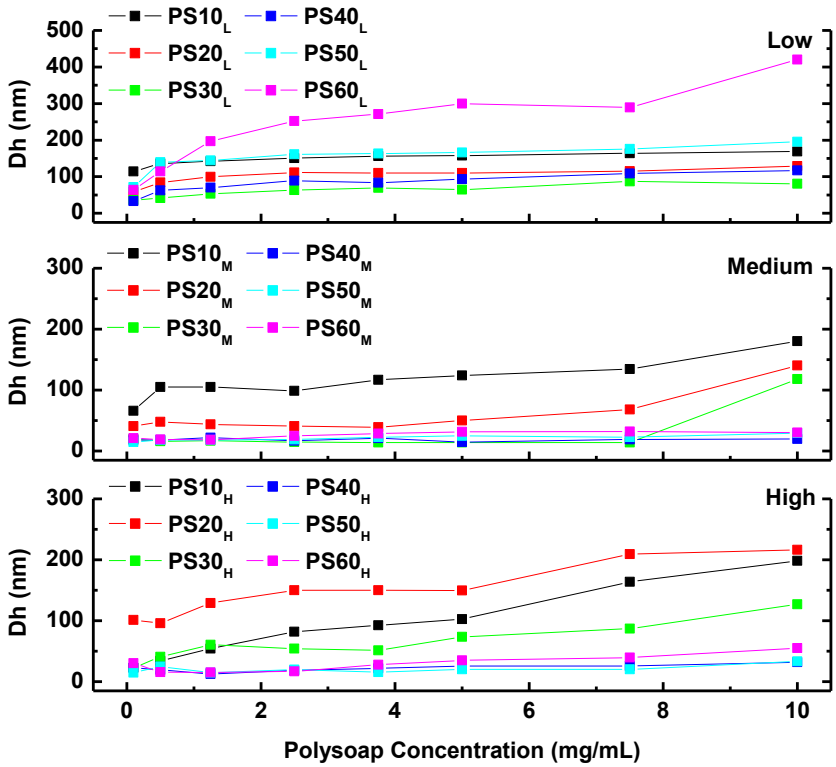

Figure 4.11 Concentration dependence of average hydrodynamic diameter of the low, medium, and high molecular weight poly(AMAPS-stat-DDAM) series as measured by DLS.

The medium molecular weight (MMw) series display mixed trends with $PS10_M$ and $PS20_M$ exhibiting clear increases in size over the entire concentration range probed. $PS30_M$ exhibits consistently low Dh values, in agreement with unimeric micelle behavior. However, this consistently low size is observed up to 10 mg/mL, at which point the sizes increase from 14 to 118 nm. This likely suggests a critical aggregation concentration (CAC) for $PS30_M$, at which a shift from unimeric micelles to multimers occurs. The $PS40_M$, $PS50_M$, and $PS60_M$ samples have constantly low diameters of around 20, 25, and 30 nm, respectively, throughout the entire concentration range. Stable, concentration independent particle sizes are characteristic of unimeric micelles.

The high molecular weight (HMw) series show significant concentration dependent behavior for $PS10_H$, $PS20_H$, and $PS30_H$, which exhibit large increases in size with increasing polymer concentration. The $PS40_H$, $PS50_H$, and $PS60_H$ samples display minor changes in size from 0.1 to 10 mg/mL. Between 0.1 and 2.5 mg/mL, a small decrease in size indicates typical unimeric micelle behavior arising from electrosteric stabilization of the corona. At concentrations above 2.5 mg/mL, micelle sizes increase, which designate a CAC for these polymers. This increase in size is an interesting result since it suggests that even once unimeric micelles could potentially aggregate into mulimeric structures if their concentration becomes high enough to do so (like seen for $PS30_M$). If this is true, it would be plausible that the opposite may occur for our observed multimeric micelles; they may eventually form unimers under more dilute conditions than measured in our study (0.1 mg/mL is the lowest concentration probed). However, these micelle structures would only exist at more dilute conditions if core domains remain intact. One way to probe the nature of these core domains is to use spectrophotometric probes or model compounds.

To probe the efficiency of the hydrophobic domains in sequestering hydrocarbon, pyrene was introduced to copolymer solutions in water and allowed to phase transfer into the core domains of the micelles. SDS was employed as a small-molecule surfactant control. Figure 4.12 shows pyrene absorbance at 341 nm as a function of polysoap concentration. For all molecular weight series, pyrene absorbance increases linearly with polymer concentration in accordance with Beers Law. The only exception to this linear trend is the $PS60_L$ sample, which shows a drop-in absorbance at 10 mg/mL. This drop is associated with a significant increase in particle size observed in the DLS data (Figure

4.11), possibly indicating that total surface area likely contributes to hydrocarbon uptake efficiency, as discussed later. SDS displays a CMC, evident by zero pyrene absorbance at 2.5 mg/mL. However, the polysoap samples do not exhibit a measurable CMC.

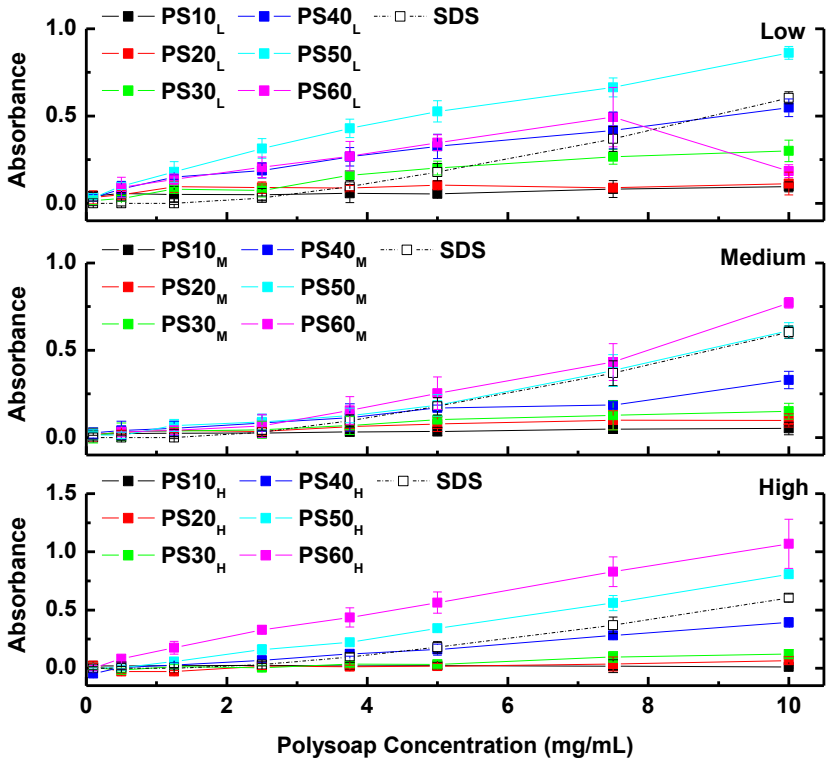

Figure 4.12 Pyrene sequestration as measured by UV absorbance at 341nm as a function of polysoap concentration for the low, medium, and high molecular weight poly(AMPS-stat-DDAM) series.

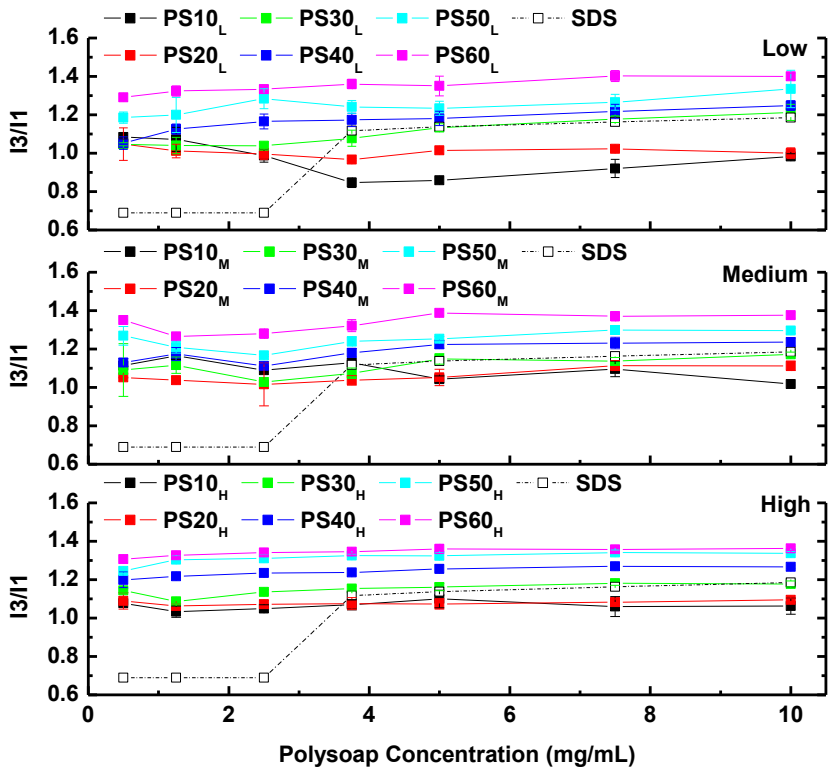

Figure 4.13 I_3/I_1 values vs polysoap concentration for the low, medium, and high molecular weight poly(AMPS-stat-DDAM) series in aqueous solution with pyrene as a probe. Excitation wavelength was 341nm.

The fluorescence spectrum of pyrene can provide information about the hydrophobicity of the core domains of the polysoaps. The ratios of the peak intensities I_3/I_1 change depending on the local microenvironment. An increase in the I_3/I_1 ratio indicates a shift from a polar aqueous environment to a more hydrophobic environment. Figure 4.13 shows the measured I_3/I_1 ratios for the copolymer series as a function of copolymer concentration, again using SDS as a control. Below the CMC of SDS, pyrene has an I_3/I_1 ratio of 0.68 in water and above the CMC the ratio increases to 1.1. All polysoap samples exhibit elevated ratios ($I_3/I_1 > 0.8$) relative to SDS below its CMC. The

samples consisting of 30, 40, 50, and 60 mole % DDAM have domains that are as hydrophobic or more hydrophobic than SDS above its CMC with I_3/I_1 ratios greater than 1.1. This ratio is consistent for these samples throughout the entire concentration range, indicating significant hydrophobic domain formation even at dilute concentrations. The 10 and 20% DDAM samples for all molecular weight series have pyrene I_3/I_1 ratios lower than SDS above its CMC, demonstrating less defined hydrophobic domains.

Altogether, DLS (Figure 4.11), UV absorbance (Figure 4.12), and fluorescence (Figure 4.13) experiments indicate that all polysoap samples form micelles capable of hydrocarbon uptake. However, the micelle properties are highly dependent on the copolymer molecular weight and molar hydrophobic content. Additionally, it is evident that only some of the polymeric micelles have unimeric characteristics ($PS30_M$, $PS40_M$, $PS50_M$, $PS60_M$, $PS40_H$, $PS50_H$, $PS60_H$). These copolymer samples have concentration-independent particle sizes with hydrophobic core domains and increased hydrocarbon uptake efficiencies; others exhibit multimeric micelle or aggregate behavior ($PS10_L$, $PS20_L$, $PS30_L$, $PS40_L$, $PS50_L$, $PS60_L$, $PS10_M$, $PS20_M$, $PS10_H$, $PS20_H$, $PS30_H$). A closer analysis of the data is necessary to better understand the individual contributing factors to micelle size, hydrophobic domain definition, and hydrocarbon sequestration.

4.2.4 Relationships between micelle size, hydrophobic domain formation and pyrene sequestration properties.

Figure 4.14 shows a 3D-plot of pyrene uptake vs micelle size and pyrene I_3/I_1 ratios. Immediately, it is evident that lower hydrodynamic diameters and increased I_3/I_1 ratios result in higher pyrene absorbance values. This behavior may be expected because increased hydrophobicity of solubilizing domains would likely aid in hydrophobic

molecule dissolution due to matching solubility parameters between the micelle core and foulant. Additionally, smaller particle sizes possess increased surface area, allowing for higher capacity and accessibility of the core domains by the diffusion of hydrophobes. Conversely, if the micelles aggregate into larger particles it is possible that the core domains buried in the center of the aggregates would be less accessible for uptake and lead to overall decreases in sequestration capability. A prime example of this can be illustrated considering the data point in Figure 4.14 exhibiting a high I_3/I_1 ratio, but a low pyrene absorbance value. Even though this sample ($PS60_L$) has well-defined hydrophobic domains, sequestration capacity is compromised by the multimeric behavior that results in a larger particle size in solution. If domain definition and micelle size are direct contributors to sequestration capability, understanding the individual structural parameters that lead to small particle sizes and increased hydrophobicity of micelle domains in these systems would be desirable. Our key candidates for this study are copolymer molecular weight (total monomer DP) and copolymer molar hydrophobic content (%DDAM).

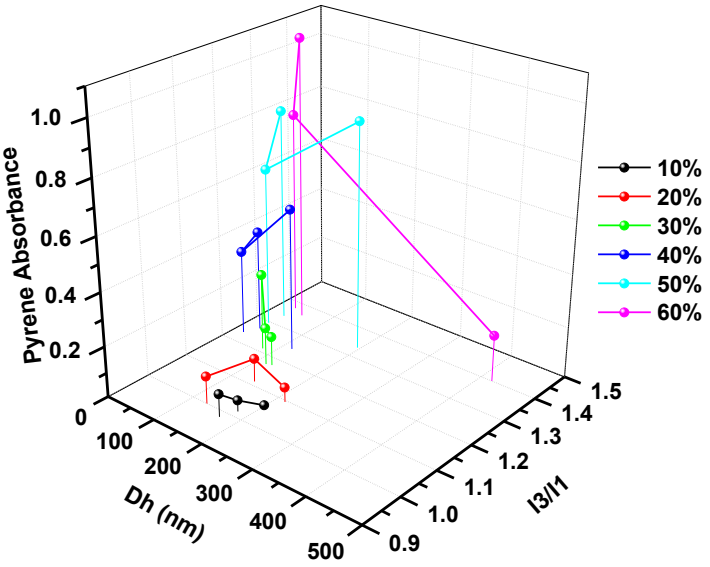

Figure 4.14 3-D plot of pyrene absorbance versus micelle size (D_h) and pyrene I_3/I_1 ratios for various polysoap hydrophobic contents.

4.2.5 Effects of hydrophobic content on polysoap micelle properties.

In order to understand how copolymer primary structure affects micelle properties in water, the data are plotted as a function of hydrophobic content for each of the molecular weight series (Figures 4.15 and 4.16). Plotting the data in this manor reveals trends relating to micelle size (D_h) and core domain definition (pyrene I_3/I_1 ratio). Additionally, we have chosen to plot the data for the 10 mg/mL solutions for all three molecular weight series. Figure 4.15 shows the hydrodynamic diameter of the polysoaps as a function of hydrophobic content at 10 mg/mL. The LMw samples exhibit a minimum in size at 30% DDAM. This observation is similar to that reported by Morishima, of which the radius of hydration (R_h) of uncontrolled, but comparable (15-30 kDa) dodecyl modified AMPS-based copolymers was studied.[27] Also, with both our LMw series and Morishima's copolymers, the 60 % hydrophobic content samples display a large size

increase compared to the other polymers. This is unique to the LMw samples and is contrary to observations in our MMw and HMw series polysoaps.

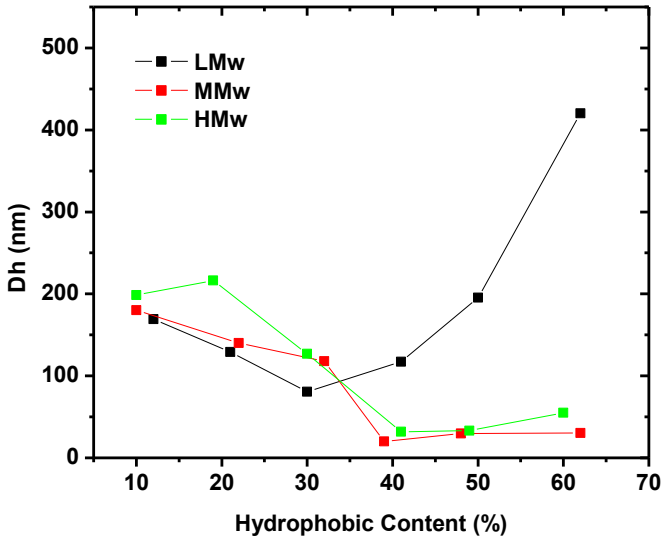

Figure 4.15 Hydrodynamic diameter dependence on hydrophobic content (% DDAM) for low (LMw), medium (MMw), and high molecular weight (HMw) polysoap series.

The general trend seen in our MMw and HMw samples is a decrease in particle size as hydrophobic content increases from 10% to 60% DDAM (Figure 4.15). The hydrodynamic diameter for the MMw series is elevated at lower hydrophobic contents (10, 20, and 30% DDAM) with sizes of 50 – 200 nm, then decreases to 10 – 25 nm and remains constant at and above 40% DDAM. For the HMw series, the diameters are also large at lower hydrophobic contents (10, 20, and 30% DDAM) with sizes at 150 – 250 nm. The size then eventually decreases to 10 – 50 nm with higher hydrophobic content (40, 50, and 60% DDAM). The observed small diameters for the higher hydrophobic content samples are expected since addition of hydrophobes attached along the backbone would strengthen the core domain interactions, further compacting the polymeric

micelles. However, this is only true if there is enough charge density in the micelle corona to stabilize these domains in solution, otherwise aggregation may occur. These effects are discussed in Section 4.2.7.

Figure 4.16 shows the pyrene I_3/I_1 ratios as a function of copolymer hydrophobic content. As a control, a dashed line represents the I_3/I_1 values of pyrene in SDS micelles. As expected, all polymer series exhibit an increase in I_3/I_1 ratio as hydrophobic content of the copolymer increases. Interestingly, the I_3/I_1 ratios, remain relatively unchanged among the three molecular weight series, indicating that domain definition may be independent of molecular weight and more of a function of hydrophobic content

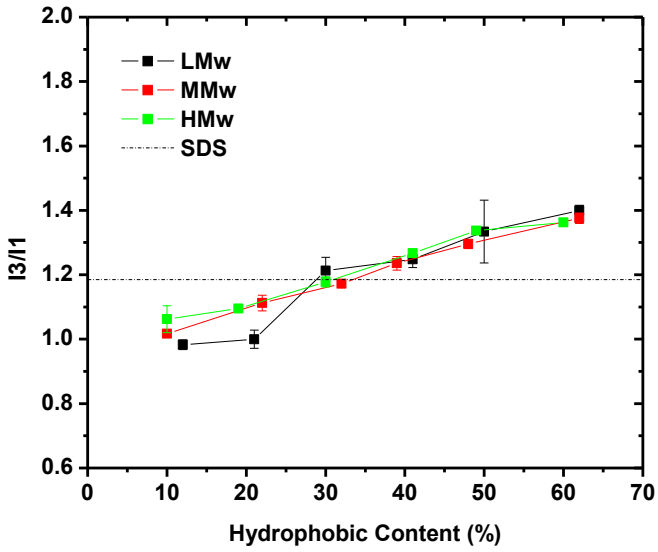

Figure 4.16 Pyrene I_3/I_1 ratio dependence on hydrophobic content (% DDAM) for low, medium, and high molecular weight polysoap series. Pyrene I_3/I_1 ratio in SDS micelle at 10 mg/mL.

4.2.6 Effects of molecular weight on polysoap micelle properties.

Micelle size (Dh) and hydrophobic domain definition (pyrene I_3/I_1 ratio) are polotted as a function of molecular weight (Figure 4.17 and 4.18). Again, we have chosen to polot the data for the 10 mg/mL solution for all six hydrophobic content series. Figure 4.17 shows the hydrodynamic diameter of the polysoaps as a function of molecular weight. The sizes of the higher hydropohobic content samples (40, 50, 60% DDAM) are influenced by the molecular weight of the copolymers more as compared to the lower hydrophobic content samples (10, 20, and 30% DDAM). The 40, 50, and 60% DDAM copolymers exhibit a large decrease in D_h between the LMw and MMw samples. The smaller size continues to be expressed at higher molecular weights. To the contrary, the 10, 20, and 30% DDAM copolymers, display small increases in micelle D_h as molecular weight increases.

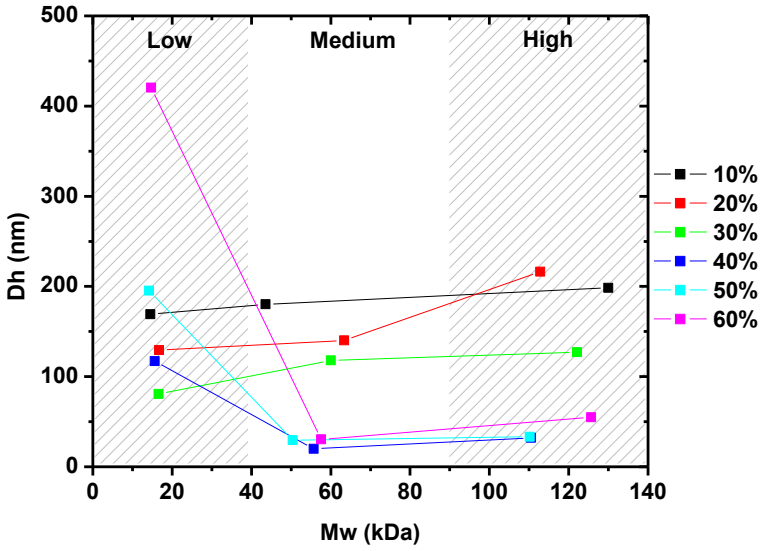

Figure 4.17 Hydrodynamic diameter dependence on polysoap molecular weight for 10, 20, 30, 40, 50, and 60% DDAM.

Figure 4.18 shows the pyrene I_3/I_1 ratios of the polymeric micelles as a function of copolymer molecular weight. The ratio of pyrene in SDS micelles is plotted as a dashed line and as a control. It is observed that for the 10 and 20% DDAM polymeric micelles, there is a slight I_3/I_1 ratio dependence on polymer molecular weight with values slightly increasing with molecular weight. The I_3/I_1 ratios of the 30, 40, 50 and 60% DDAM samples exhibit an insignificant dependence on molecular weight.

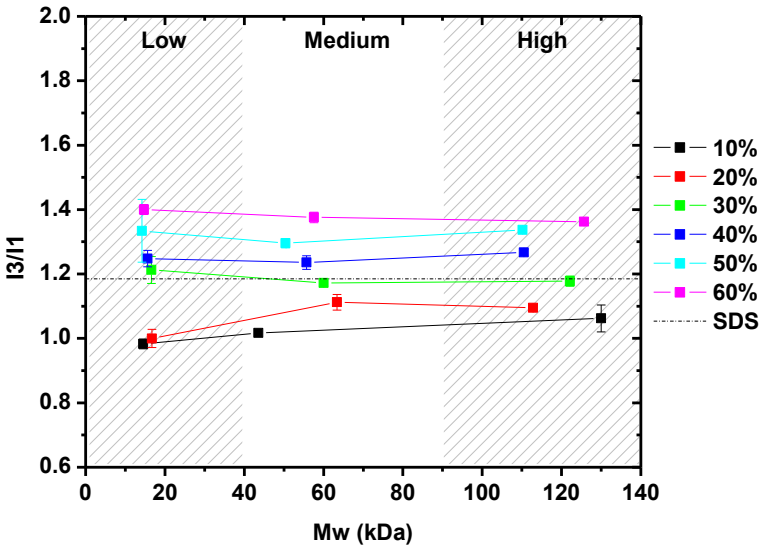

Figure 4.18 Pyrene I_3/I_1 ratio dependence on polysoap molecular weight for 10, 20, 30, 40, 50, and 60% DDAM. Pyrene I_3/I_1 ratio in SDS micelle at 10 mg/mL.

Combining the constant hydrophobic domain definition between the higher hydrophobic content samples and their measured micelle sizes, we can distinguish an important shift in behavior from multimeric to unimeric micelles based on copolymer molecular weight at 10 mg/mL, which suggests that copolymer DP is an important factor in unimeric micelle formation and core domain stabilization. Increasing the copolymers DP eventually allows for a sufficient number of units in the corona to stabilize highly

hydrophobic cores. Additionally, unimeric micelles may form if a single polysoap chain has a sufficient number of hydrophobic monomer units to contribute to a single stable domain; otherwise multiple chains would need to associate to have adequate hydrophobic interactions to form a stable core. This relationship is not surprising, especially since we can see slight indications of these trends when plotting the micelle D_h and pyrene I_3/I_1 ratios versus copolymer concentration (Figure 4.11 and 4.13). However, this closer look at the micelle properties at one concentration (10 mg/mL) now gives further insight into how copolymer molecular weight and hydrophobic content, cooperatively lead to unimeric versus multimeric micelle behavior.

4.2.7 Degree of polymerization of AMPS and DDAM in each polysoap.

As mentioned above, the copolymer DP influences the extent to which individual polymer chains associate to form micelles. Table 4.3 shows the calculated experimental degree of polymerization of AMPS and DDAM in each copolymer. Our observed trend of the LMw series having a minimum in micelle size at 30% DDAM is in agreement with literature reports.[27] Below 30% DDAM ($DP_{DDAM} < 13$), intramolecular interactions strengthen with increasing hydrophobic content because there is enough charge in the corona (>70% AMPS or $DP_{AMPS} > 31$) to stabilize the core domain; however, above 30% DDAM ($DP_{DDAM} > 13$), there are not enough charged repeating units in the corona to stabilize the core in water (<70% AMPS or $DP_{AMPS} < 31$). Therefore, further aggregation occurs with a shift from intramolecular to intermolecular association of hydrophobic moieties until an equilibrium driven multimeric structure or aggregate is reached.

Table 4.3 Calculated experimental degree of polymerization (DP) of AMPS and DDAM in each copolymer.

Sample	%Conversion [a]	Total DP [b]	F_{DDAM} [c]	F_{AMPS} [c]	DP_{DDAM} [d]	DP_{AMPS} [d]
Low Molecular Weight [e]						
aPS10$_L$	90	45	0.12	0.88	5.0	40
aPS20$_L$	94	47	0.21	0.79	10	37
aPS30$_L$	89	44	0.30	0.70	13	31
aPS40$_L$	81	40	0.41	0.59	16	24
aPS50$_L$	76	38	0.50	0.50	19	19
aPS60$_L$	80	40	0.62	0.38	25	15
Medium Molecular Weight [e]						
aPS10$_M$	58	145	0.10	0.90	15	130
aPS20$_M$	76	190	0.22	0.78	42	148
aPS30$_M$	75	187	0.32	0.68	60	127
aPS40$_M$	73	182	0.39	0.61	71	111
aPS50$_M$	68	170	0.48	0.52	82	88
aPS60$_M$	56	140	0.62	0.38	87	53
High Molecular Weight [e]						
aPS10$_H$	81	405	0.10	0.90	41	364
aPS20$_H$	66	330	0.19	0.81	63	267
aPS30$_H$	57	285	0.30	0.70	86	199
aPS40$_H$	73	365	0.41	0.59	150	215
aPS50$_H$	67	335	0.49	0.51	164	171
aPS60$_H$	59	295	0.60	0.40	177	118

[a] Total monomer conversion.
[b] Total monomer DP based on experimental % conversion.
[c] Molar fraction of AMPS and DDAM in each copolymer.
[d] Calculated experimental degree of polymerization of AMPS and DDAM.
[e] Theoretical DP at 100% conversion of monomer is 50 (LMw), 250 (MMw), and 500 (HMw).

For the 40, 50, and 60% DDAM samples, when the molecular weight or total DP of the copolymers increases (MMw and HMw series), increasing hydrophobic content does not lead to large aggregates. The drastic increase in the number of charged AMPS groups that make up the corona (from 15 to 53 or 118 for the 60% DDAM samples) helps stabilize the domains of the micelles, even those with highly hydrophobic cores.

4.2.8 Hydrophilic lipophilic balance of polysoaps.

A parameter that can be used to describe the nature of a surfactant's behavior in solution is the hydrophilic lipophilic balance (HLB). HLB values between 15-18 usually suggest dispersing capabilities. Additionally, values of 13 or greater produce transparent, homogenous solutions. Below HLB values of 13, inhomogeneous and turbid solutions usually develop. As shown in Figure 4.19, the HLB of the polysoaps range from 7 to 18. We would expect a wide range of solution properties from these values, however all polysoap samples of this study result in stable homogenous micelles, suggesting these polysoaps do not follow the conventional trends that small molecule or other polymeric surfactants do.

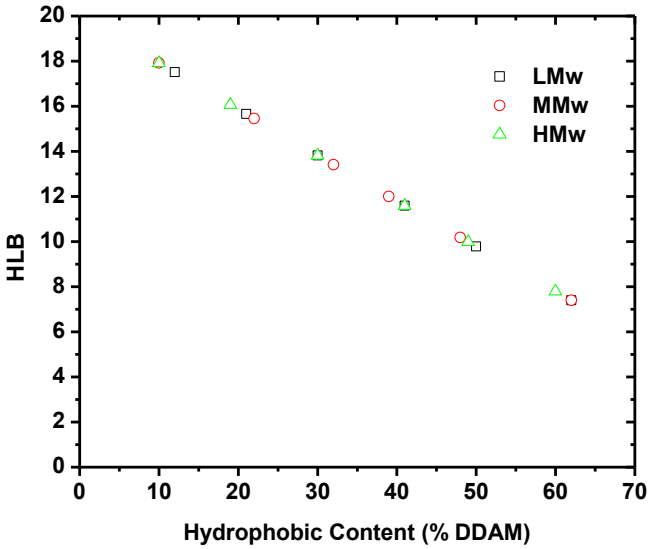

Figure 4.19 Hydrophilic lipophilic balance of polysoaps as a function of hydrophobic content.

4.3 Amphoteric, sulfonamide-functionalized "polysoaps": CO_2-induced phase-separation for water remediation.[137]

4.3.1 Overview.

Amphiphilic copolymers, or polysoaps, that reversibly form multimeric or unimeric micelles are of particular interest for water remediation since they potentially combine surfactant-like behavior and hydrophobe capture/sequestration capabilities at high dilution.[4,27,33,34,46,60,128,138] In this section, taking advantage of work described in previous sections (4.1 and 4.2), we now report the synthesis and CO_2-responsive behavior of two series of statistical copolymers that reversibly undergo phase changes and meet requisites discussed above for the envisioned second-generation polymeric micelles (Scheme 4.3). These copolymers, based on mSAC and mSMZ, possess pH-responsive coronas and phase-separation behavior that can be controlled through variation of comonomer composition and sulfonamide structure. Hydrophobic molecules can be captured and subsequently removed from solution through precipitation, simply by water acidification via CO_2 addition.

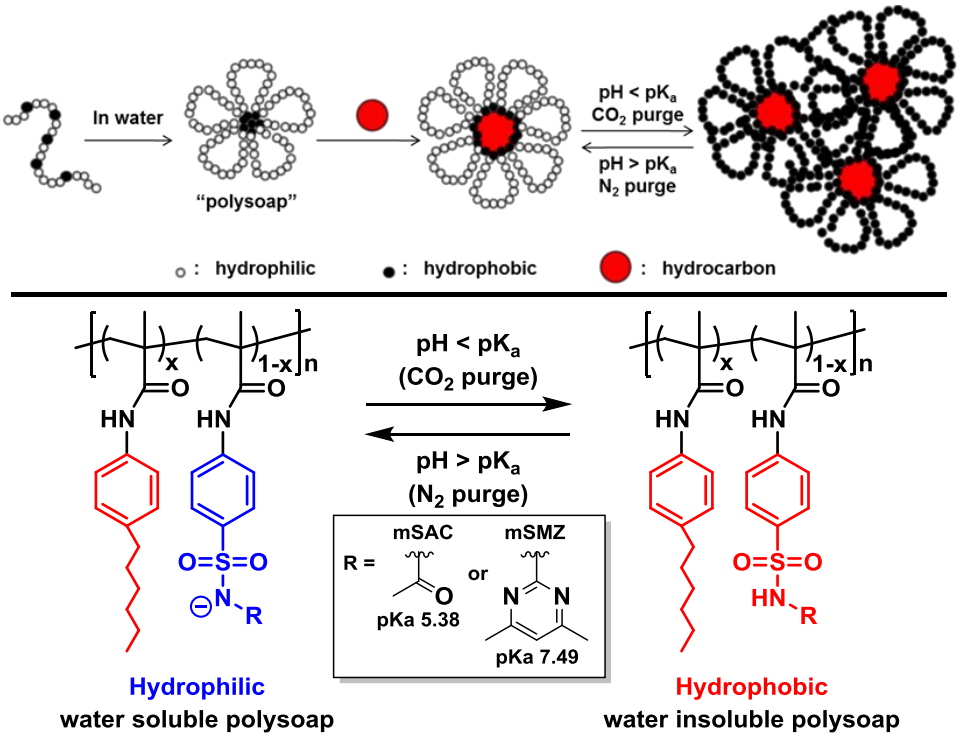

Scheme 4.3 (top) Second-generation polymeric micelles with pH/CO_2-responsive coronas representing hydrocarbon sequestration and recovery capabilities; (bottom) chemical structure of pH/CO_2-responsive sulfonamide-based polysoaps.

4.3.2 Structural design of sulfonamide polysoaps.

In order to study the solution properties of sulfonamide-based, pH- and CO_2-responsive polysoaps, two series of statistical amphoteric copolymers were synthesized via RAFT copolymerization. 4-Hexylphenyl methylacrylamide (4HPhMA) was copolymerized with either sulfonamide-based methacryloyl sulfacetamide (mSAC, pK_a = 5.38) or methacryloyl sulfamethazine (mSMZ, pK_a = 7.49) (Scheme 4.4). The 4HPhMA structure was rationally chosen as the hydrophobic monomer since it comprises the same polymerizable phenyl methacrylamide moiety as the sulfonamide monomers, resulting in similar reactivity ratios between the comonomers. Additionally, the hexyl alkyl chain on 4HPhMA increases the hydrophobicity of the monomer which, by design, will associate

into the hydrophobic core domain of the micelles. The sulfonamide-based mSAC or mSMZ monomers were chosen as components of the pH-responsive coronas. When solution pH > sulfonamide pK_a, formation of micelles is expected. Conversely, when solution pH < pK_a, the entire polymer (along with any sequestered hydrocarbon) should form an insoluble coagulate. Mole percentages of 10, 20, 30, and 40 4HPhMA were targeted for this study; pertinent structural data are reported in Table 4.4. The amphoteric polysoap samples are identified accordingly as follows: A or B indicate the sulfonamide monomer incorporated (mSAC or mSMZ, respectively) followed by the targeted mole % of 4HPhMA in the copolymer.

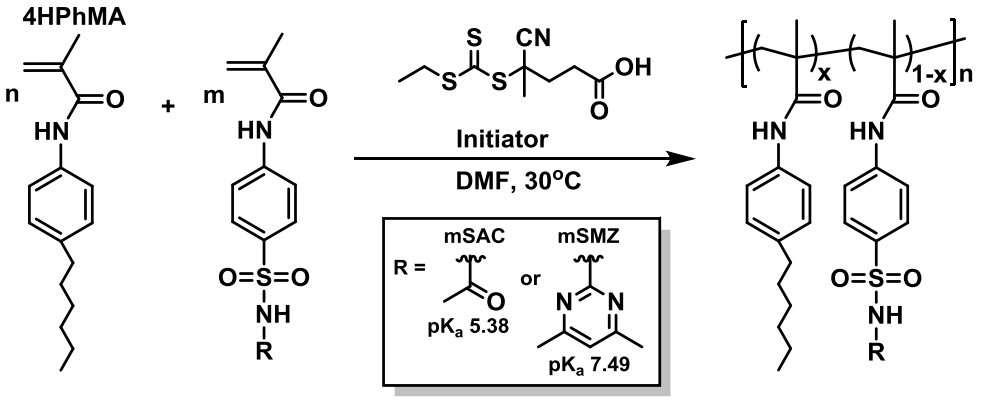

Scheme 4.4 Amphoteric sulfonamide polysoap structure and synthetic pathway.

Table 4.4 Structural data for amphoteric sulfonamide copolymers.

Sample	Sulfonamide Monomer	ρ [a]	4HPhMA content [a]	M_{nexp} [b] (kDa)	Đ [b]
A0*	mSAC	79%	0%	57.1	1.34
A10	mSAC	51%	8%	77.3	1.36
A20	mSAC	86%	17%	79.4	1.39
A30	mSAC	56%	27%	53.4	1.28
A40	mSAC	76%	43%	52.2	1.30
B0*	mSMZ	87%	0%	21.6	1.39
B10	mSMZ	52%	10%	67.2	1.35
B20	mSMZ	44%	20%	45.0	1.40
B30	mSMZ	61%	29%	60.0	1.35
B40	mSMZ	42%	42%	51.1	1.35

[a]Total monomer conversion (ρ) and mol % composition determined by ^{1}H NMR.
[b]Determined by SEC-MALLS.
*Homopolymer samples are used as controls for the CO_2/N_2 purge and remediation experiments.

4.3.3 Micellar properties of amphoteric sulfonamide polysoaps in water.

4.3.3.1 Dynamic and Static light scattering.

Dynamic light scattering (DLS) was utilized to determine the hydrodynamic diameter (D_h) values of micelles as a function of concentration for each copolymer in water at pH 12. The experimental data in Figure 4.20 indicate increases in the D_h values with increasing concentration for each copolymer in the A series, consistent with multimer formation. On the other hand, B10 and B20 have constant D_h values of ~8 nm across the entire concentration range. Additionally, Zimm analysis (Figures 4.21 and 4.22) for B10 and B20 indicates weight average molecular weights of 83.8 kDa and 55.8 kDa, respectively, consistent with single chain micelles. B30, although exhibiting a near-

constant particle size of ~35 nm over the concentration range, obviously contains multiple chains based on SEC-MALLS molecular weight. B40 is insoluble, even at high pH values, due to increased polymer hydrophobicity. Also, static light scattering at 90 degrees (Figures 4.23 and 4.24) further support the DLS observations.

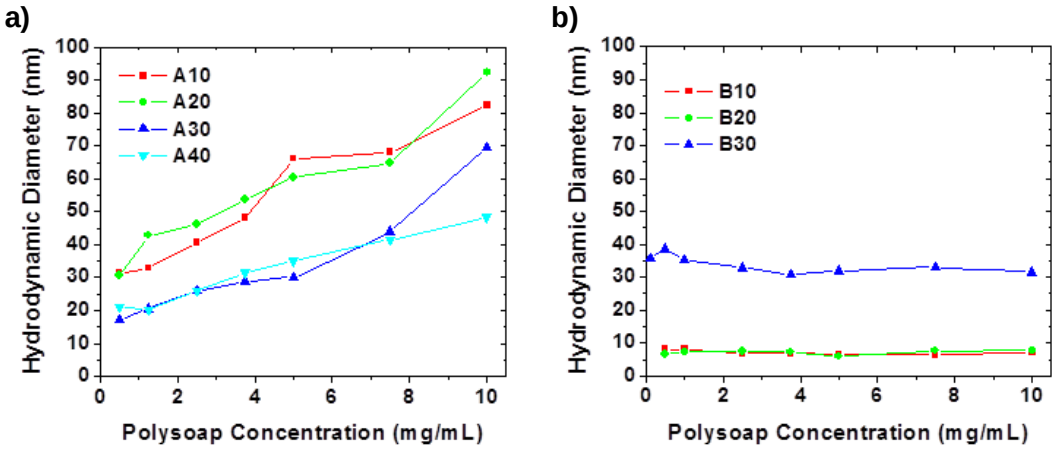

Figure 4.20 Hydrodynamic diameter (D_h) vs. polysoap micelle concentration as measured by dynamic light scattering: a) A series; b) B series.

Since the B10 and B20 samples are thought to be unimeric micelles we provide additional data to support this. If the micelle size does not change as a function of concentration (which is observed for B10 and B20), then scattering intensity should increase linearly as discussed above. Therefore, a multivariate static light scattering measurement can provide weight average molecular weights through a Zimm analysis. The Zimm equation is presented by

$$\frac{Kc}{R_\theta} = \frac{1}{M_w}\left(1 + \frac{(qR_g)^2}{3} + \cdots\right) + 2A_2c + \cdots$$

in which R_θ is the Rayleigh ratio ($(I_{solution} - I_o)r^2/I_o$), K is the optical constant, M_w is the weight average molecular weight, R_g is the radius of gyration, and A_2 is the second virial

osmotic coefficient. The dependent variables in this equation are concentration (c) and the scattering vector (q) which is a function of scattering angle (θ). After data collection, the Zimm plot data points can be extrapolated to determine lines associated to c = 0 mg/mL and θ = 0°. The y-intercept of these extrapolated lines equals $1/M_w$. The slope of the c = 0 mg/mL line equals $R_g^2/2M_w$ and the slope of the θ = 0° line equals $2A_2/\gamma$, in which γ is a spreading factor used during analysis of the data. The first measurement necessary to determine the molecular weight of the polymers is how the refractive index changes with polymer concentration (Figure 4.21). The slope provides the differential, dn/dc value. This value appears in the optical constant (K) in the Zimm equation. The calculated dn/dc values for B10 and B20 are 0.2016 and 0.1912, respectively.

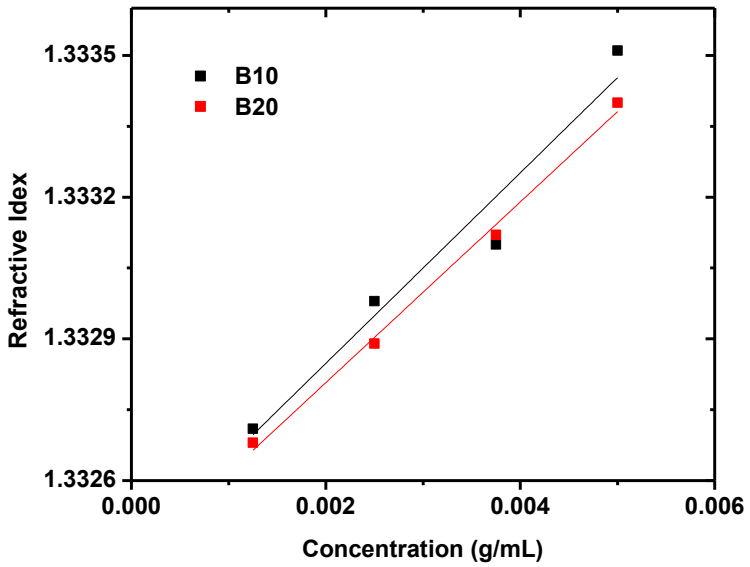

Figure 4.21 Refractive index as a function of polymer concentration for B10 and B20 to calculate dn/dc values for Zimm analysis (0.2016 and 0.1912, respectively).

Using the dn/dc values calculated from Figure 4.21, Zimm plots were generated for B10 and B20 in 0.05N NaOH (aq, pH 12) (Figure 4.22). Concentrations of 0.5, 1.25,

2.5, 3.75, and 5.0 mg/mL were measured, each at 60, 75, 90, 105, and 120°. Extrapolation of the data to c = 0 mg/mL and θ = 0° yields y-intercepts equal to 1.19E-5 and 1.79E-5 for B10 and B20, correspondingly. These intercept values provide weight average molecular weights of 83.8 kDa and 55.8 kDa, respectively.

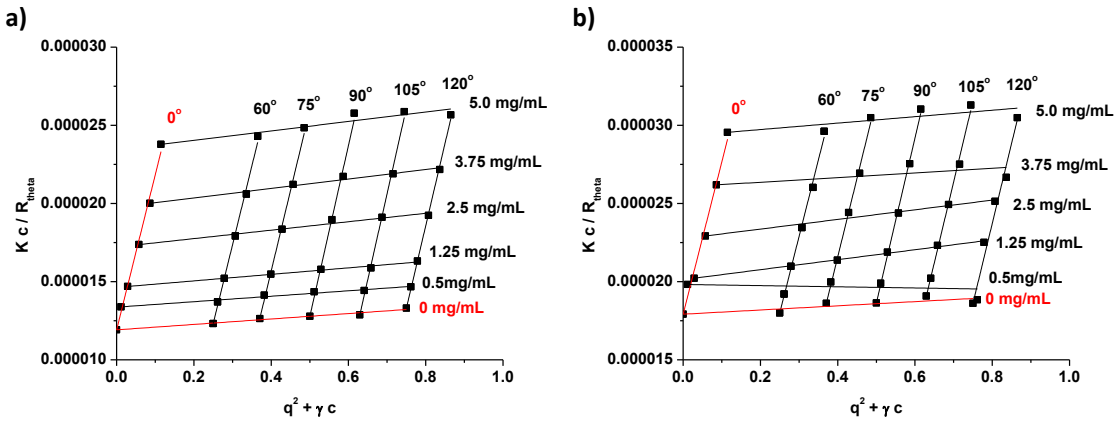

Figure 4.22 Zimm plots of B10 (a) and B20 (b) to calculate micelle weight average molecular weights (Refractive index of solvent was 1.33237; B10 dn/dc = 0.2016; B20 dn/dc = 0.1912; spreading factor (γ) = 23).

When comparing the measured molecular weights of the individual polymer chains from SEC-MALLS to the effective molecular weights of the micelles from the Zimm analysis, the nature of B10 and B20 can be elucidated. The weight average molecular weights determined in DMF, a good solvent for the entire copolymer chain, are 90.7 kDa for B10 and 63.0 kDa for B20. The corresponding weight average molecular weights of 83.8 kDa and 55.8 kDa for the micelles suggest that these micelles are likely unimeric. The measured molecular weights are slightly lower than expected since collapsed coils would artificially lower the observed scattering intensities as compared to extended chains.

Figure 4.23 shows the excess scattering intensity (I_{ex}/I_o) of the A and B series polysoaps as a function of concentration. As expected, the excess scattering intensity increases with concentration for all samples. The change in slope of the A series lines are consistent with the increase in size seen in the DLS experiment. This indicates a clear distinction of multimeric aggregates. The B10 and B20 samples exhibit a linear increase in excess scattering intensity with a constant slope. This indicates that these samples are either intramolecular or stable concentration independent intermolecular assemblies. B30 is unique as it has a significantly higher excess scattering profile which correlates well with increased micelle sizes relative to the B10 and B20 samples. B30 also displays a slight decrease in the slope at higher concentrations. This change in slope agrees with the small decrease in particle size seen in the DLS experiment as concentration increases.

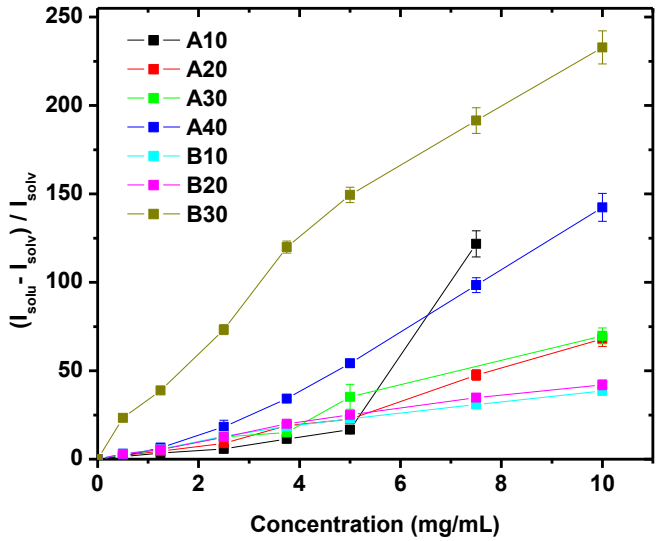

Figure 4.23 Concentration dependence of light scattering intensity ratio of A and B series polysoaps in water. Solu and solv are short for solution and solvent, respectively.

We can also observe the effects of concentration on particle size by normalizing the excess scattering intensity to concentration. This is done by plotting I_{ex}/cI_o vs. concentration, which is presented in Figure 4.24. This method is qualitative; however, it provides information about the particle size contribution to scattering intensity as the concentration increases. This type of information compliments the DLS data well since any change in particle size correlates to a change in normalized scattering intensity regardless of the concentration. For the A series polysoaps there is a noticeable increase in normalized scattering intensity as concentration increases. This is expected since DLS data suggests multimeric aggregates for these samples. The B10 and B20 normalized intensities show a zero slope as concentration increases. This correlates well with what we would expect for intramolecular (unimeric association) or concentration independent multimeric assemblies. B30 expresses a slight decrease in normalized scattering intensity as concentration increases which is consistent with the slight decrease in particle size seen in the DLS data.

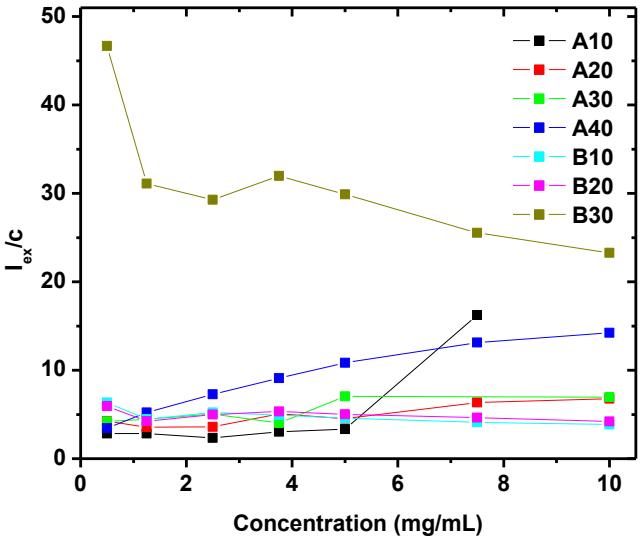

Figure 4.24 Concentration dependence of light scattering intensity ratio of polysoap in water normalized to concentration. I_{ex} is short for $(I_{solu} - I_{solv})/I_{solv}$.

4.3.3.2 UV-absorbance spectroscopy.

In order to study the nature of the hydrophobic domains in each sulfonamide series, pyrene was introduced as a probe and its absorbance at 341 nm monitored as a function of increasing copolymer concentration (Figure 4.25). Sodium dodecyl sulfate (SDS) was employed as a small-molecule surfactant control. For all samples, pyrene absorbance values increase as the number of polysoap domains increase. The entire B series and A40 show sequestration behavior similar or superior to SDS above its critical micelle concentration (CMC). As expected, SDS exhibits virtually no observable pyrene absorbance below its CMC (2.3 mg/ml); however, all samples except for A10 exhibit noticeable to moderate pyrene absorbance at lower polysoap concentrations (0.1 – 2.5 mg/mL).

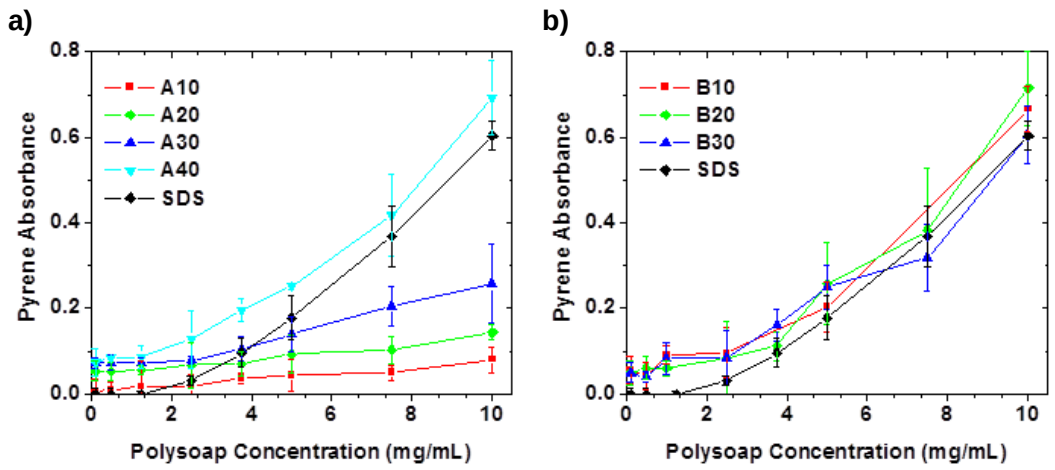

Figure 4.25 Pyrene sequestration as measured by UV-absorbance at 341 nm as a function of polysoap concentration for the sPS series: a) A series; b) B series.

4.3.3.3 Fluorescence spectroscopy

The fluorescence spectrum of pyrene in micellar solution can provide further information about the hydrophobic/hydrophilic microenvironment of core domains. The ratio of the peak intensities I_3/I_1 changes depending on the polarity of the local microenvironment in which the pyrene resides.[72,136] Increasing I_3/I_1 ratios indicate a shift from a polar aqueous environment to a less polar, hydrophobic environment. In Figure 4.26, measured I_3/I_1 values are plotted as a function of copolymer solution concentration with SDS used as a control. In water, pyrene exhibits an I_3/I_1 value of 0.68 below the CMC of SDS and an I_3/I_1 value of ~1.1 above the CMC. All polysoap samples tested (A10-40 and B10-30) exhibit $I_3/I_1 > 1$ over the entire range, even at very low copolymer concentrations (0.1 mg/mL). Taken together, the light scattering, UV-absorbance, and fluorescence experiments indicate that the A series polysulfonamides and B30 exist as multimeric assemblies while B10 and B20 form single-chain micelles. All polymers are capable of sequestering pyrene.

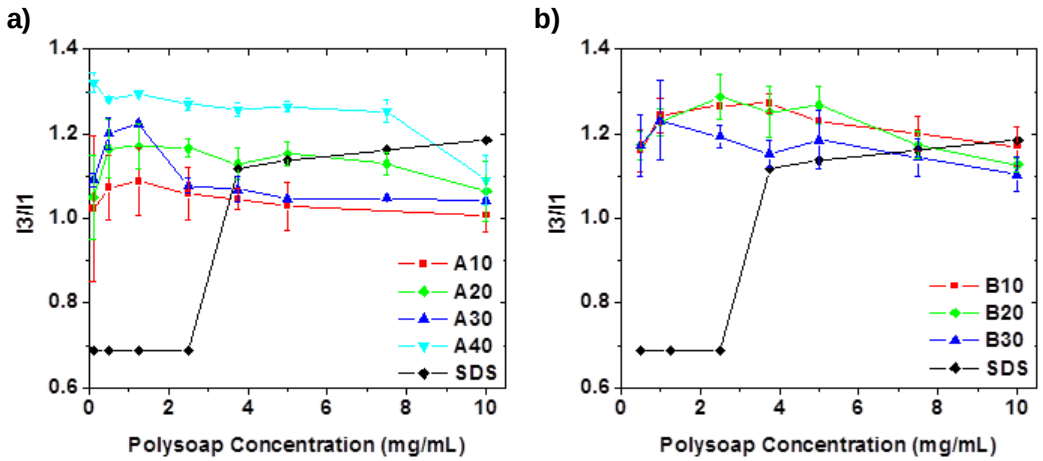

Figure 4.26 Pyrene I_3/I_1 values of the polysoaps at varying polymer concentrations: a) A series; b) B series.

4.3.4 pH-responsive behavior of the sulfonamide-based polysoaps.

Having studied the micellar nature of the A and B series of amphoteric polysoaps at pH = 12, the pH-dependent solubility of these copolymers was subsequently examined by turbidimetry while titrating with HCl. The pH-dependent turbidity measurements of each amphoteric polysoap solution is shown in Figure 4.27. As expected, sharp phase transitions are observed at pH values at or near the pK_a of the constituent sulfonamide monomers (A series, mSAC, pK_a = 5.38; B series, mSMZ, pK_a = 7.49).

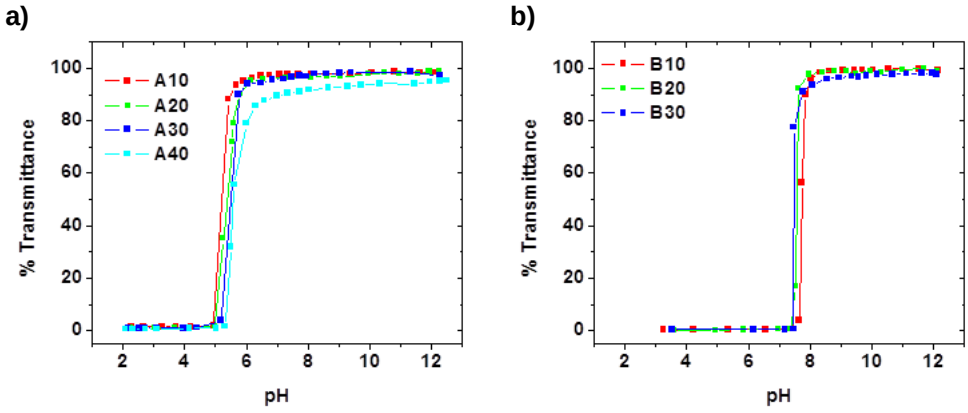

Figure 4.27 Percent Transmittance (533 nm) of amphoteric polysoap series at 10mg/mL in water as a function of solution pH titrated with HCl: a) A series; b) B series.

4.3.5 CO_2-responsive behavior of the sulfonamide-based polysoaps.

The concept of "tuning" reversible phase transitions in amphoteric, micelle-forming sulfonamide copolymers, suggests utility in practical applications, including water remediation. For example, the pH of water can be lowered to 3.9 by entraining with CO_2,[139] and subsequently returned to its original pH by purging with nitrogen (or air). Series A and B polysoap solutions were subjected to repeated CO_2/N_2 purge cycles of specific duration and visually inspected for phase-separation (Figure 4.28). To further quantitate the phase behavior of the copolymers, turbidimetric measurements were performed over 4 purge cycles as shown in Figure 4.29 (times were chosen to best illustrate the visual differences in phase-behavior). The extent of phase-separation and re-dissolution for both series is dependent on the hydrophobic content and proximity of the respective pK_a values of the sulfonamide units to the solution pH (Table 4.5). Table 4.5 shows the calculated values for the molar fractions of ionized sulfonamide units (σ_i) for each solution based on the Henderson-Hasselbach equation. A30 and A40 show significant decreases in percent transmittance (%T) and A10 and A20 display only minimal drops after each CO_2 purge cycle (Figure 4.27). After purging with N_2, the %T and clarity of each A series solution recovers. Conversely, all B series polysoaps show complete phase-separation upon CO_2 entrainment. After purging with N_2, the %T and clarity of the B10 and B20 solutions moderately recover. B30, however, does not completely re-dissolve when purging with N_2 due to increased copolymer hydrophobicity and additional chain aggregation compared to B10 and B20. Additional experiments reveal a small but noticeable time dependency on copolymer re-dissolution, which is presented in Figure 4.30. As a reference, Table 4.6 shows the %T values of the homopolymers A0 and B0 during a single CO_2/N_2 purge cycle.

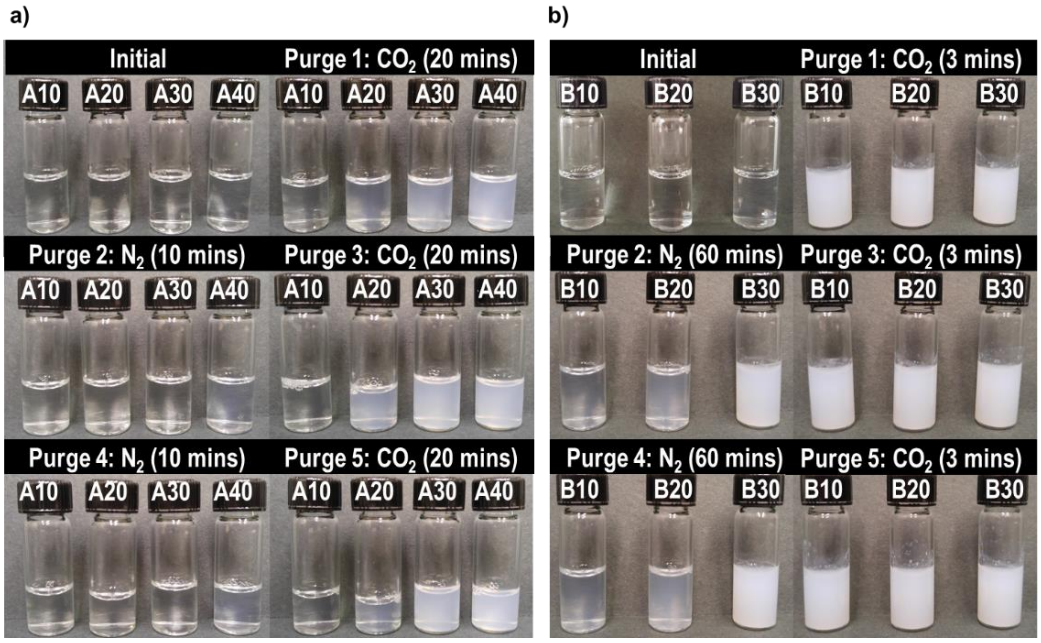

Figure 4.28 The visual turbidity of the CO_2-responsive A series (a) and B series (b) copolymers (concentrations of 10 mg/mL).

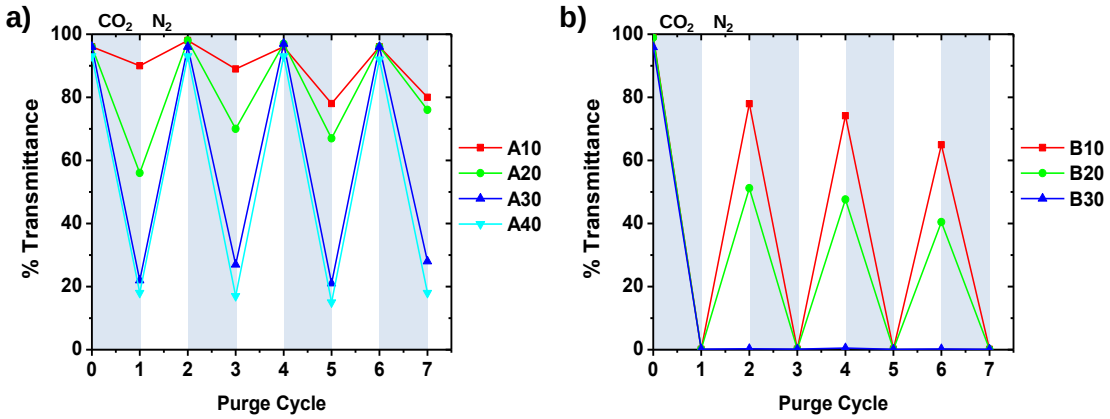

Figure 4.29 Percent transmittance of amphoteric polysoap solutions showing reversible CO_2-responsiveness in water during CO_2/N_2 purge cycle: a) A series; b) B series.

Table 4.5 Solution pH and respective molar fraction of ionized sulfonamide units for A and B series polysoaps during CO_2/N_2 purge cycles.

Sample	Initial		CO_2[a]		N_2[b]		
	pH	σ_i[c]	pH	σ_i[c]	pH	σ_i[c]	pKa
A10	11.4	1.00	6.07	0.826	7.51	0.992	5.38
A20	11.6	1.00	6.13	0.848	7.55	0.993	
A30	11.7	1.00	6.13	0.848	7.82	0.996	
A40	11.8	1.00	6.14	0.851	7.81	0.996	
B10	11.7	1.00	6.29	0.0592	8.86	0.957	7.49
B20	11.7	1.00	6.33	0.0646	8.78	0.948	
B30	11.8	1.00	6.27	0.0567	8.82	0.953	
DI H_2O	7.64	-	3.92	-	7.55	-	-
H_2O/NaOH	12.0	-	6.13	-	8.99	-	-

[a] CO_2 purge time was 10 minutes for the A series and 3 minutes for the B series.
[b] N_2 purge time was 20 minutes for the A series and 60 minutes for the B series.
[c] Molar fraction of ionized sulfonamide units calculated using Henderson Hasselbach equation.

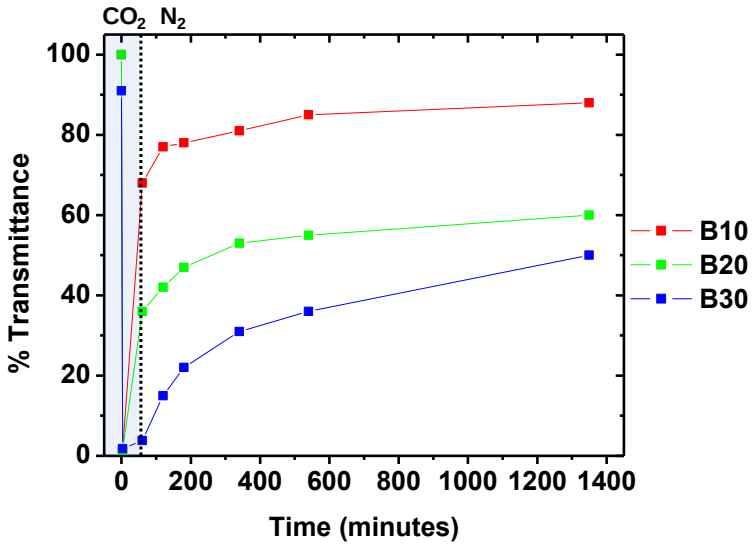

Figure 4.30 % Transmittance of B series polysoap solution showing time-dependent reversibility after a N_2 purge (60 minutes).

Table 4.6 %T values for homopolymers A0 and B0 during a single CO_2/N_2 purge cycle.

Sample	Initial	CO_2[a]	N_2[b]
A0	100	97.7	98.5
B0	98.8	1.35	96.7

[a] CO_2 purge time was 10 minutes for the A0 and 3 minutes for the B0.
[b] N_2 purge time was 20 minutes for the A0 and 60 minutes for the B0.

4.3.6 Hydrocarbon remediating properties of amphoteric sulfonamide polysoaps.

4.3.6.1 Removal of pyrene from water using HCl.

To demonstrate the ability of each amphoteric polysoap in the A and B series to remove dissolved aromatic hydrocarbons from aqueous solution upon pH-induced phase-separation, pyrene was chosen as a model compound since it possesses a high molar absorptivity, allowing detection of minimally soluble quantities in water. The pyrene absorbance values as a function of pH through the phase-transitions of A40, B10, B20, and B30 are shown in Figure 4.31. As the pH 12 micellar solutions are titrated with HCl, pyrene is removed via copolymer precipitation, as evidenced by an absorbance decrease at the corresponding pH of phase-separation (Figure 4.27). It should be noted that the A10, A20, and A30 data are not shown since these solutions remained turbid after acidification and centrifugation. A40 displays partial pyrene removal capability, as some copolymer and pyrene remain in solution after centrifugation with absorbance values expressing a minimum of 0.2. The B series demonstrates excellent hydrocarbon removal with pyrene absorbance values reaching zero after precipitation and centrifugation. Additionally, it is important to note that homopolymers A0 and B0 were studied as a control at pH 12. As expected, the homopolymers do not possess the hydrophobic core domain or micelle properties required for hydrocarbon dispersion in water.

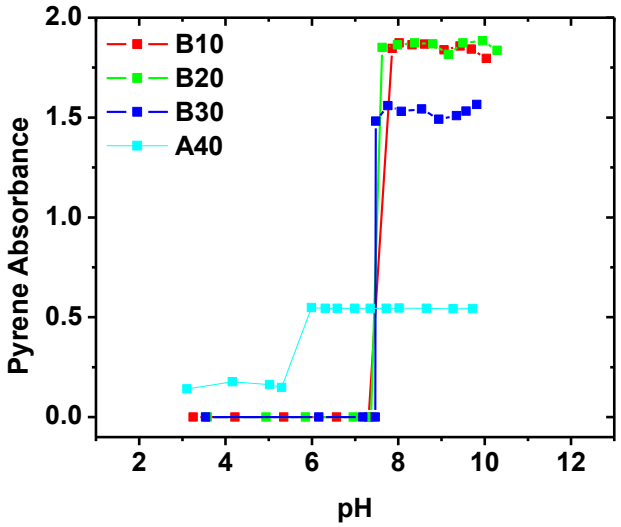

Figure 4.31 Pyrene absorbance (341 nm) as a function of pH through the phase-transitions of A40 and B series polysoaps.

4.3.6.2 Amphoteric polysoap remediation of 9-anthracenemethanol from water.

B10 and B20 were selected for water remediation studies based on our initial observations of phase behavior and an ability to partition the aromatic hydrocarbon pyrene into hydrophobic domains (Figure 31). 9-Anthracenemethanol (9-AM) was chosen as an appropriate model due to its high molar extinction coefficient and moderate water solubility. 9-AM is also a good model for aromatic contaminants found in trace amounts in ground and drinking water.[117,140] Utilizing the procedure outlined in Scheme 4.5, amphoteric polysoaps B10 and B20 were subjected to multiple dissolution/precipitation cycles to remediate 9-AM from water using CO_2-induced phase-separation.

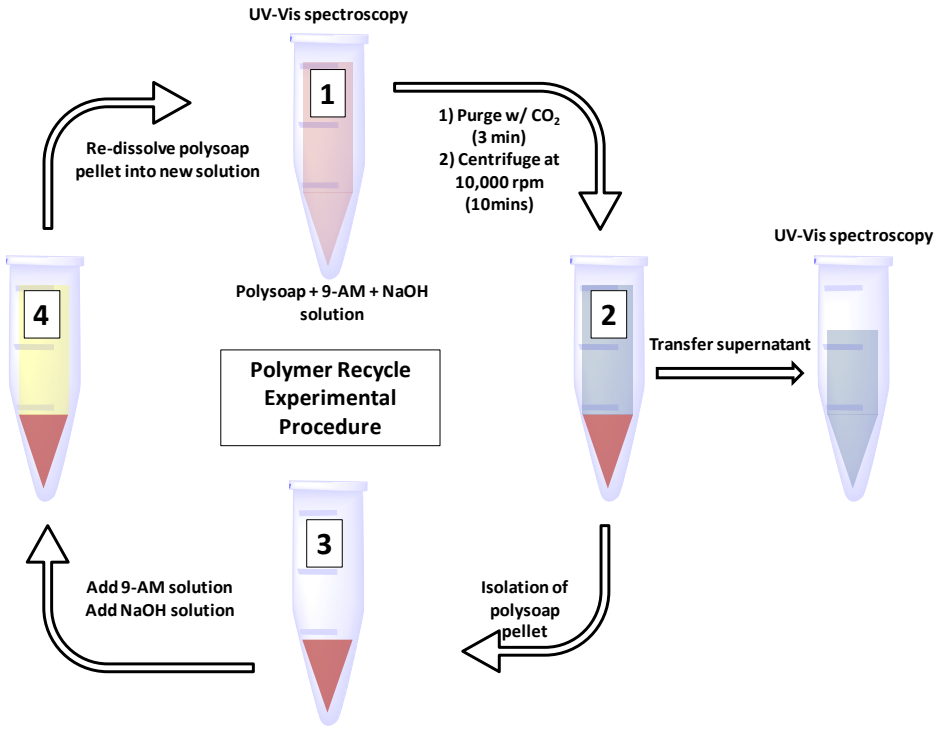

Scheme 4.5 Procedure for B10 and B20 recycle experiments involving the removal of 9-AM from multiple batches of contaminated water.

Figure 4.32 shows 9-AM absorbance values at 388 nm for each copolymer solution and its respective supernatant after remediation. As new solutions of 9-AM are introduced, the polymers continue to sequester 9-AM until saturation of the micelle core domains occurs. Based on calculations described in the experimental section, B10 and B20 have the capacity to sequester 4.5 and 5.2 molecules of 9-AM per polymer chain, respectively. Interestingly, at this concentration of 9-AM in the micelle core domains, excimer formation occurs, resulting in a decrease in the measured absorbance values. This is commonly observed when anthracene derivatives associate at high concentrations.[141–144] Overall, this experiment demonstrates the ability of these amphoteric polysoaps to be re-used (recycled) to remediate successive solutions of 9-AM, suggesting utility as sustainable remediating materials.

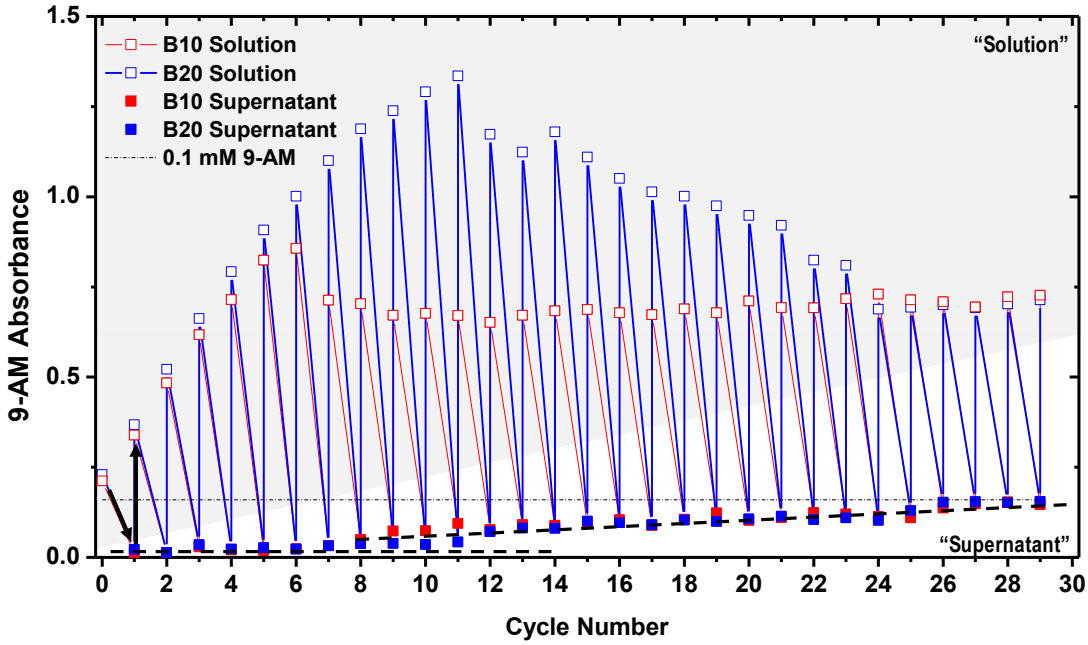

Figure 4.32 Incremental absorbance values of 9-AM at 388 nm as a function of the number of dissolution/precipitation cycles for B10 and B20. Each cycle shows dissolution followed by CO_2-induced (3 min purge) precipitation of B10 and B20 (10.3 mg) from 1 mL increments of 9-anthracenemethanol solution (0.1 mM).

Further absorbance and fluorescence data are presented in Figures 4.33-4.38. The homopolymer B0 was studied as a control for the remediation of 9-AM from water experiments. This data is presented in Figure 4.33. Figure 4.34 shows the absorbance values of the supernatants of B10, B20, and B0 during the 9-AM remediation experiment. The B0 supernatant expresses significantly higher supernatant absorbance values at initial recycle numbers than B10 and B20, indicating lower efficiencies of remediating the hydrocarbon from water.

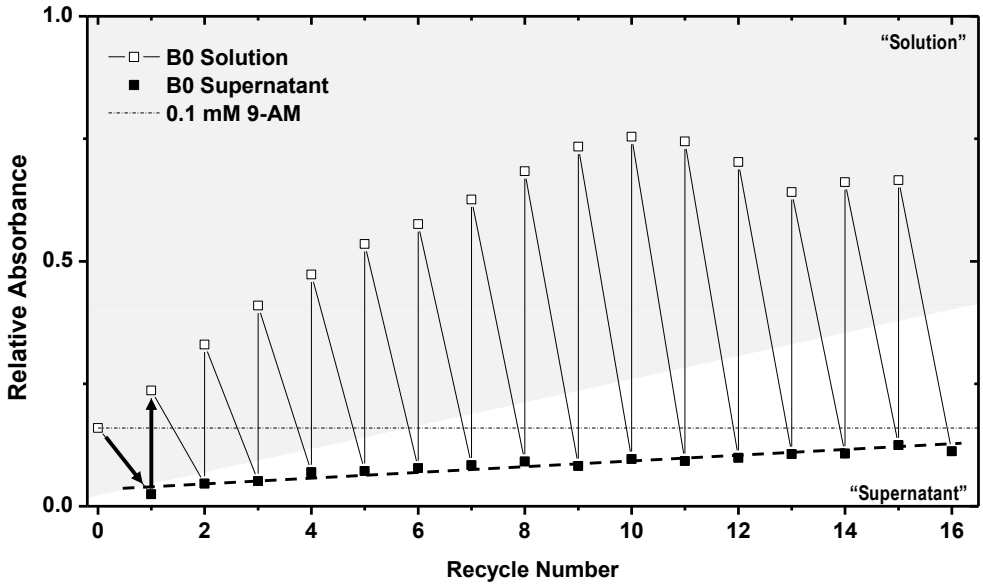

Figure 4.33 The absorbance of 9-anthracenemethanol as a function of the number of B0 recycles. Each cycle shows dissolution followed by CO_2-induced (3 min purge) precipitation of B0 (10.3 mg) from 1 mL increments of 9-anthracenemethanol solution (0.1 mM).

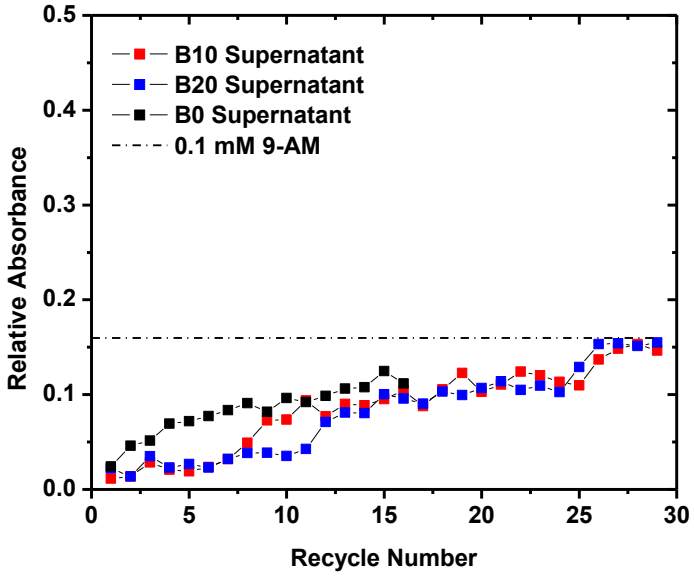

Figure 4.34 9-AM absorbance values for B10, B20, and B0 supernatant during 9-AM remediation experiments.

Figure 4.35 shows the UV-Vis spectra of the B10, B20, and B0 solutions during the 9-AM remediation experiment. The black dashed line is a visual aid for the 9-AM unimer absorbance at 388 nm. The red dashed line is a visual aid for the 9-AM excimer absorbance at 403 nm. Figure 4.36 shows the absorbance values of the 9-AM excimer at 403 nm during the remediation experiment. It is interesting to note that the slope of the absorbance values of the excimer increases for the B10 and B20 samples at the same recycle number that the unimer absorbance decreases to a steady value.

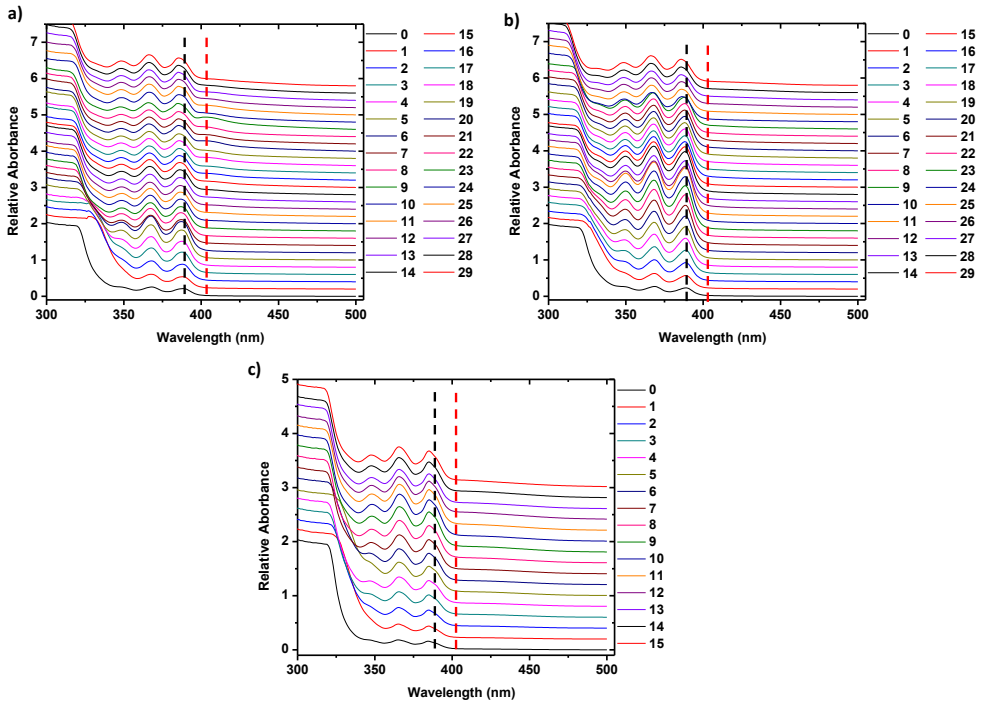

Figure 4.35 UV-Vis absorbance spectra of 9-AM in the B10 (a), B20 (b), and B0 (c) solutions during the recycle experiment.

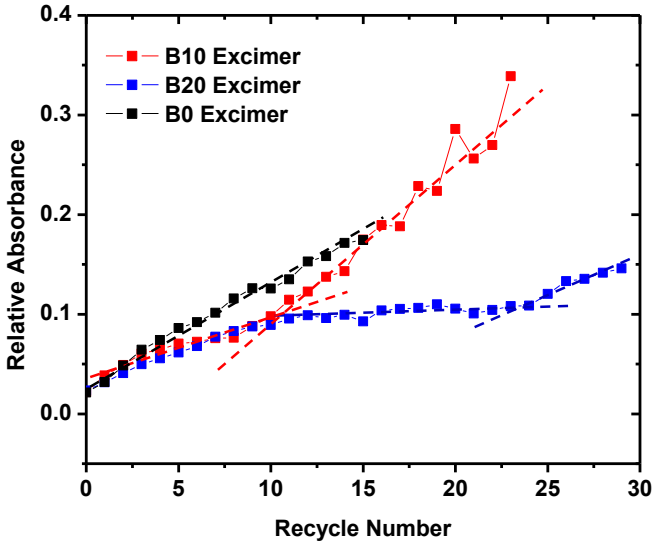

Figure 4.36 Relative absorbance of 9-AM excimer in the B10, B20, and B0 solutions at 403 nm during the recycle experiment.

Figure 4.37 shows the 9-AM absorbance spectra in the presence of SDS micelles (2.5 mg/mL) and shows excimer formation at higher hydrophobe concentrations, further confirming that the observed change in absorbance spectra and values is due to increased 9-AM concentrations in the micelle domains forming excimer. Figure 4.38 shows the fluorescence spectra of 9-AM in water, in the presence of B0, and in the initial polymer solution (0) and after recycling the polymer (23rd recycle). The spectra are normalized to the peak max intensity of 9-AM in water. It is noticed that the spectra shift towards higher wavelengths when 9-AM is sequestered into the polysoap core domains. Also, an increase in the shoulder emission at 440 nm compared to the initial solution is observed when the peak max is normalized, signifying the presence of excimer. These additional data agree with excimer absorbance and fluorescence trends observed in the literature for anthracene derivatives.[52-55]

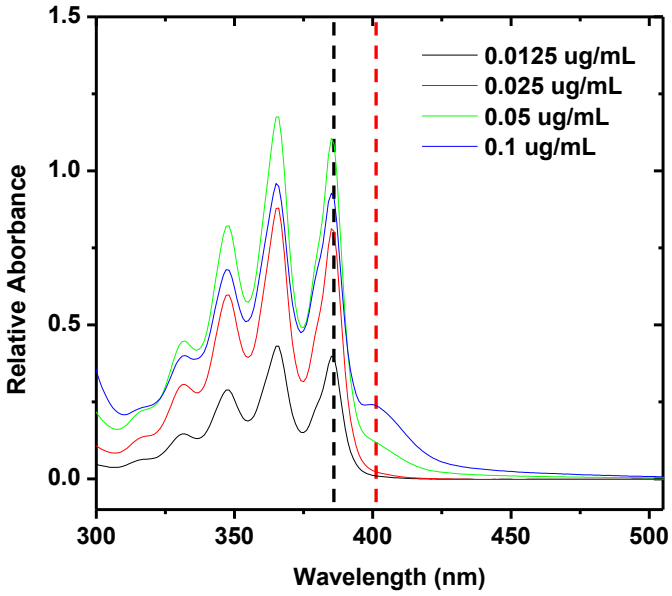

Figure 4.37 UV-Vis absorbance spectra of 9-AM at various concentrations in the presence of SDS micelles (2.5 mg/mL).

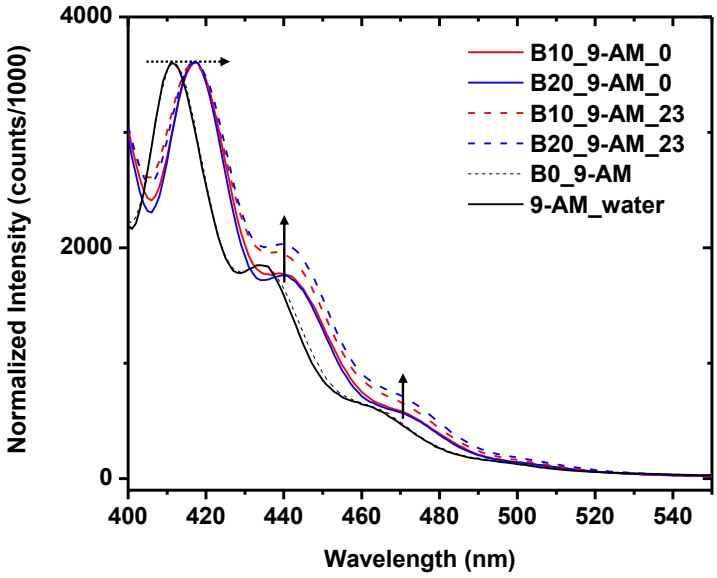

Figure 4.38 Fluorescence spectra of 9-AM in water, in the presence of B0, and in the initial (0) and the 23rd recycled B10 and B20 solutions.

CHAPTER V – CONCLUSIONS

5.1 Structurally controlled "polysoaps" via RAFT copolymerization of AMPS and n-doedcyl acrylamide for environmental remediation.

RAFT copolymerization has been utilized to prepare a series of well-defined, statistical copolymers from AMPS and DDAM. Light scattering, surface tension, and fluorescence studies suggest that PS40, PS50, and PS60a form unimeric micelles while PS10, PS20, and PS30 form multimeric micelles with increases in concentration. Composition- and concentration- dependence as well as hydrodynamic dimensions are consistent with flower-like micelle models proposed for hydrophobically-modified polyelectrolytes.[20,37,145,146] Unimolecular micelles form with increasingly collapsed structures with increasing DDAM content. This behavior is consistent with the collapse from second to third order unimeric micelles previously reported by Morishima.[27,135] Increasing hydrodynamic dimensions are observed with concentration increments indicating association of amphiphilic chains in both intra- and intermolecular fashion. UV absorbance studies using pyrene indicate that the unimeric micelles have enhanced capabilities of sequestering hydrophobic molecules on a molar basis as compared to SDS. Cell viability studies of the polysoap series as functions of concentration, composition, and molecular weight indicate up to 60x less cytotoxicity as compared to SDS. The control of structure afforded by RAFT polymerization and the demonstrated ability to form well-defined associates in aqueous media suggest a number of technological applications for these amphiphilic polymers including environmental remediation targeted in this work.

5.2 Structurally controlled anionic "polysoaps" to serve as dispersants for hydrocarbon uptake in aqueous media: Structural contributions of hydrophobic content and molecular weight.

Anionic polysoaps from the statistical RAFT copolymerization of DDAM and AMPS have been prepared. Three different molecular weight series were studied (low, medium, and high; DP_{target} = 50, 250, and 500, respectively), each with varying targeted hydrophobic monomer contents (10, 20, 30, 40, 50, and 60% DDAM). With these polymers we are able to determine how copolymer molecular weight and hydrophobic monomer content, individually influence micelle size and hydrophobic domain definition. This also allows us to recognize structural markers that predict unimeric versus multimeric micelle behavior and hydrocarbon sequestration properties in these systems. All samples in the low molecular weight series formed multimeric assemblies with concentration dependent micelle sizes (increasing size with polymer concentration; $PS10_L$, $PS20_L$, $PS30_L$, $PS40_L$, $PS50_L$, $PS60_L$). Within the medium and high molecular weight series, $PS10_M$, $PS20_M$, $PS10_H$, $PS20_H$, $PS30_H$ also formed concentration dependent multimeric micelles. Potential unimeric micelles were observed for $PS30_M$, $PS40_M$, $PS50_M$, $PS60_M$, $PS40_H$, $PS50_H$, $PS60_H$, which are identified as having small, stable, concentration independent Dh values and well-defined hydrophobic core domains (pyrene I_3/I_1 ratios). Overall, increased pyrene absorbances are observed for micelles with smaller Dh values and increased I_3/I_1 ratios. Pyrene I_3/I_1 ratios increased with copolymer hydrophobic content but remained relatively constant among varying molecular weight samples. Micelle size was determined to be influenced by both molecular weight and hydrophobic content. Lower hydrophobic content polymers (10, 20, and 30% DDAM) exhibit very small increases in micelle size as

molecular weight increased. However, the 40, 50, and 60% DDAM copolymers showed a large decrease in D_h from the low molecular weight series to the medium and high molecular weight series. These variances in micelle sizes indicate that assembly in these systems is a complicated process. However, we have been able to clarify to what extent these assemblies are influenced by the most basic structural parameters, molecular weight and hydrophobic monomer content. Other parameters, like chain flexibility or monomer secondary structure, may contribute to polymer assembly behavior as well. Therefore, it would be useful to expand upon this study in future work by including monomer structure and rigidity of the copolymer backbone to determine how other structural parameters effect unimeric versus multimeric micelle formation. The data collected from this work would allow for predictive structure-property models for polysoaps and other polymeric micelles which would be beneficial for the development of new materials for environmental and biomedical applications.

5.3 Amphoteric, sulfonamide-functionalized "polysoaps": CO_2-induced phase-separation for water remediation.

Amphoteric polysoaps have been prepared utilizing the RAFT copolymerization of sulfonamide-based mSAC or mSMZ and permanently hydrophobic 4HPhMA. At high pH values the copolymers are water-soluble and exist as micelles; below a critical pH value, phase separation occurs, and the polymers become water insoluble. These amphoteric sulfonamide polysoaps have pK_a values in a range allowing for CO_2-responsive behavior. The A series of polysoaps (mSAC derivatives) has minimal responsiveness as demonstrated by limited increases in solution turbidity. On the other hand, the B series

(mSMZ derivatives) exhibits excellent CO_2-responsiveness with sharp phase-separation. The amphoteric nature of these copolymers allows sequestration of hydrocarbon impurities from water. Specifically, B10 and B20 were efficient at removing the model foulant 9-AM from aqueous solutions via CO_2-induced phase-separation. We believe the demonstrated potential of these pH/CO_2-responsive amphoteric sulfonamide polysoaps will have future implications in deriving commercially-feasible water remediation technologies.

APPENDIX A - pH-RESPONSIVE SULFONAMIDE-BASED POLYSOAPS VIA RAFT COPOLYMERIZATION FOR OIL REMEDIATION AND RECOVERY[147]

A.1 Overview.

Previous sections (4.1 and 4.2) report first-generation micelles composed of AMPS and DDAM capable of hydrocarbon sequestration. Those amphiphilic systems rely on indigenous bacteria for oil remediation. This section (Appendix A) discusses the development of third-generation, stimuli-responsive systems that would allow for removal of sequestered oil or foulants as well as recycling of the "polysoaps." We have prepared a series of polysoaps via the statistical RAFT copolymerization of mSAC and mSMZ. By incorporating the two sulfonamide-based monomers into a copolymer backbone, we aimed to create three distinct phase responses by adjusting pH (Scheme A.1): full water solubility at alkaline pH, micelle formation at neutral pH, and full phase separation at acidic pH. This tri-phasic behavior allows for hydrocarbon sequestration and removal from water, followed by hydrocarbon recovery and separation from the copolymer. The copolymer can then be recycled, markedly improving the efficiency of current oil spill remediation technologies.

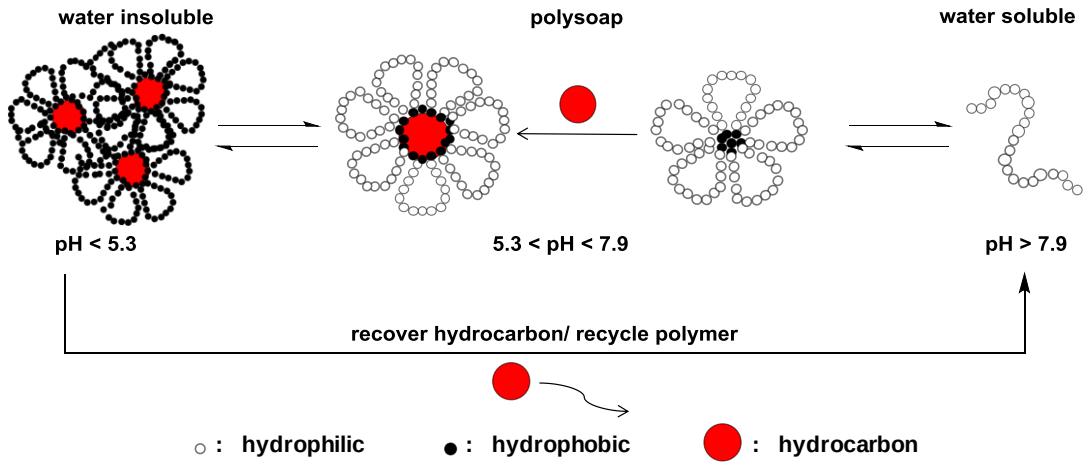

Scheme A.1 Third-generation, pH-responsive polysoaps for oil spill remediation and recovery.

A.2 Results and discussion.

A.2.1 Structural design of polysoaps.

In order to study the solution properties of third-generation, sulfonamide-based, pH-responsive polysoaps, a series of statistical copolymers was synthesized via the RAFT copolymerization of sulfonamide-based mSAC (pKa = 5.38) and mSMZ (pKa = 7.49) (Scheme A.2). These monomers were chosen due to their respective pK_a values and sharp segmental solubility transitions upon ionization in water at values of solution pH > pKa. This creates three distinct phase behaviors dictated by the pH of the solution (Scheme A.3). At high solution pH (> 7.9), both the mSAC and mSMZ units are ionized, creating a water-soluble polyelectrolyte. When the solution pH < mSMZ pK_a, but above the pK_a of mSAC, the mSMZ groups are water-insoluble and create the hydrophobic domain of the micelles. Between the two pK_a values, the core domains are stabilized by the charged mSAC groups that form solubilizing coronas. In this phase (5.3 < pH < 7.9), the hydrophobic core domains formed by the mSMZ are capable of solubilizing hydrocarbons. At solution pH values < mSAC pK_a (5.3), the entire copolymer becomes

hydrophobic, resulting in precipitation. This phase separated product can be readily removed from solution by filtration or centrifugation. Once the polymer is separated from the solution, the clean water can be removed, and the polymer reused until saturation of the polymers core domain. Additionally, when the polymeric micelles reach their saturation limit, they can then be re-dissolved in an alkaline solution to solubilize the entire chain, dissociate the hydrophobic domains, and thus releasing the sequestered hydrocarbon foulant. After hydrocarbon extraction with a nonpolar solvent, the copolymer can be recovered for further use. Based on previous work, mole percentages of 10, 20, 30, and 40 mSMZ were targeted for this study, and pertinent structural data are reported in Table A.1. Copolymers of the desired M_w were synthesized with low dispersity Đ.

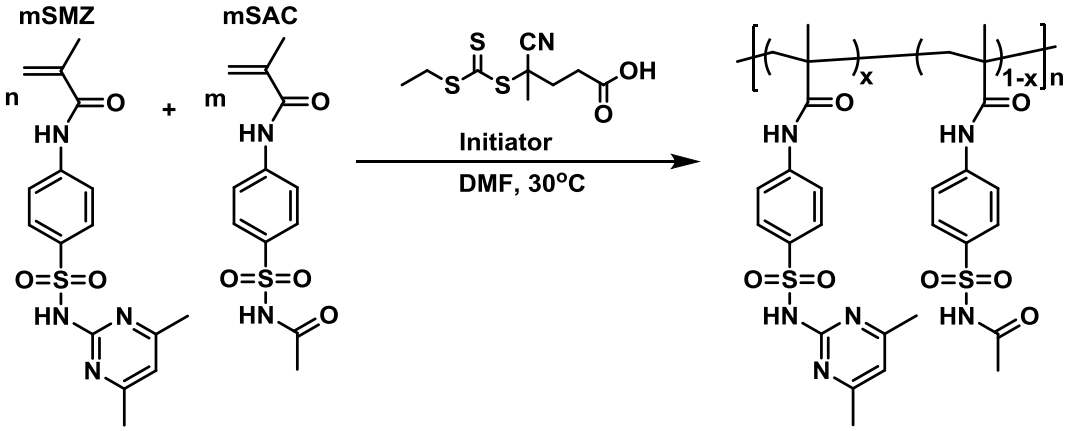

Scheme A.2 Synthesis of sulfonamide-based polysoap, poly(mSMZ-stat-mSAC).

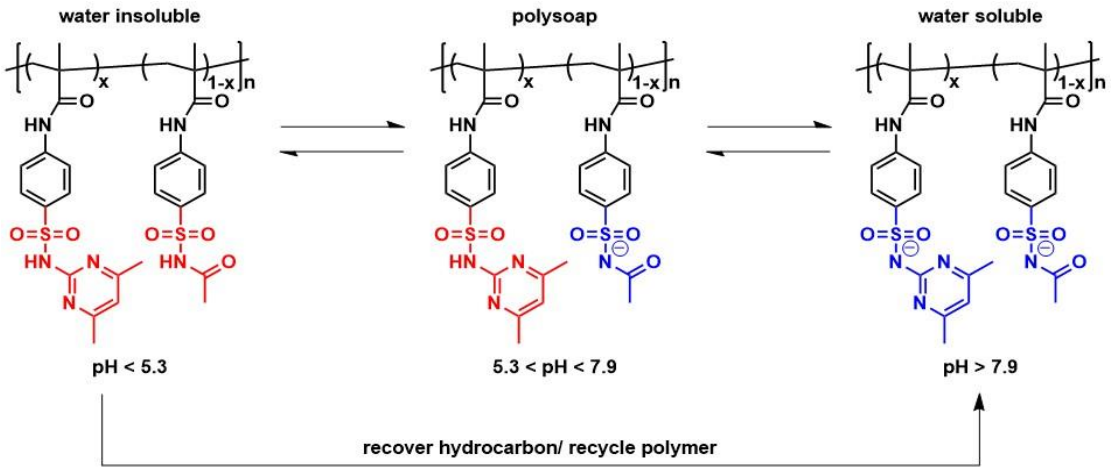

Scheme A.3 Solubility transitions of sulfonamide-based polysoap, poly(mSMZ-stat-mSAC).

Table A.1 Structural Details of poly(mSMZ-stat-mSAC) series.

Sample	Conversion [a]	Targeted mSMZ Content [b]	Experimental mSMZ Content [a]	M_w / kDa [c]	Đ [c]
PS10s	35%	10%	6.20%	72.0	1.04
PS20s	44%	20%	13.4%	70.5	1.05
PS30s	42%	30%	20.0%	71.7	1.10
PS40s	45%	40%	27.4%	83.8	1.13

[a]Monomer conversion and experimental mSMZ content determined by ^{1}H NMR.
[b]Targeted mol % of mSMZ.
[c]Determined by SEC-MALLS.

A.2.2 pH-dependent phase behavior of polysoaps

To determine the pH range of micelle formation, we used dynamic and static light scattering. Figure A.1 shows the static light scattering intensities and hydrodynamic diameters of the polysoaps as a function of pH. As the solution is titrated with HCl, the scattering intensity initially decreases. Near pH 11 a slight drop in Dh is observed for all polymers. This indicates a conformational shift from an expected rod-like polyelectrolyte in solution to a collapsed coil due to the polyelectrolyte effect of added electrolytes to the solution upon titration. As the pH drops even further, eventually a second intensity drop

occurs around pH 8, This likely corresponds to an initial collapse of the polymer into a micelle. As the pH approaches the pK_a of the mSMZ units (7.5), neutralization of the charges becomes more prevalent which drives the start of hydrophobic core domain formation. At this point, when the copolymers form micelles, a steady auto-correlation function emerges during DLS measurements, allowing us to determine the hydrodynamic diameters of the polymeric micelles. All polymers demonstrated micellar behavior at 5.3 < pH < 7.3, with PS40s exhibiting a narrower window (5.5 < pH < 6.5), probably due to its increased hydrophobicity. The polymers display sharp increases in scattering intensity and particle size as the pH approaches the pKa of the mSAC monomer units, indicating aggregation and a change in copolymer solubility. As the pH drops further below 5.3, the polymers fully phase separate and the scattering intensities become orders of magnitude larger.

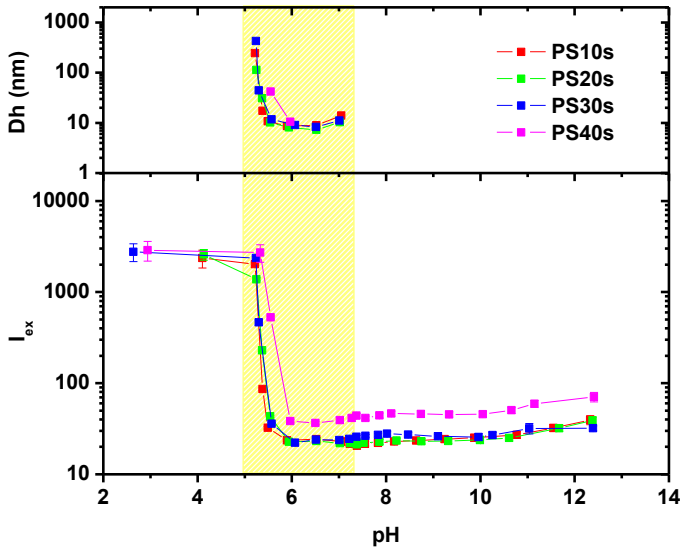

Figure A.1 90° scattering intensity and hydrodynamic diameter dependence on pH at 10 mg/mL of polysoap in water.

A.2.3 Polysoap properties in water at pH 6.5.

A.2.3.1 Dynamic and static light scattering.

The concentration dependent properties of the polymers were probed at pH = 6.5, which lies within the pH range of observed micelle formation ($pH_{micelle}$ = 5.3 – 7.3). Dynamic light scattering was used to probe the hydrodynamic diameter of the particles formed in solution as a function of polymer concentration (Figure A.2). PS10s, PS20s, and PS40s show increased sizes at higher concentrations, indicating concentration dependent multimeric associations. PS30s, however, exhibits a consistent particle size throughout the concentration range probed, suggesting possible unimeric assemblies. Figure A.3 shows the excess scattering intensities (I_{ex}) of the copolymer series as a function of concentration. As is expected, all samples exhibit increasing excess scattering intensities with concentration corresponding well with the DLS data.

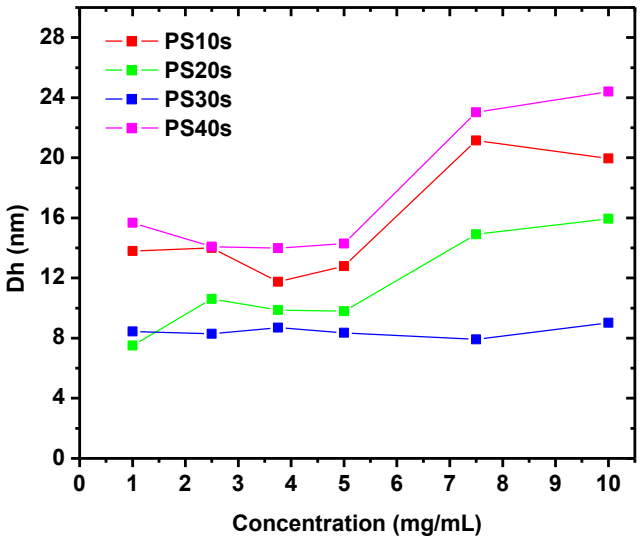

Figure A.2 Hydrodynamic diameter dependence on polysoap concentration as measured by dynamic light scattering at pH = 6.5.

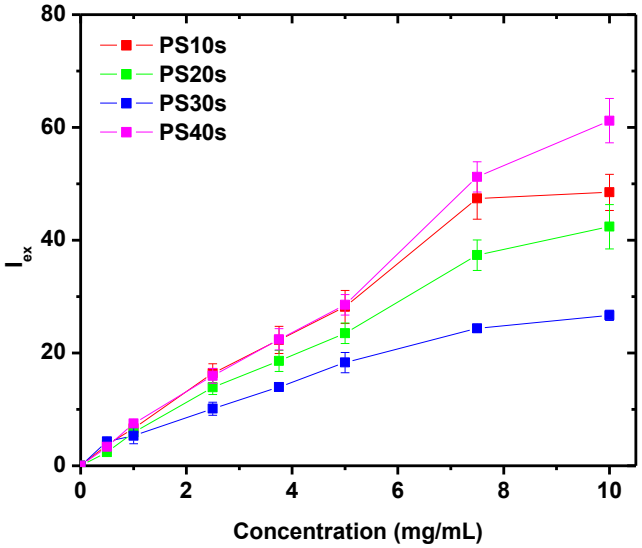

Figure A.3 Excess scattering intensity $I_{ex} = (I_{solu} - I_{solv})/I_{solv})$ dependence on polysoap concentration as measured by static light scattering at 90°. Experiments conducted at solution pH ~ 6.5.

A.2.3.2 UV-absorbance and Fluorescence spectroscopy.

Pyrene was utilized to assess the sequestration properties of the polysoaps. Sodium dodecyl sulfate (SDS) was used as a small molecule surfactant control, and as expected, exhibited no absorbance below its CMC (Figure A.4). All copolymers show absorbance values. The absorbance of PS10s increases linearly up to 10 mg/mL. For PS20s, PS30s, and PS40s the absorbance values initially increase linearly as a function of concentration up to 2.5 mg/mL and then plateau to an absorbance value of ~0.19. Figure A.5 shows the UV-absorbance spectra of the pyrene/polysoap solutions at varying concentrations. The appearance of an excimer peak around 350 nm at higher concentrations is indicative of pyrene excimer formation, which would explain the observed asymptotic trend in the pyrene monomer absorbance.

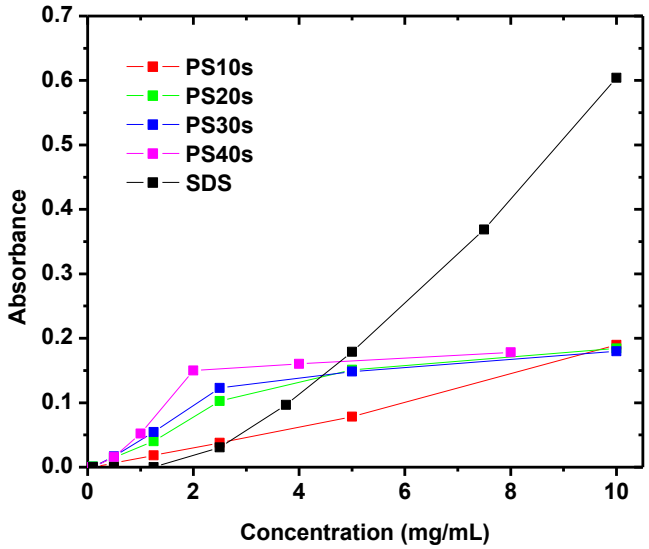

Figure A.4 Pyrene sequestration as measured by UV-absorbance at 338 nm as a function of polysoap concentration for the polysoap series (polysoap samples at pH = 6.5, SDS in DI water as a control).

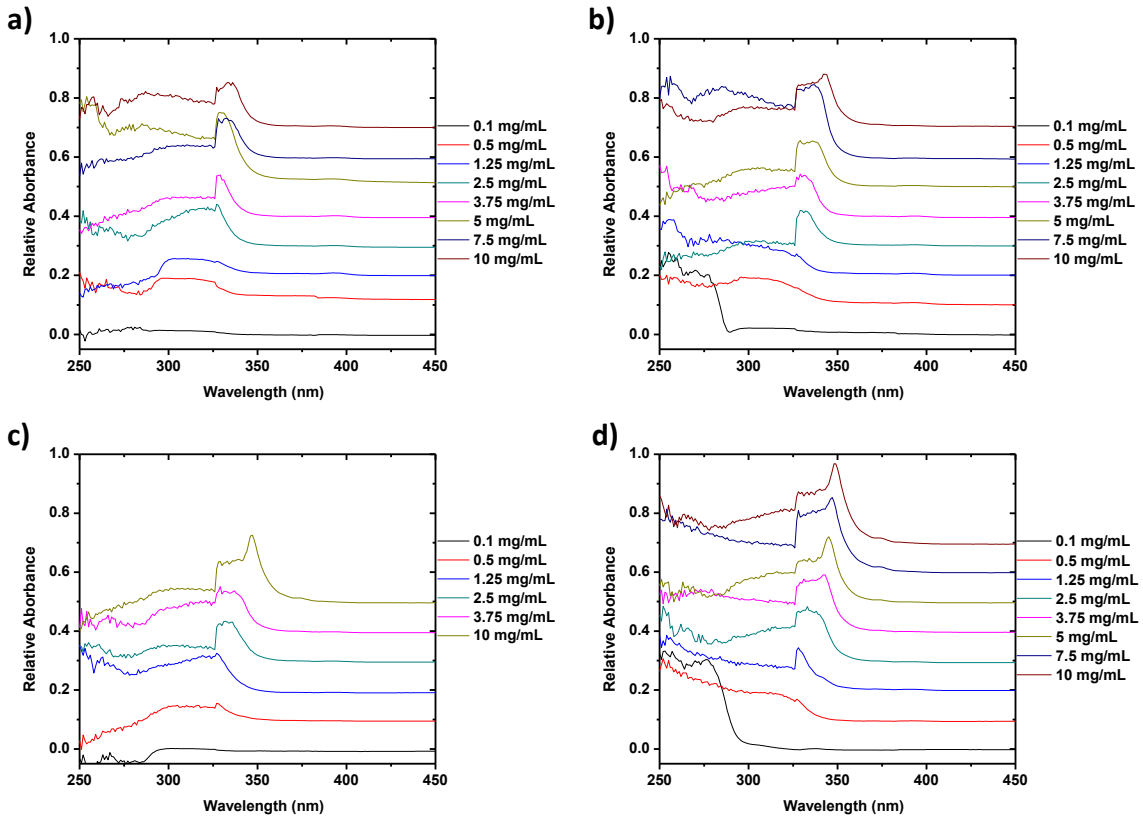

Figure A.5 UV-Absorbance spectra of pyrene/polysoap solutions: a) PS10s; b) PS20s; c) PS30s; d) PS40s.

All copolymers exhibited steady I_3/I_1 ratios above 0.68, demonstrating the presence of a hydrophobic core domain at high dilution and a lack of CMC in these polysoaps (Figure A.6). However, the existence of pyrene excimer limits our ability to probe the environment of the micelle domains at higher concentrations. Additionally, all polymer I_3/I_1 ratios that could be measured show lower values than the SDS micelles, which indicates that the polysoap core domains are very weakly defined. This would explain why such little pyrene is absorbed prior to excimer forming in these systems.

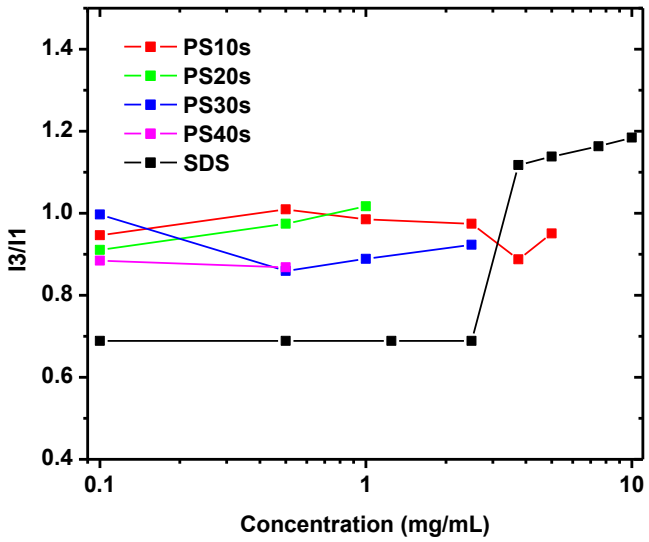

Figure A.6 Probing the hydrophobic domain at varying polysoap concentrations using pyrene I_3/I_1 ratios. (polysoap samples at pH ~6.5, SDS in DI water as a control)

A.2.4 Hydrocarbon removal, recovery, and polysoap recycling.

To assess the capability of the sulfonamide-based polysoaps to remove hydrocarbon from water, the procedure outlined in Scheme A.1 was used. Each polymer (10 mg) was dissolved into a solution of 9-AM (0.1 mM, 1 mL) at pH 6.5. The solutions were then characterized via UV-absorbance spectroscopy. Upon titration with HCl to pH

2.5, the polymers phase-separated and the solutions were centrifuged, allowing for characterization of the supernatant. The supernatant was absent of 9-AM, indicating that the polymer was able to remove the 9-AM upon phase-separation from water. The corresponding data are shown in Figure A.7. After hydrocarbon removal, the supernatant was reintroduced to the polymer pellet and was titrated to pH 10 to fully solubilize the copolymer and to release the hydrocarbon through dissociation of a hydrophobic environment. A small amount of ether (1 mL) was added to extract the hydrocarbon from the water. The decrease in absorbance of the aqueous polymer solution suggests that extraction with ether removed a significant amount of the 9-AM from the aqueous solution. Since the polymer is fully charged, it is insoluble in ether and remains in the water layer. This allows for the polymer to be re-used for further hydrocarbon purification and recovery cycles.

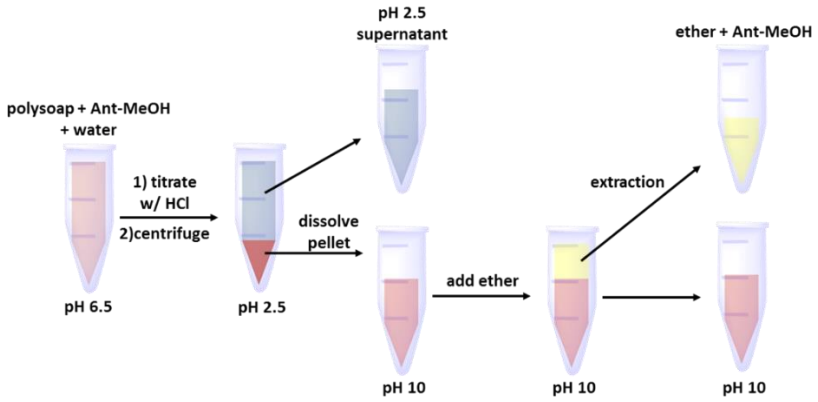

Scheme A.4 Polysoap recycle and hydrocarbon removal experimental description.

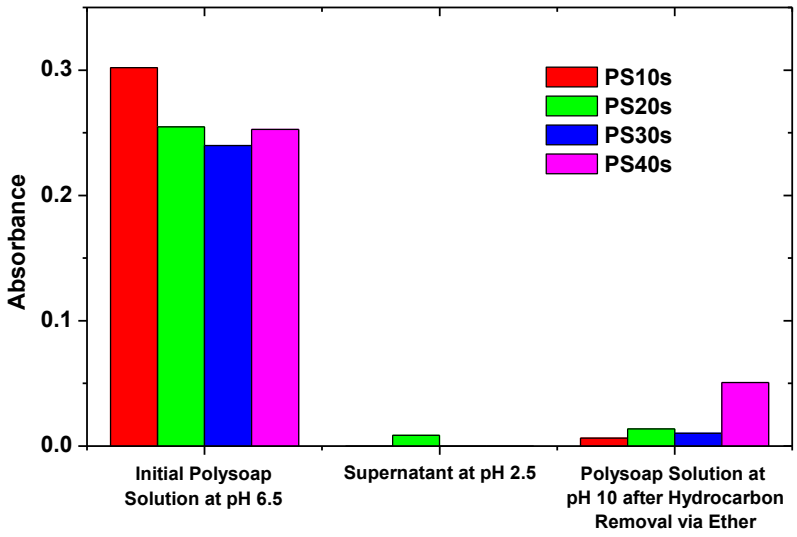

Figure A.7 Absorbance of 9-anthracenemethanol at 384 nm for initial polysoap solution, the supernatant after polymer precipitation and removal, and the polysoap solution at pH 10 after hydrocarbon removal using ether.

A.3 Conclusions.

A series of pH-responsive sulfonamide-based polysoaps have been prepared via RAFT copolymerization and characterized. All polysoap samples form assemblies capable of sequestering hydrophobic molecules in water. These polysoaps show three distinct phase responses by adjusting pH: full water solubility at alkaline pH (>7.3), assembly behavior at pH = 5.3 – 7.3, and phase separation at acidic pH (<5.3). This tri-phasic behavior allows for hydrocarbon sequestration and removal from water followed by hydrocarbon recovery and separation from the copolymer. The copolymer can be recycled, thus offering a potential pathway for improving the efficiency of current oil spill remediation technologies. Further studies may include using other sulfonamide monomer pairs in order to optimize hydrocarbon uptake and micelle behavior.

APPENDIX B - BIOCOMPATIBLE, RESPONSIVE "POLYSOAPS" VIA RAFT COPOLYMERIZATION FOR THE DELIVERY OF HYDROPHOBIC CANCER DRUGS[148]

B.1 Overview.

The research presented in this section (Appendix B) investigates the development of bio-compatible polysoaps that are capable of triggered drug release *in vivo*. To do this, we explore an initial polysoap scaffold that allows for the dissociation of the hydrophobic domain in the presence of the reducing environment of the cell, allowing for triggered intracellular drug release. This first-design will help develop directions for future systems with the potential to uptake, transport, and release hydrophobic cancer therapeutic drugs in the body regardless of delivery vehicle concentration. The copolymers prepared for this research are through the RAFT copolymerization of N-(2-hydroxypropyl) methacrylamide (HPMA) and dodecylpropyldisulfide methacrylamide (DPDMA). The facile synthesis of these polysoaps and their ability to function at high dilution are promising indicators of their utility in future applications.

B.2 Results and discussion.

B.2.1 Structural design of biocompatible polysoaps.

To study the solution properties and feasibility for drug delivery of responsive polysoaps, we prepared two statistical copolymers via the RAFT copolymerization of HPMA and DPDMA (Scheme B.1). The DPDMA monomer was designed to form the hydrophobic domain of the micelles. Additionally, as desired for our polysoap design, the hydrophobic dodecyl disulfide functionality can be reductively cleaved to a thiol, providing for responsive hydrophobic domain dissociation and subsequent payload

release. The HPMA monomer was chosen to form the water-soluble corona of the micelle because it is biocompatible and non-immunogenic. This is important since biocompatibility and a neutral immune response would be necessary for *in vivo* use. Monomer content for this study was based on previous work conducted in our group,[128] which indicated the necessity of sufficient hydrophobic content to form core domains in the micelles. However, since the coronas in our polymeric micelles are neutral, water solubility can be compromised with too high a hydrophobic content. To ensure water solubility and micelle formation, mole percentages of 5 and 10% DPDMA were initially targeted for this work. The resulting copolymers had weight average molecular weights of 37.9 and 33.7kDa and M_w/M_n values of 1.08 and 1.09, respectively (Table B.1). Figure B.1 shows the SEC traces of the polysoap samples. From these traces we observe that the polymerizations result in narrow and unimodal molecular weight distributions, a characteristic that is necessary for preparing well-defined micelles for drug delivery applications.

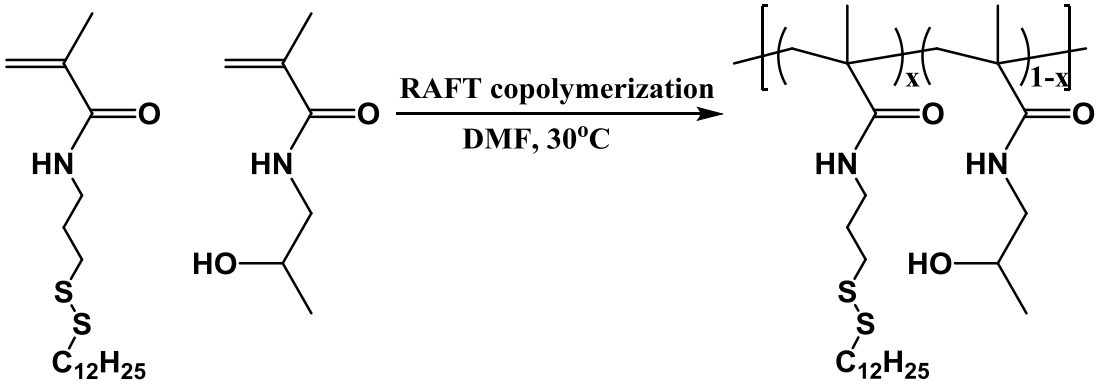

Scheme B.1 Synthesis of biocompatible, responsive polysoap poly(DPDMA-stat-HPMA).

Table B.1 Structural Details of poly(DPDMA-stat-HPMA) series.*

Sample	Conversion [a]	DPDMA Content [a]	M_w / kDa [b]	M_w/M_n
PS5s-s	33%	7.77%	37.9	1.08
PS10s-s	33%	15.4%	33.8	1.06

[a]Determined by ^{1}H NMR.
[b]Determined by SEC-MALS.
*All polymerizations were conducted at 30°C in DMF until desired monomer conversion was achieved.

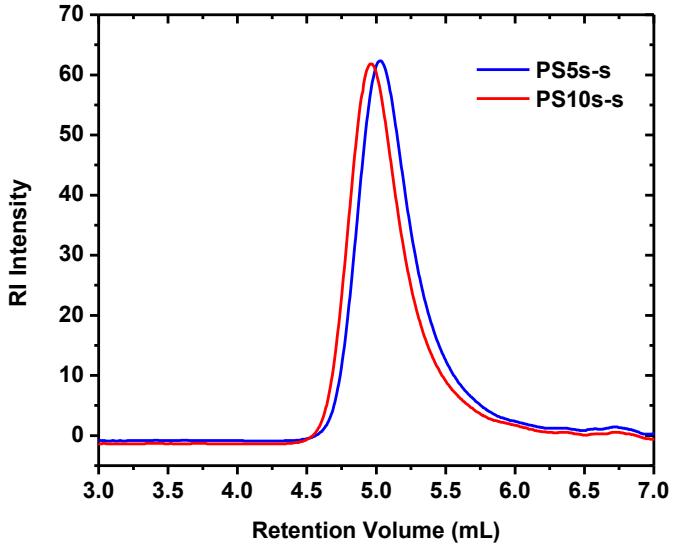

Figure B.1 Size exclusion chromatography (SEC) traces of polysoaps. Eluent 0.05M LiClO4 in MeOH. Flow rate: 0.3 mL/min.

B.2.2 Polysoap properties in water.

B.2.2.1 Dynamic and static light scattering.

Figure B.2 shows the hydrodynamic sizes of the PS5s-s and PS10s-s micelles as a function of copolymer concentration. The size of the PS5s-s sample indicates unimeric assemblies are possibly formed with consistent values of about 11 nm across the concentration range. PS10s-s, however, exhibits larger sizes of around 60 nm, suggesting that multimeric associates are formed based on the measured molecular weight of the

individual polymer chains. This can be attributed to increased hydrophobicity, and, without a charged corona to stabilize the assemblies, electrosterically, inter-core mixing may be prominent at higher hydrophobic contents. Notably, the hydrodynamic diameters of both samples do not increase with concentration, which reveals that these assemblies or micelles are stable at the experimentally measured concentrations and hydrophobic contents.

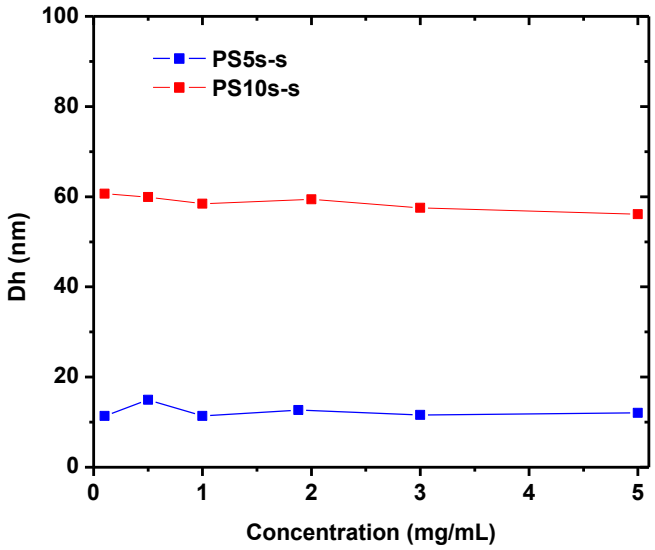

Figure B.2 Hydrodynamic diameter dependence on polysoap concentration in water as measured by dynamic light scattering.

Figure B.3 shows the excess scattering intensity of PS5s-s and PS10s-s solutions as a function of polymer concentration. PS10s-s has consistently higher intensities and a greater slope compared to the PS5s-s. Since scattering intensity scales with the size of a point scatterer, this agrees with the larger particle sizes observed in the DLS experiments for PS10s-s. The scattering intensity of PS5s-s increases linearly with concentration, indicating a consistent aggregation number and size of the copolymers in solution. PS10-

s-s has a slight decrease in slope at higher concentrations which is consistent with the slight decrease in particle size observed in the DLS experiments over the concentration range measured.

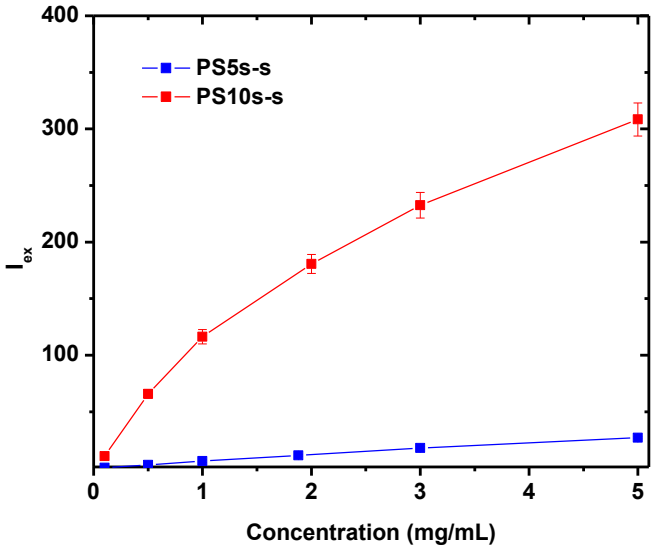

Figure B.3 Scattering intensity dependence on polysoap concentration in water as measured by static light scattering at 90°.

B.2.2.2 Fluorescence and UV-absorbance spectroscopy.

Now that the formation of particles has been confirmed via DLS, the formation of well-defined hydrophobic core domains capable of hydrocarbon uptake was probed. This was accomplished through fluorescence spectroscopy measurements of pyrene in solution with increasing concentration of polysoap. As is shown in Figure B.4, pyrene is sequestered into the hydrophobic core domain of the polysoap micelles. At lower concentrations of 0.1 and 0.5 mg/mL, low I_3/I_1 values indicate the absence of a core domain. As the polysoap concentration increases, the I_3/I_1 ratios approach those of the SDS micelles, indicating a more defined hydrophobic microdomain in the core of the

micelles. This may suggest a CMC for these polysoap samples. Furthermore, it is observed that PS10s-s, with the higher hydrophobic content, exhibits higher ratios than PS5s-s.

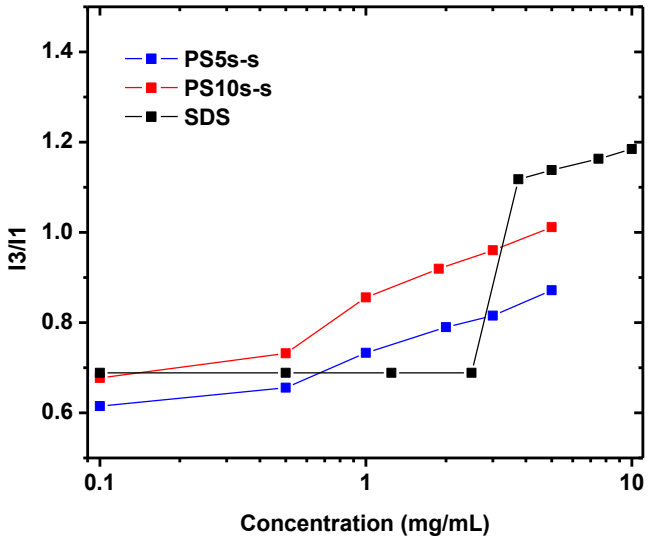

Figure B.4 Probing the hydrophobic domain of the polysoaps at varying concentrations using pyrene I_3/I_1 ratios.

Next, the capacity for hydrocarbon uptake was tested and measured using UV-absorbance spectroscopy. Shown in Figure B.5, the absorbance of pyrene increases with increasing polysoap concentration in deionized water. This demonstrates the ability of the polysoaps to take up hydrocarbon. PS10s-s exhibits a greater uptake efficiency with greater absorbance values compared to PS5s-s. This is in agreement with the increased hydrophobe content and elevated I_3/I_1 ratios observed from the fluorescence experiments.

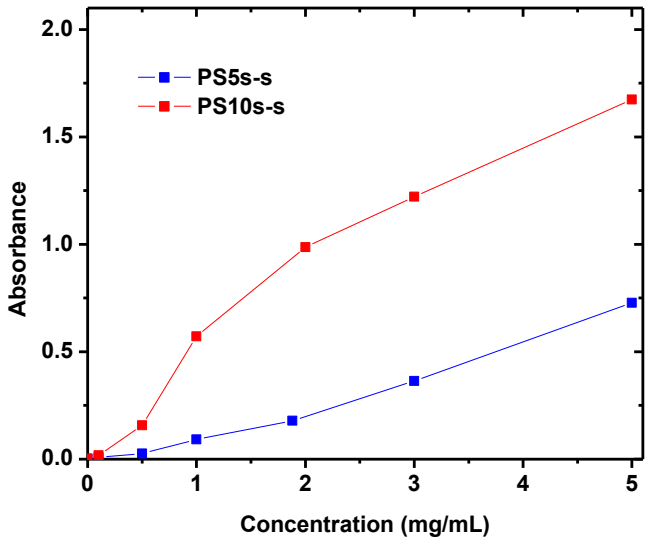

Figure B.5 Pyrene sequestration as measured by UV-absorbance at 338 nm as a function of polysoap concentration.

B.2.3 Hydrocarbon retention and release experiments.

The retention and triggered release of hydrocarbon is essential for effective drug delivery. The polysoaps were studied for their hydrocarbon retention and release in the presence and absence of glutathione as the reducing agent. 9-AM was used as a model hydrophobe capable of partitioning into water to a small extent. This experiment relied on dialysis of the analyte through a membrane that retained the polymer. A signal in the dialysate would indicate hydrocarbon release. As is seen in Figure B.6, the polysoap was sufficient at retaining the hydrocarbon in water. Additionally, glutathione was observed to be ineffective as a reducing agent in the time frame of the experiment, as its addition to solution did not significantly increase the relative absorbance of the hydrophobe in the dialysate. Had the desired release mechanism occurred, the glutathione would have reduced the disulfide bond of the DPDMA units, changing those units to hydrophilic, and

thus disrupting the hydrophobic core domain. This triggered release would of lead to a change of slope in the data in Figure B.6.

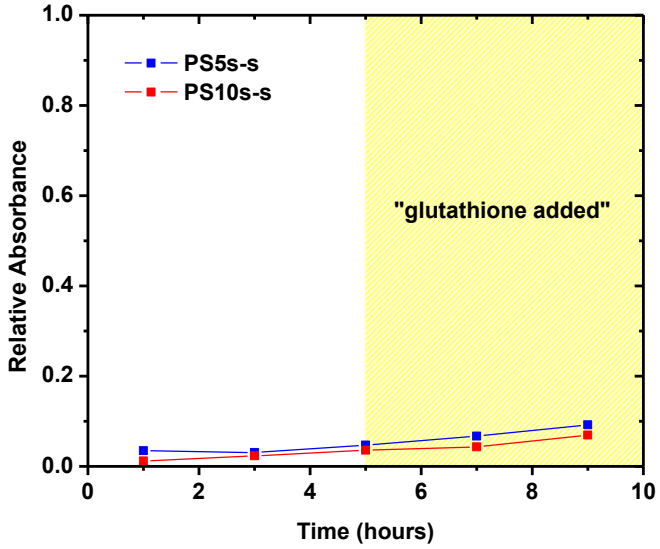

Figure B.6 Absorbance of 9-anthracenemethanol in dialysate via dialysis against water (1 mL of polymer solution, 5 mg/mL).

Retention of the hydrocarbon in the presence of a nonpolar solvent was also examined. Proper utility and circulation of a loaded drug delivery vehicle requires resistance to premature release or leakage of its payload. As partitioning of the payload may occur inside the body to other tissue, it is important to determine if this will occur for our polymers. As is shown in Figure B.7, using ethyl acetate, an organic solvent, premature partitioning of the 9-AM into the organic layer occurs. This is undesired, as the loaded drug delivery vehicle needs to be able to withstand similarly hydrophobic areas in the body, such as in fat tissue that would potentially lead to drug partitioning out of the core domain of the polysoap. Furthermore, the addition of glutathione had no significant effect on the release of hydrophobe, likely due to significant release of hydrophobe prior

to glutathione addition. This illustrates that the current polysoap system must be altered to increase hydrophobic core domain stability and definition to avoid premature partitioning of the hydrophobe from the delivery vehicle by increasing hydrophobe retention in the core.

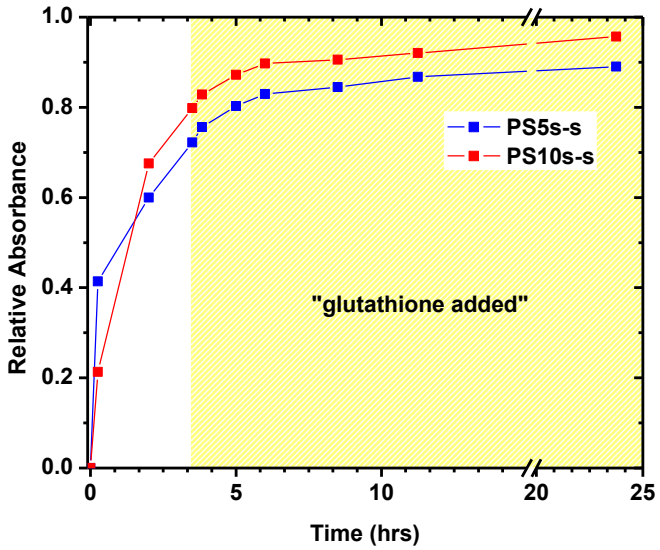

Figure B.7 Absorbance of 9-anthracenemethanol in ethyl acetate (5 mL) via extraction from 5 mL of polymer solution (5 mg/mL).

B.2.4 Cell toxicity.

The cell toxicity of the polysoaps was tested to determine biocompatibility with KB cells. As is seen in Figure B.8, the relative toxicities of the polysoap samples are indistinguishable from the control. Differences in toxicity in this test are within experimental error. Further experiments with larger sample sizes will be required for statistical confirmation of the overall toxicity of our polymers; however, initial experiments conclude that these polysoaps may safely be used *in vitro*.

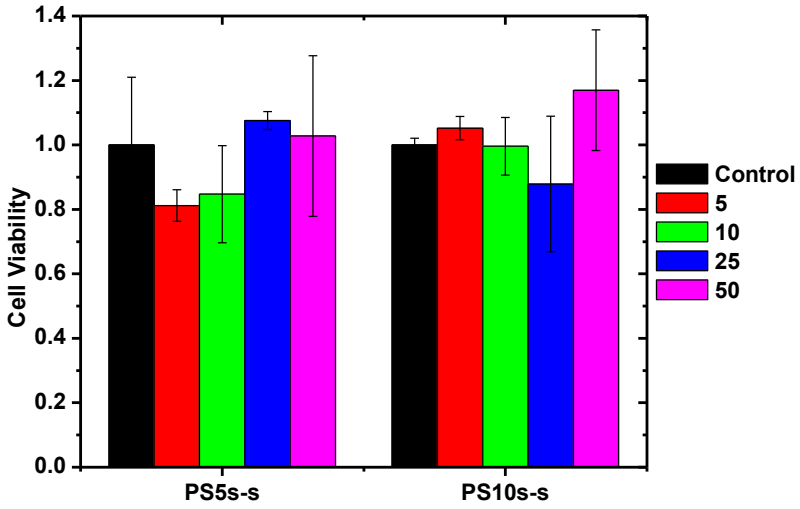

Figure B.8 Cell viability determined via MTT cell assay at different concentrations of polymer sample, in μg/mL.

B.3 Conclusions.

A series of biocompatible, responsive polysoaps was prepared via RAFT copolymerization. As determined by DLS, UV-absorbance, and fluorescence spectroscopy, the polysoaps assemble into in structures capable of sequestering hydrocarbons in water. Hydrocarbon retention experiments indicate that polymeric domains retain 9-AM in water, indicated by relatively small amount of hydrophobe in the dialysate. Furthermore, addition of glutathione to the dialysis solution does not result in the expected release of the hydrocarbon within the time frame of the experiment. This may be due to poor diffusion of the reducing agent to the disulfide bonds. Hydrocarbon partitioning experiments in the presence of ethyl acetate indicate that the polysoaps do not retain the hydrophobe in the presence of organic solvent. This is evidenced by complete partitioning of 9-AM into the organic layer. Additionally, the partitioning does

not require glutathione cleavage of the disulfide linkage. The polysoaps are relatively non-toxic, as determined by negligible changes cell viability as compared to the control. Though the polysoap design is promising for drug delivery based on efficient hydrocarbon uptake and biocompatibility, further studies and alterations to the structural design will be necessary to optimize hydrocarbon retention and triggered release for such applications.

APPENDIX C – SUPPLEMENTARY INFORMATION

C.1 Pertinent chemical structures.

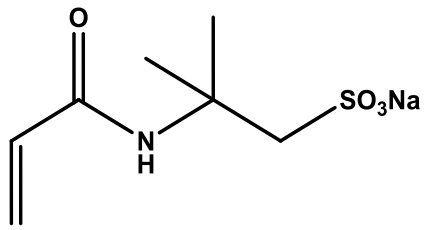

1

Figure C.1 2-Acrylamido-2-methylpropane sulfonic acid (AMPS).

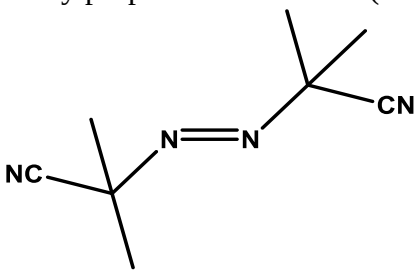

2

Figure C.2 azobisisobutyronitrile (AIBN).

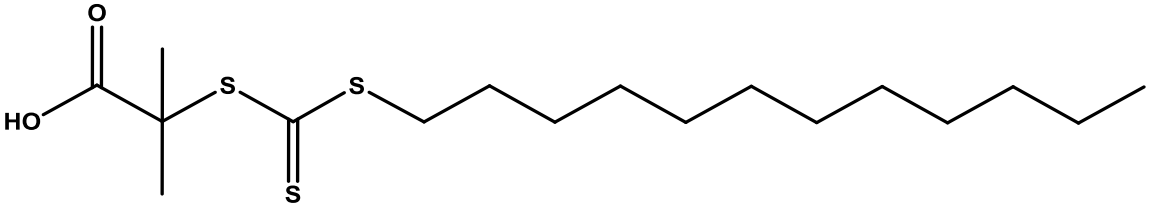

3

Figure C.3 2-dodecylsulfanylthiocarbonylsulfanyl-2-methyl propionic acid (DMP).

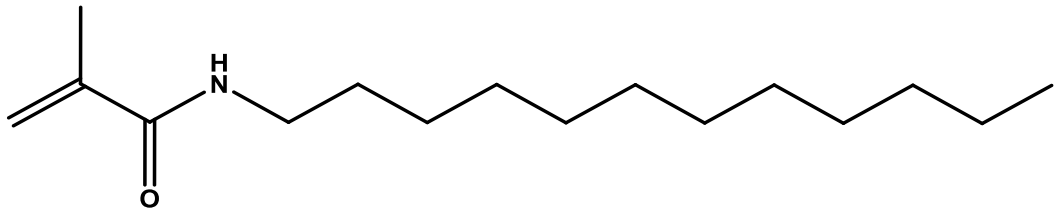

4

Figure C.4 Dodecylacrylamide (DDAM) chemical structure and ^{1}H-NMR.

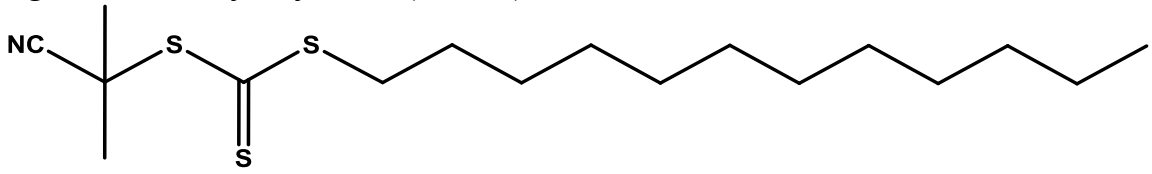

5

Figure C.5 2-Cyano-2-propyl dodecyl trithiocarbonate (CPDT).

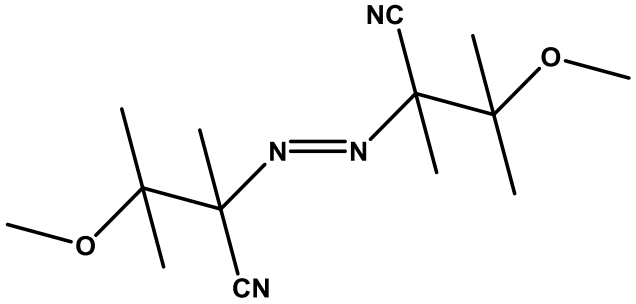

6

Figure C.6 2,2′-Azobis(4-methoxy-2,4-dimethylvaleronitrile) (V-70).

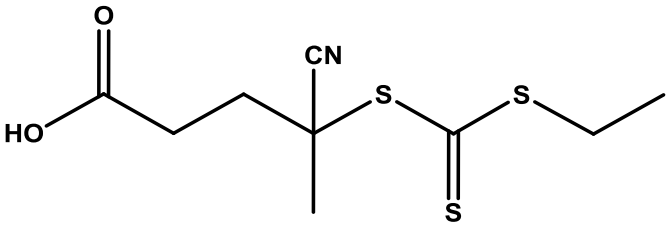

7

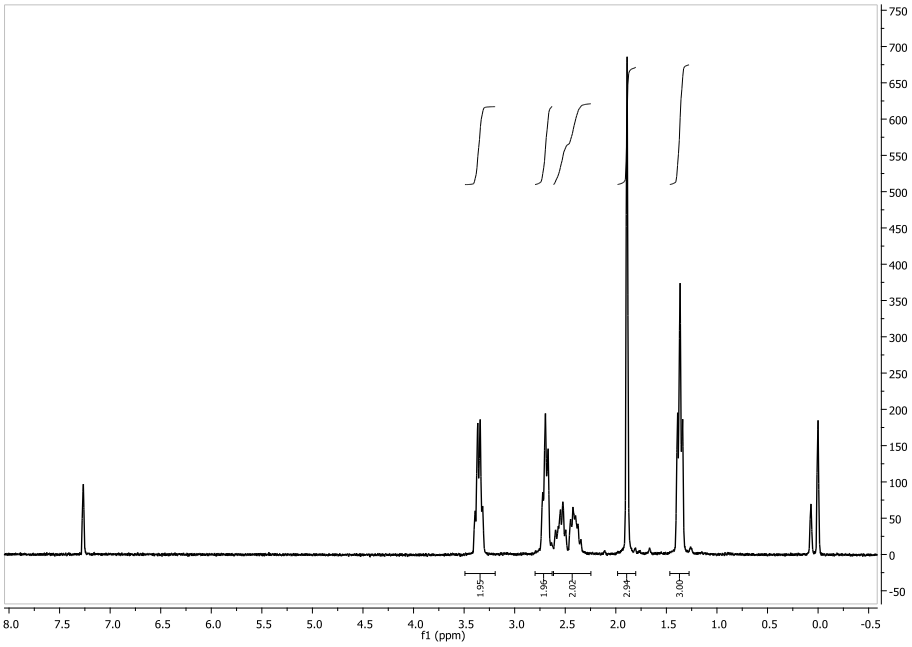

Figure C.7 4-cyano-4-(ethylsulfanylthiocarbonylsulfanyl)pentanoic acid (CEP) chemical structure and 1H-NMR.

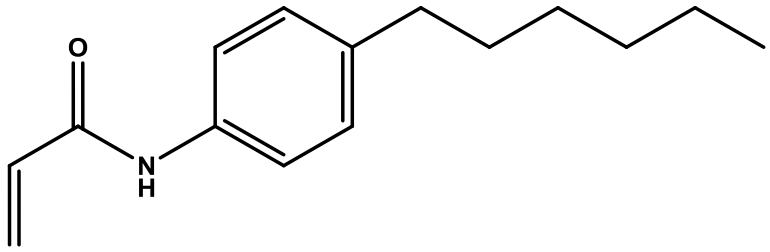

8

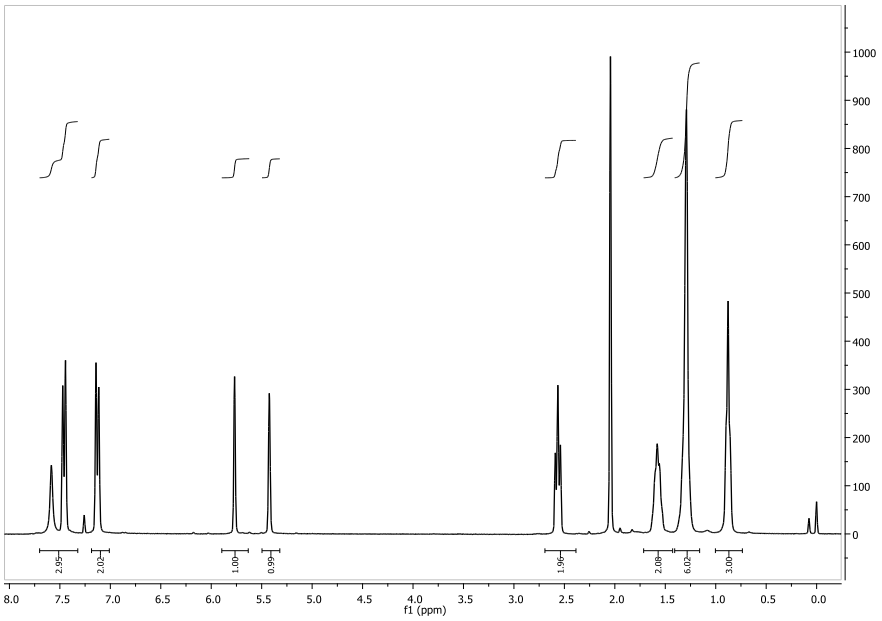

Figure C.8 4-Hexylphenyl Methlyacrylamide (4HPhMA) chemical structure and 1H-NMR.

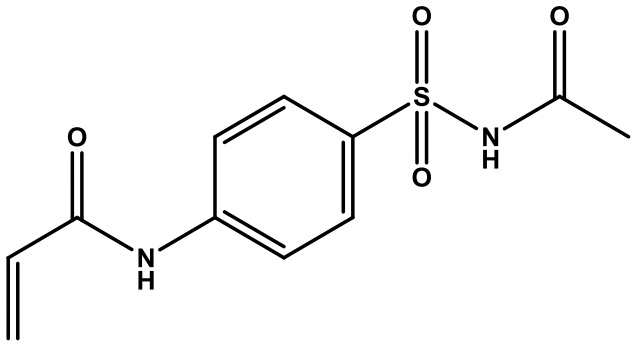

9

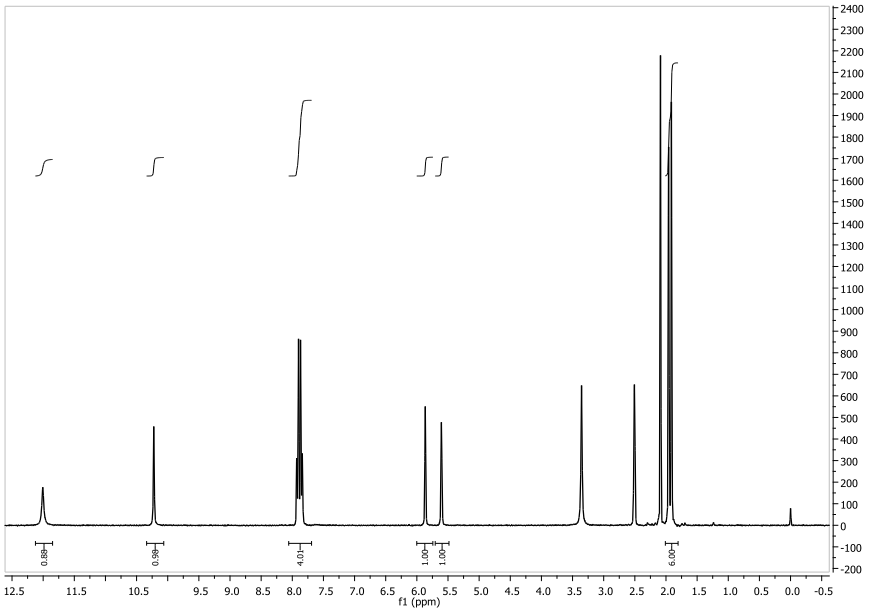

Figure C.9 Methacryloyl Sulfacetamide (mSAC) chemical structure and 1H-NMR.

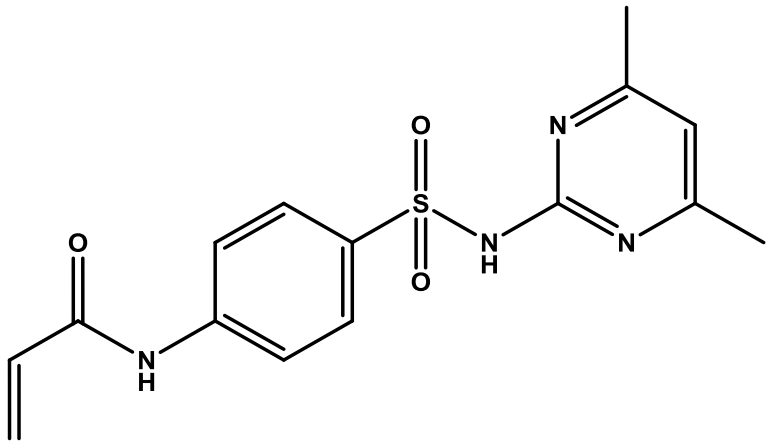

10

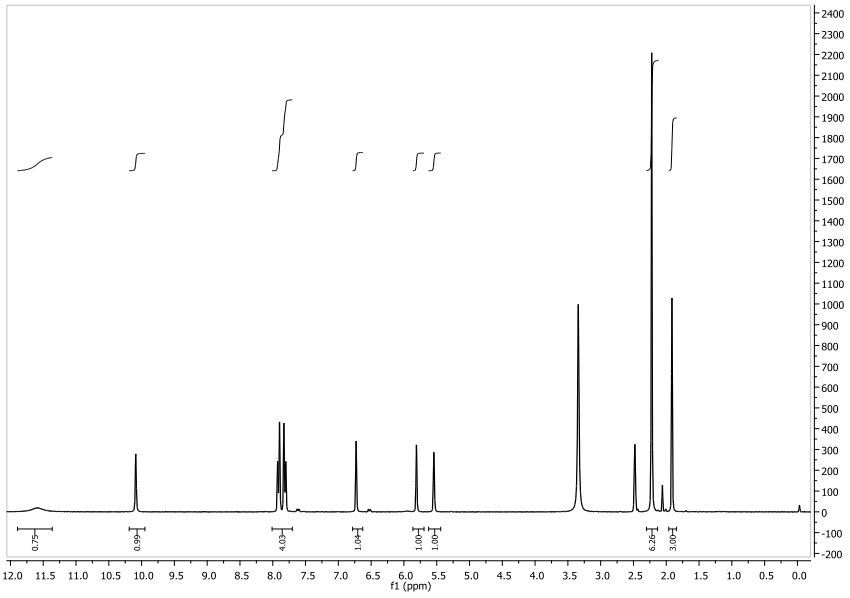

Figure C.10 Methacryloyl Sulfamethazine (mSMZ) chemical structure and 1H-NMR.

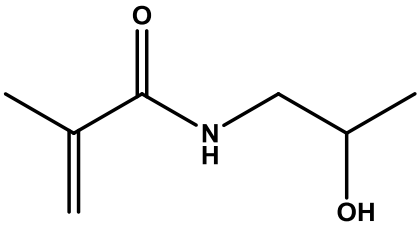

11

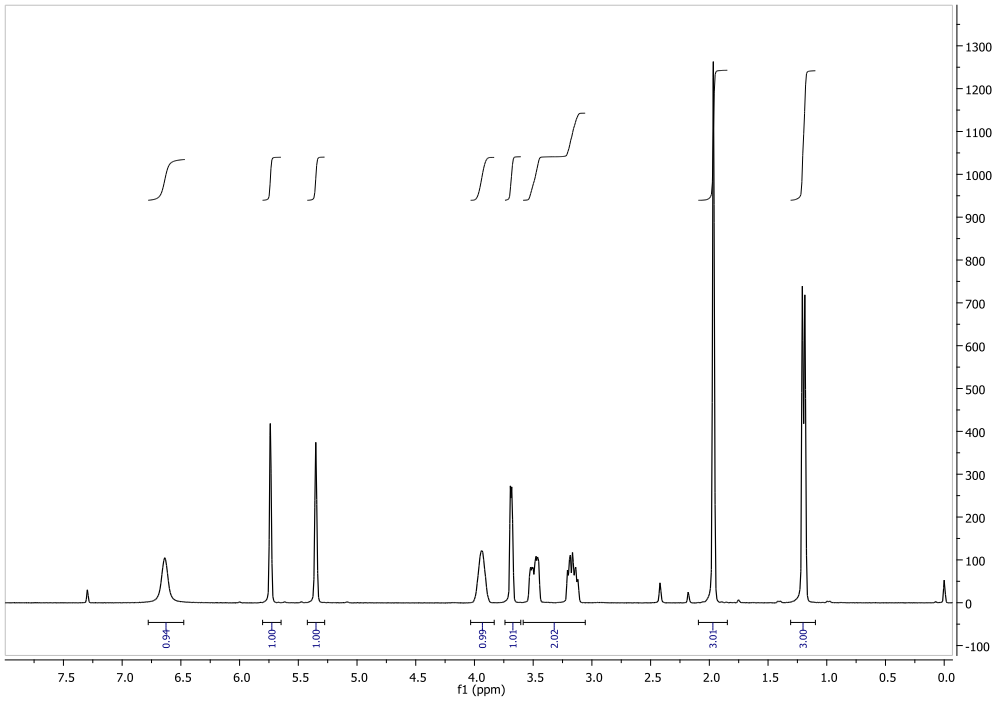

Figure C.11 N-(2-hydroxypropyl)methacrylamide (HPMA) chemical structure and 1H-NMR.

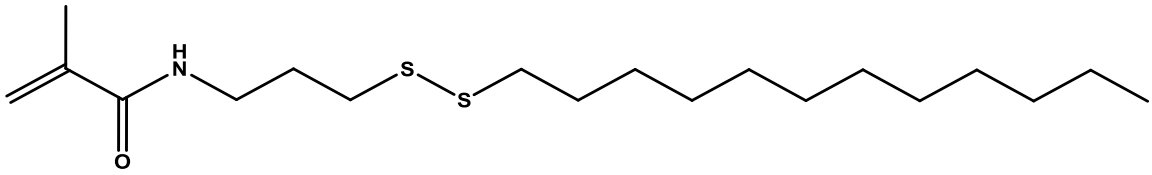

12

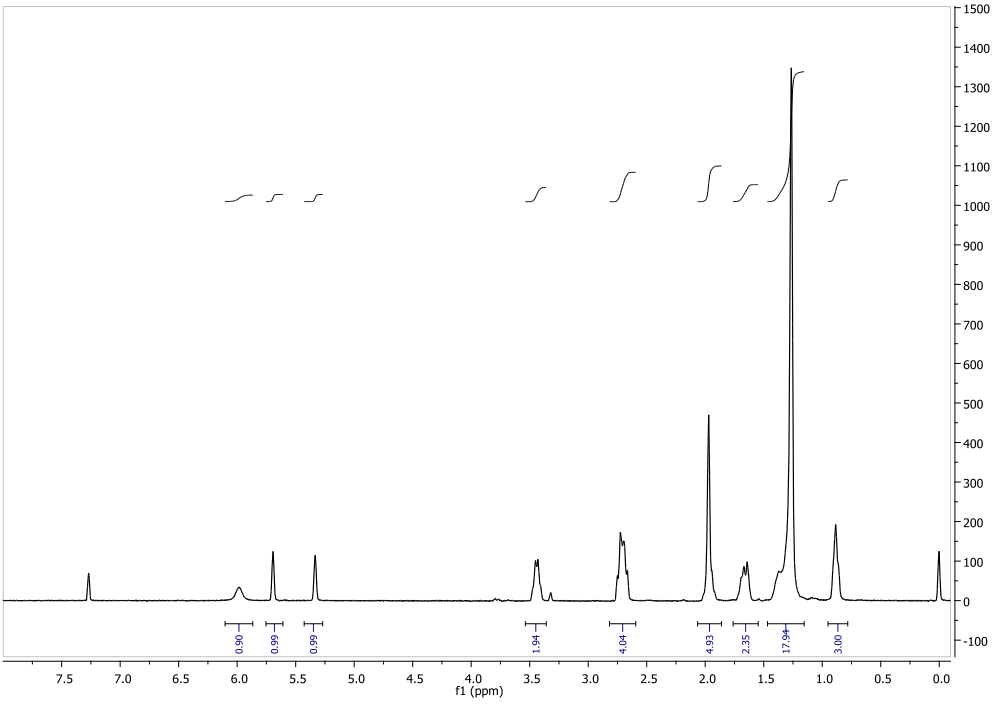

Figure C.12 (dodecylpropyldisulfide)methacrylamide (DPDMA) chemical structure and 1H-NMR.

REFERENCES

(1) Domínguez, A.; Fernández, A.; González, N.; Iglesias, E.; Montenegro, L. *J. Chem. Ed.* **1997**, *74*, 1227–1231.

(2) Chatterjee, a.; Moulik, S. P.; Sanyal, S. K.; Mishra, B. K.; Puri, P. M. *J. Phys. Chem. B* **2001**, *105*, 12823–12831.

(3) Schick, B. Y. M. J. *J. Phys. Chem.* **1963**, *67*, 1796–1799.

(4) Laschewsky, A. *Adv. Polym. Sci.* **1995**, *124*, 1–86.

(5) Abraham, M. H. *J. Am. Chem. Soc.* **1982**, *104*, 2085–2094.

(6) Rosen, M. J.; Liu, L. *J. Am. Oil Chem. Soc.* **1996**, *73*, 885–890.

(7) Frank, H. S.; Evens, M. W. *J. Chem. Phys.* **1945**, *13*, 507–532.

(8) Phillips, J. N. *Transf. Faradays Scociety* **1954**, *51*, 561–569.

(9) Sugihara, G.; Hisatomi, M. *J. Colloid Interface Sci.* **1999**, *219*, 31–36.

(10) Matijevio, E.; Pethica, A. *Transf. Faradays Scociety* **1957**, *54*, 587–592.

(11) Griffin, W. C. *J. Soc. Cosmet. Chem.* **1949**, *1*, 311–326.

(12) Schott, H. *J. Pharm. Sci.* **1995**, *84*, 1215–1222.

(13) Gadhave, A. *Int. J. Sci. Res.* **2014**, *3*, 573–575.

(14) *The HLB System a time-saving guide to emulsifier selection*; Chemmunique, Ed.; ICI Americas Inc.: Wilmington, Delaware 19897, 1976.

(15) Schott, H. *J. Colloid Interface Sci.* **1989**, *133*, 527–529.

(16) Davies, J. In *Proceedings of 2nd International Congress Surface Activity*; Butterworths, London, 1957; pp 426–438.

(17) Kumthekar, K. R. Studies in Mixed Surfactant Systems and Oil Emulsions, Institute of Chemical Technology, Mumbai, 2012.

(18) Alexandridis, P. *Curr. Opin. Colloid Interface Sci.* **1996**, *1*, 490–501.

(19) Liu, S.; Armes, S. P. *Curr. Opin. Colloid Interface Sci.* **2001**, *6*, 249–256.

(20) Winnik, M.; Yekta, A. *Curr. Opin. Colloid Interface Sci.* **1997**, *2*, 424–436.

(21) Kwon, G. S.; Kataokab, K. *Adv. Drug Deliv. Rev.* **1995**, *16*, 295–309.

(22) Riess, G.; Labbe, C. *Macromol. Rapid Commun.* **2004**, *25*, 401–435.

(23) York, A. W.; Kirkland, S. E.; McCormick, C. L. *Adv. Drug Deliv. Rev.* **2008**, *60*, 1018–1036.

(24) Kikuchi, A.; Nose, T. *Macromolecules* **1996**, *29*, 6770–6777.

(25) Laukkanen, A.; Valtola, L. *Polymer* **2005**, *46*, 7055–7065.

(26) Mizusaki, M.; Morishima, Y.; Winnik, F. M. *Macromolecules* **1999**, *32*, 4317–4326.

(27) Yamamoto, H.; Morishima, Y. *Macromolecules* **1999**, *32*, 7469–7475.

(28) Riess, G. *Prog. Polym. Sci.* **2003**, *28*, 1107–1170.

(29) McCormick, C. L.; Sumerlin, B. S.; Lokitz, B. S.; Stempka, J. E. *Soft Matter* **2008**, *4*, 1760–1773.

(30) Zhou, Y.; Yan, D. *Chem. Commun.* **2009**, 1172–1188.

(31) Dai, S.; Ravi, P.; Tam, K. C. *Soft Matter* **2008**, *4*, 435.

(32) Zhou, J.; Wang, L.; Ma, J. *Des. Monomers Polym.* **2009**, *12* (1), 19–41.

(33) Strauss, U. P.; Jackson, E. G. *J. Polym. Sci.* **1950**, *6*, 649–659.

(34) Jackson, E. G.; Strauss, U. P. *J. Polym. Sci.* **1951**, *7*, 473–484.

(35) Strauss, U. P.; Williams, B. L. *J. Phys. Chem.* **1961**, *65*, 1390–1395.

(36) Borisov, V. *Langmuir* **1995**, *11*, 2911–2919.

(37) Morishima, Y.; Nomura, S.; Ikeda, T.; Seki, M.; Kamachi, M. *Macromolecules*

1995, *28*, 2874–2881.

(38) Strauss, U. P.; Schlesinger, M. S. *J. Phys. Chem.* **1978**, *82*, 571–574.

(39) Vuillaume, P. Y.; Galin, J.; Bazuin, C. G. *Macromolecules* **2001**, *34*, 859–867.

(40) Cochin, D.; Schryver, F. C. De; Stam, J. Van. *Langmuir* **2001**, *17*, 2579–2584.

(41) Cooper, J. E.; Corpoi, D. *J. Polym. Sci. Part A Polym. Chem.* **1971**, *9*, 2361–2369.

(42) Kramer, M. C.; Steger, J. R.; Hu, Y.; McCormick, C. L. *Macromolecules* **1996**, *29*, 1992–1997.

(43) Jaeger, W.; Wendler, U.; Lieske, A.; Bohrisch, J. *Langmuir* **1999**, *15*, 4026–4032.

(44) Laschewsky, A.; Marsat, J.-N.; Skrabania, K.; von Berlepsch, H.; Bottcher, C. *Macromol. Chem. Phys.* **2010**, *211*, 215–221.

(45) Science, P.; Mississippi, S.; Station, S. *Macromolecules* **1994**, *27*, 2151–2158.

(46) Hashidzume, A.; Kawaguchi, A.; Tagawa, A.; Hyoda, K.; Sato, T. *Macromolecules* **2006**, *39*, 1135–1143.

(47) Hu, Y.; Smith, G. L.; Richardson, M. F.; McCormick, C. L. *Macromolecules* **1997**, *30*, 3526–3537.

(48) Smith, G. L.; McCormick, C. L. *Langmuir* **2001**, *17*, 1719–1725.

(49) Smith, G. L.; McCormick, C. L. *Macromolecules* **2001**, *34*, 5579–5586.

(50) Sato, Y.; Hashidzume, A.; Morishima, Y. *Macromolecules* **2001**, *34*, 6121–6130.

(51) Chang, Y.; McCormick, C. L. *Polymer* **1994**, *35*, 3503–3512.

(52) Kathmann, E. E.; White, L. A.; McCormick, L. *Polymer* **1997**, *38*, 879–886.

(53) Morimoto, H.; Hashidzume, A.; Morishima, Y. *Polymer* **2003**, *44*, 943–952.

(54) Morikawa, H.; Morishima, Y.; Motokucho, S.; Morinaga, H.; Nishida, H.; Endo, T. *J. Polym. Sci. Part A Polym. Chem.* **2007**, *45*, 5022–5030.

(55) Chang, Y.; McCormick, C. L. *Macromolecules* **1993**, *26*, 6121–6126.

(56) Hu, Y.; Kramer, M. C.; Boudreaux, C. J.; McCormick, C. L. *Macromolecules* **1995**, *28*, 7100–7106.

(57) Mizusaki, M.; Morishima, Y.; Raju, B. B.; Winnik, F. M. *Eur. Phys. J.* **2001**, *5*, 105–115.

(58) Hu, Y.; Armentrout, R. S.; McCormick, C. L. *Macromolecules* **1997**, *30*, 3538–3546.

(59) Armentrout, R. S.; McCormick, C. L. *Macromolecules* **2000**, *33*, 419–424.

(60) Armentrout, R. S.; McCormick, C. L. *Macromolecules* **2000**, *33*, 2944–2951.

(61) Kathmann, E. E.; White, L. A.; McCormick, L. *Polymer* **1997**, *38*, 871–878.

(62) Mainz, J. G. U. *Macromolecules* **1991**, *24*, 1678–1686.

(63) Binana-Limbele, W.; Zana, R. *Macromolecules* **1990**, *23*, 2731–2739.

(64) Binana-Limbele, W.; Zana, R. *Macromolecules* **1987**, *20*, 1331–1335.

(65) Anghela, D. F.; Alderson, V.; Winnik, F. M. *Polymer* **1998**, *39*, 3035–3044.

(66) Zana, R.; Anthony, O. *Macromolecules* **1994**, *27*, 3885–3891.

(67) Strauss, U. P.; Vasnaver, G. *J. Phys. Chem.* **1975**, *79*, 2426–2429.

(68) Ezell, R. G.; Lowe, A. B.; McCormick, C. L. In *Polyelectrolytes and Polyzwitterions: Synthesis, Properties, and Applications*; 2006; pp 47–63.

(69) Lowe, Andrew, B.; McCormick, C. In *Stimuli-Responsive Water-Soluble and Amphiphilic Polymers*; McCormick, C. L., Ed.; American Chemical Society, 2001; pp 1–13.

(70) Morishima, Y.; Takashi, N.; Kohji, T. *Molecular Interactions and Time-Space Organization in Macromolecular Systems*; Springer-Verlag Berlin Heidelberg:

Osaka, Japan, 1999.

(71) Lowe, A. B.; McCormick, C. L. *Chem. Rev.* **2002**, *102*, 4177–4189.

(72) Winnik, F. M. *Chem. Rev.* **1993**, *93*, 587–614.

(73) Hsu, J. L.; Strauss, U. P. *J. Phys. Chem.* **1987**, *91*, 6238–6241.

(74) Straws, U. P.; Barbieri, B. W. *Macromolecules* **1982**, *15*, 1347–1349.

(75) Anton, P.; Kdberle, P.; Laschewsky, A. *Makromol. Chem* **1993**, *194*, 1–27.

(76) Note, C. Influence of Hydrophobically Modified Polyelectrolytes on Nanoparticle Synthesis in Self-Organized Systems and in Water, 2006.

(77) Kotz, J.; Kosmella, S.; Beitz, T. *Prog. Polym. Sci.* **2001**, *26*, 1199–1232.

(78) Guillet, J. E.; Rendall, W. A. *Macromolecules* **1986**, *19*, 224–230.

(79) Hamad, E.; Qutubuddin, S. *J. Chem. Phys.* **1992**, *96*, 6222–6228.

(80) Hamad, E.; Qutubuddin, S. *Macromolecules* **1990**, *23*, 4185–4191.

(81) Morishima, Y. *ACS Symposium Series 937: Polyelectrolytes and Polyzwitterions: Synthesis, Properties, and Applications*; Lowe, A. B., McCormick, C. L., Eds.; American Chemical Society: Washington, DC, 2006.

(82) Hashidzume, A.; Noda, T.; Morishima, Y. *ACS Symposium Series 780: Stimuli-Responsive Water Soluble and Amphiphilic Polymers*; McCormick, C. L., Ed.; American Chemical Society: Washington, DC, 2001.

(83) Semenov, A. N.; Joanny, J. F.; Khokhlov, A. R. *Macromolecules* **1995**, *28*, 1066–1075.

(84) Halperin, A. *Macromolecules* **1991**, *24*, 1418–1419.

(85) Tominaga, Y.; Mizuse, M.; Hashidzume, A.; Morishima, Y.; Sato, T. *J. Phys. Chem.* **2010**, *114*, 11403–11408.

(86) Morishima, Y. *Chinese J. Polym. Sci.* **2000**, *18*, 323–336.

(87) Blanazs, A.; Armes, S. P.; Ryan, A. J. **2009**, 267–277.

(88) Voets, I. K.; de Keizer, A.; Cohen Stuart, M. a. *Adv. Colloid Interface Sci.* **2009**, *147–148*, 300–318.

(89) McCormick, C. L.; Lowe, Andrew, B. *Polyelectrolytes and Polyzwitterions: Synthesis, Properties, and Applications*, Symposium.; American Chemical Society: Washington, DC, 2006.

(90) Perry, S. L.; Yue, L.; Dimitrios, P.; Lorraine, L.; Matthew, T. *Polymers (Basel).* **2014**, 1756–1772.

(91) Yang, H.; Zheng, Q.; Cheng, R. *Colloids Surfaces A Physicochem. Eng. Asp.* **2012**, *407*, 1–8.

(92) Wang, F.; Yang, J.; Zhao, J. *Polym Int* **2015**, *64*, 999–1005.

(93) Smith, A. E.; Xu, X.; McCormick, C. L. *Prog. Polym. Sci.* **2010**, *35*, 45–93.

(94) Gandhi, A.; Paul, A.; Sen, S. O.; Sen, K. K. *Asian J. Pharm. Sci.* **2015**, *10*, 99–107.

(95) Abel, B. A.; Sims, M. B.; McCormick, C. L. *Macromolecules* **2015**, *48*, 5487–5495.

(96) Wang, J.; Matyjaszewski, K. *J. Am. Chem. Soc.* **1995**, *117*, 5614–5615.

(97) Lowe, A. B.; McCormick, C. L. *Prog. Polym. Sci.* **2007**, *32*, 283–351.

(98) Moad, G.; Rizzardo, E.; Thang, S. H. *Aust. J. Chem.* **2009**, *62*, 1402.

(99) Moad, C. L.; Moad, G.; Rizzardo, E.; Thang, S. H. *Macromolecules* **1996**, *29*, 7717–7726.

(100) McCormick, C. L.; Lowe, A. B. *Acc. Chem. Res.* **2004**, *37*, 312–325.

(101) Van Den Dungen, E. T. A.; Matahwa, H.; McLeary, J. B.; Sanderson, R. D.; Klumperman, B. *J. Polym. Sci. Part A Polym. Chem.* **2008**, *46*, 2500–2509.

(102) Barner-Kowollik, C.; Buback, M.; Charleux, B.; Coote, M. L.; Drache, M.; Fukuda, T.; Goto, A.; Klumperman, B.; Lowe, A. B.; Mcleary, J. B.; Moad, G.; Monteiro, M. J.; Sanderson, R. D.; Tonge, M. P.; Vana, P.; Marie, P. *J. Polym. Sci. Part A Polym. Chem.* **2006**, *44*, 5809–5831.

(103) Chiefari, J.; Mayadunne, R. T. A.; Moad, C. L.; Moad, G.; Rizzardo, E.; Postma, A.; Skidmore, M. A.; Thang, S. H. *Macromolecules* **2003**, *36*, 2273–2283.

(104) Chong, B. Y. K.; Krstina, J.; Le, T. P. T.; Moad, G.; Postma, A.; Rizzardo, E.; Thang, S. H. *Macromolecules* **2003**, *36*, 2256–2272.

(105) Goto, A.; Hirai, N.; Wakada, T.; Nagasawa, K.; Tsujii, Y.; Fukuda, T. *Macromolecules* **2008**, *41*, 10–13.

(106) Strube, O. I.; Nothdurft, L.; Drache, M.; Schmidt-Naake, G. *Macromol. Chem. Phys.* **2011**, *212*, 574–582.

(107) Lowe, A. B.; Sumerlin, B. S.; McCormick, C. L. *Polymer* **2003**, *44*, 6761–6765.

(108) Bruheim, P.; Bredholt, H.; Eimhjellen, K. *Appl. Environ. Microbiol.* **1999**, *65*, 1658–1661.

(109) Celik, G. Y.; Aslim, B.; Beyatli, Y. *J. Environ. Biol.* **2008**, *29*, 867–870.

(110) Camilli, R.; Reddy, C. M.; Yoerger, D. R.; Van Mooy, B. A. S.; Jakuba, M. V; Kinsey, J. C.; McIntyre, C. P.; Sylva, S. P.; Maloney, J. V. *Science* **2010**, *330*, 201–204.

(111) White, H. K.; Hsing, P.-Y.; Cho, W.; Shank, T. M.; Cordes, E. E.; Quattrini, A. M.; Nelson, R. K.; Camilli, R.; Demopoulos, A. W. J.; German, C. R.; Brooks, J.

M.; Roberts, H. H.; Shedd, W.; Reddy, C. M.; Fisher, C. R. *Proc. Natl. Acad. Sci. U. S. A.* **2012**, *109*, 20303–20308.

(112) Stackelberg, P. E.; Furlong, E. T.; Meyer, M. T.; Zaugg, S. D.; Henderson, A. K.; Reissman, D. B. *Sci. Total Environ.* **2004**, *329*, 99–113.

(113) Stehle, S.; Schulz, R. *PNAS* **2015**, *112*, 5750–5755.

(114) Ying, G.; Kookana, R. S.; Ru, Y. *Environ. Int.* **2002**, *28*, 545–551.

(115) Meyer, B.; Pailler, J.-Y.; Guinard, C.; Hoffmann, L.; Krein, A. *Env. Monit Assess* **2011**, *180*, 127–146.

(116) Celino, J. J.; Corseuil, H. X.; Fernandes, M.; Garcia, K. S. *Rev. Esc. Minas* **2010**, *63*, 211–218.

(117) Niño, L. R.; Torres, R. J.; Mozeto, A. A.; Fadini, P. S. *Polycycl. Aromat. Compd.* **2014**, *34*, 37–41.

(118) Hartmann, J.; Beyer, R.; Harm, S. *Environ. Process* **2014**, *1*, 87–94.

(119) Ciesielczuk, T.; Kusza, G.; Poluszynska, J.; Kochanowska, K. *Water Air Soil Pollut* **2014**, *225*, 2145.

(120) Lau, E. Von; Gan, S.; Ng, H. K.; Poh, P. E. *Environ. Pollut.* **2014**, *184*, 640–649.

(121) Brette, F.; Shiels, H. A.; Galli, G. L. J.; Cros, C.; Incardona, J. P.; Scholz, N. L.; Block, B. A. *Sci. Rep.* **2017**, *7*, 41476.

(122) Flotron, V.; Delteil, C.; Bermond, A.; Camel, V. *Polycycl. Aromat. Compd.* **2003**, *23*, 353–376.

(123) Andersen, H.; Siegrist, H.; Halling-Sorensen, B.; Ternes, T. A. *Environ. Sci. Technol.* **2003**, *37*, 4021–4026.

(124) Gogate, P. R.; Pandit, A. B. *Adv. Environ. Res.* **2004**, *8*, 553–597.

(125) Sonune, A.; Ghate, R. *Desalination* **2004**, *167*, 55–63.

(126) Lai, J. T.; Filla, D.; Shea, R. *Macromolecules* **2002**, *35*, 6754–6756.

(127) Thomas, D. B.; Convertine, A. J.; Hester, R. D.; Lowe, A. B.; McCormick, C. L. *Macromolecules* **2004**, *37*, 1735–1741.

(128) Wan, W.-M.; Pickett, P. D.; Savin, D. A.; McCormick, C. L. *Polym. Chem.* **2014**, *5*, 819–827.

(129) Kalyanasundaram, K.; Thomas, J. K. *J. Am. Chem. Soc.* **1977**, *99*, 2039–2044.

(130) Turro, N. J.; Yekta, A. *J. Am. Chem. Soc.* **1978**, *100*, 5951–5952.

(131) Neidlinger, H. H.; Chen, G.-S.; McCormick, C. L. *J. Appl. Polym. Sci.* **1984**, *29*, 713–730.

(132) McCormick, C. L.; Elliott, D. L. *Macromolecules* **1986**, *19*, 542–547.

(133) McCormick, C. L.; Chen, G.-S.; Hutchinson, B. H. *J. Appl. Polym. Sci.* **1982**, *27*, 3103–3120.

(134) Ezzell, S. A.; McCormick, C. L. *Macromolecules* **1992**, *25*, 1881–1886.

(135) Yamamoto, H.; Tomatsu, I.; Hashidzume, A.; Morishima, Y. *Macromolecules* **2000**, *33*, 7852–7861.

(136) Kalyanasundaram, K. *Photochemistry in Microheterogeneous Systems*; Academic Press, Inc.: Orlando, FL, 1987.

(137) Pickett, P. D.; Kasprzak, C. R.; Siefker, D. T.; Abel, B. A.; Dearborn, M. A.; McCormick, C. L. *Macromolecules* **2018**, *51*, 9052–9059.

(138) Borisov, O. V; Halperin, A. *Curr. Opin. Colloid Interface Sci.* **1998**, *3*, 415–421.

(139) Peng, C.; Crawshaw, J. P.; Maitland, G. C.; Martin Trusler, J. P.; Vega-Maza, D. *J. Supercrit. Fluids* **2013**, *82*, 129–137.

(140) Qiao, M.; Qi, W.; Liu, H.; Qu, J. *Water Res.* **2013**, *52*, 11–19.

(141) Chandross, E. A.; Ferguson, J.; McRae, E. G. *J. Chem. Phys.* **1966**, *45*, 3546–3553.

(142) Chandross, E. A.; Ferguson, J. *J. Chem. Phys.* **1966**, *45*, 3554–3564.

(143) Abdel-Mottaleb, M. S. A.; Galal, H. R.; Dessouky, A. F. M.; El-Naggar, M.; Mekkawi, D.; Ali, S. S.; Attya, G. M. *Int. J. Photoenergy* **2000**, *2*, 47–53.

(144) Ferguson, J.; Mau, A. W. *Mol. Phys.* **1974**, *27*, 377–387.

(145) Tam, K. C.; Jenkins, R. D.; Winnik, M. A.; Bassett, D. R. *Macromolecules* **1998**, *31*, 4149–4159.

(146) Yusa, S.; Kamachi, M.; Morishima, Y. **1998**, *7463*, 6059–6067.

(147) Stevens, K. pH-Responsive Sulfonamide-Based Polysoaps via RAFT Copolymerization for Oil Remediation and Recovery, 2018.

(148) Dearborn, M. A. Biocompatible, Responsive Polysoaps via RAFT Copolymerization for the Delivery of Model Cancer Therapeutics, University of Southern Mississippi, 2018.